Technical Report HL 94-15
September 1994

AD-A286 423

US Army Corps
of Engineers
Waterways Experiment
Station

Review and Evaluation of Hydrodynamic Modeling for the Lower St. Johns River Estuary

by Lisa Roig

DTIC
ELECTE
NOV 22 1994
S B D

Approved For Public Release; Distribution Is Unlimited

94 11 22 005

94-35839

Prepared for U.S. Army Engineer District, Jacksonville
and St. Johns River Management District

The contents of this report are not to be used for advertising, publication, or promotional purposes. Citation of trade names does not constitute an official endorsement or approval of the use of such commercial products.

PRINTED ON RECYCLED PAPER

Technical Report HL-94-15
September 1994

Review and Evaluation of Hydrodynamic Modeling for the Lower St. Johns River Estuary

by Lisa Roig

U S Army Corps of Engineers
Waterways Experiment Station
3909 Halls Ferry Road
Vicksburg, MS 39180-6199

Final report

Approved for public release, distribution is unlimited

Prepared for U S Army Engineer District, Jacksonville
Jacksonville, FL 32232-0019

and St Johns River Water Management District
Palatka, FL 32178-1429

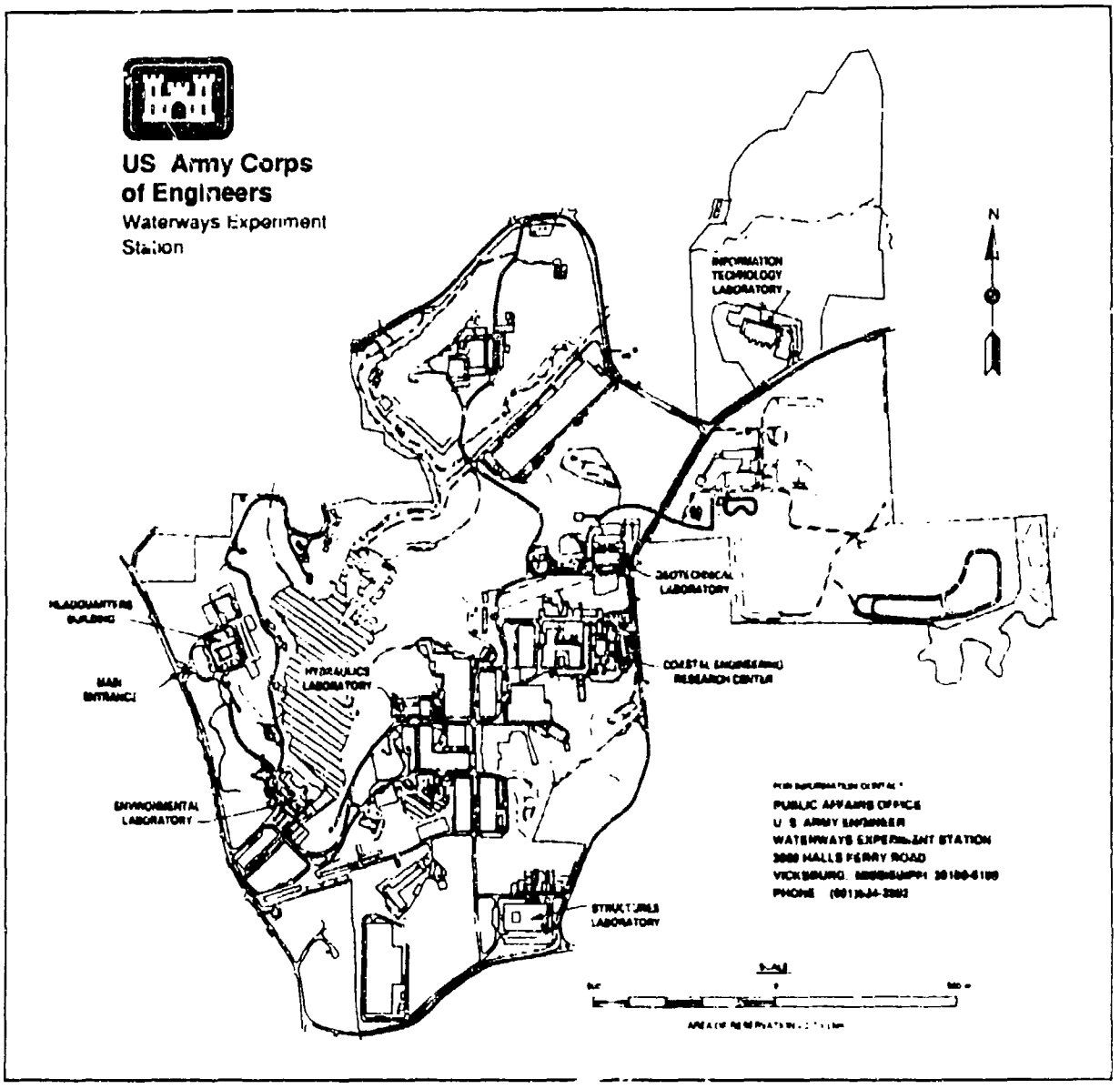

Waterways Experiment Station Cataloging-In-Publication Data

Roig, Lisa.

Review and evaluation of hydrodynamic modeling for the lower St. Johns River Estuary / by Lisa Roig ; prepared for U.S. Army Engineer District, Jacksonville and St. Johns River Water Management District.

76 p. : ill. ; 28 cm. — (Technical report ; HL-94-15)

Includes bibliographic references.

1. Saint Johns River Estuary (Fla.) — Mathematical models. 2. Sediment transport — Florida — Saint Johns River — Mathematical models. 3. Water quality — Florida — Saint Johns River — Mathematical models. 4. Hydrodynamics — Data processing. I. United States. Army. Corps of Engineers. Jacksonville District. II. U.S. Army Engineer Waterways Experiment Station. III. Hydraulics Laboratory (U.S.) IV. St Johns River Water Management District. V. Title. VI. Series: Technical report (U.S. Army Engineer Waterways Experiment Station) ; HL-94-15.

TA7 W34 no.HL-94-15

NTIS GRA&I ☑
DTIC TAB ☐
Unannounced ☐
Justification
By
Distribution/
Availability Codes
Dist | Avail and/or Special
A-1

Contents

Preface v

1—Introduction 1

2—Equations of Estuarine Hydrodynamics 3

Three-dimensional Hydrodynamic/Salinity Equations 3
Hydrostatic Pressure Assumption (Shallow-Water Approximation) 6
Viscous Forces 6
Reynolds Stresses 7
Parameterizations of the Turbulent Fluctuation Terms 8
Two-dimensional, Vertically Averaged Equations 10
Mode Splitting 13
Wave Continuity Equation for Vertically Averaged Flow 14
Constant Density, Vertically Averaged Approximation 14
Two-dimensional Laterally Averaged Equations 15
One-dimensional Equations 16
Multidimensional Approximations 18
Spectral Methods 18

3—Numerical Solution Techniques 20

Discretization of the Solution Domain 20
Numerical Methods 21
Grid Resolution 22
Time-Stepping Schemes 23
Computational Efficiency 24

4—Current Issues in Hydrodynamic Modeling 26

Lateral Momentum Transport 26
Wetting and Drying 27
Vertical Coordinate Transformations 27
Resolution of Sharp Fronts 28
Treatment of the Convective Term 28
Supercritical Flows 29
Residual Flows 29
Model Testing and Verification 30

5—Compatibility with Sediment Transport and Water Quality Models 31

6—Estuarine Hydrodynamic/Salinity Models 33

Figure

8. Intensity and line width of NMR of quasi-liquid layer against inverse temperature 7
9. Correlation time for rotational motion τ of quasi-liquid layer against inverse temperature 8
10. Diffusion coefficient of quasi-liquid layer against inverse temperature 8
11. Temperature dependence of the relative concentration of the mobile aqueous suspension of Aerosil 8
12. Typical configuration for measurements of surface and bulk conductivity 9
13. Variations of the real part of conductivity of pure polycrystalline ice at –10°C .. 10
14. Temperature dependence of surface conductivity of the (0001) plane for pure and doped ice 12
15. Surface conductivity of ice as a function of crystallographic orientation and temperature 12
16. Variations of surface conductance after evacuation of pure water for "pure" natural ice 13
17. Typical thickness dependence of the measured current intensity obtained for ice films deposited onto a glass substrate 13
18. Hall mobility μ at 157 Hz as a function of temperature for normal and rubbed surfaces 14
19. Space distribution of electric charges in ice near the surface 15
20. Kelvin's method 18
21. Temperature dependence of $\Delta W_{im} = 1/k'$ 19
22. Change in ice surface potential when the surface was rimed with supercooled droplets 19
23. Static electric potential at the surface of freshwater columnar ice 20
24. Schematic diagram of experimental setup for measurements of static electric potential of ice surface 20
25. Electric potential on the surface of ice sample assembled of pure and KOH-doped ice 21
26. Separation force as a function of temperature 23
27. Strength as a function of temperature for snow–ice sandwiched between stainless steel disks 23
28. Grain-boundary grooves 25
29. Temperature dependencies of quasi-liquid layer thickness 26
30. Calculated temperature dependence of a thickness of liquid film on an ice surface 29
31. Calculated dependence of the equilibrium thickness of the liquid-like layer on ice 30
32. Representation of protonic point defects concentration 31
33. Calculated temperature dependence of the liquid film on ice thickness 31

TABLES

Table

1. Temperature dependence of the thickness of a liquid-like layer on the ice/Aerosil interface 8
2. Surface conductivity of ice 10
3. Summary of estimates of grain boundary thickness 14

FOREWORD

At the present time, thousands and thousands of people around the world deal with ice, snow and permafrost. They are scientists, educators, engineers, navigators, meteorologists and others. While a small fraction of these people contribute to the knowledge base in ice physics, all of them use knowledge from it frequently. Moreover, successful applied research is based upon fundamental science—one more reason for ice specialists to have a textbook on ice physics on their desks.

The first modern ice physics text was Fletcher's book on *The Chemical Physics of Ice* (1970). Fletcher's book is in typical textbook format: it is reasonably brief and easy to understand. He touched on a few of the most important topics, but not all of them.

The most comprehensive book on ice physics to date was published by Hobbs in 1974. Hobbs considered almost all of the basic aspects of ice as understood at that time. Moreover, he described and compared several (sometimes opposing) viewpoints. This fundamental and rather large (837 pages) book is commonly known as the "Ice Bible" by specialists in the field. In 1974 and 1975, two CRREL Monographs on ice were produced by John Glen. These were briefly and clearly written and reviewed almost all ice-related subjects. This work was (and in some respects still is) a magnificent introduction to ice.

Finally, in 1981 Maeno wrote a simple, popular book for the express purpose of attracting people's attention to the subject.

During the past 20 years, a significant amount of new experimental and theoretical work has appeared, dramatically changing our views on ice physics. As a result, we are now able to formulate physical laws using more simple and direct methods. We have found some of the physical models used in the past to be completely wrong. The physics of ice is a much better developed subject than it was 20 years ago.

For the above reasons, I feel the time is ripe for a contemporary book on ice physics, incorporating the known and proven with almost 20 years worth of material not covered by previous works.

I have tried to prepare a "readable" book, and not one that requires the reader to be a uniquely educated person. It is my intent to present the material in such a way that any reader attracted by the title *Ice Physics* will be able to comprehend it. This is quite difficult for a book dedicated, not to a particular field of knowledge, but to a specific material. Indeed, for ice it means we have to consider a wide variety of subjects, including quantum chemistry, solid state physics, the theory of elasticity, ionic conductivity, synchrotron X-ray topography, crystal growth, the physics of surfaces and more.

The primary goal is to produce as simple a book as possible without sacrificing scientific accuracy. Experimental facts, physical ideas and theories will be strongly organized and bound together cohesively. The reader will be introduced to a wide variety of material on a step by step basis. Then the picture will be whole.

To accelerate publication, this book will appear first in the form of a series of joint CRREL–Dartmouth reports, later to be published in CRREL's Monograph series, on:

1. The structure of ordinary ice
   Part I: "Ideal" structure of ice. Ice crystal lattice
   Part II: Defects in Ice
   Volume 1: Point defects
   Volume 2: Dislocations and planar defects
2. Electrical properties of ice
   Part I: Conductivity and dielectric permittivity of ice
   Part II: Advanced topics and new physical phenomena

3. Optical properties
4. Electro–optical effects in ice
5. Thermal properties
6. Mechanical properties of ice. Elasticity and anelastic relaxation. Plastic properties. Fracture of ice
7. Electromechanical effects in ice
8. The Surface of ice
   Part I: Experimental results on the structure and properties of the ice surface
   Part II: Theoretical models of the ice surface
9. Other forms of ice and their properties
10. Ice in space
11. Ice research laboratories

The reports will be prepared in a sequence convenient to the author. The present report is the fifth in the series.

NOMENCLATURE

a	length of hop
$\varkappa_1^{-1}$	length of screening by Bjerrum defects
$\varkappa_2^{-1}$	length of screening by ions
$\varkappa^{-1}$	screening length when $\lvert e_i\varphi_s \rvert >> k_BT$
α_o	fraction of surface molecules in the liquid-like layer with dipole moments (i.e., protons) oriented towards the surface
B	magnetic induction
C_s	concentration of adsorbed molecules on the surface
C_M	maximum concentration of adsorbed molecules
d	thickness of the quasi-liquid layer
D_i	diffusion coefficient
Δ,Ψ,ϑ	angles
E_a	heat of adsorption
E, $\vec{E}$	electric field strength
e_i	electric charge of i^{th} type of charge carrier, $i = 1,2,3,4$
ε_0	dielectric permittivity of vacuum
ε_s	static dielectric permittivity of ice, $\varepsilon_s = 100$ ($T = -10°C$)
E_s	activation energy of surface conductivity
E'	effective electric field acting on a molecule
ε_∞	high-frequency dielectric permittivity of ice, $\varepsilon_\infty \approx 3.2$
Φ	$= 3.85\, k_BTr_{oo}$
ϕ	wetting angle
G	Gibbs free energy
g	gyromagnetic constant
γ	surface energy
γ_{SL}	surface energy of ice/water interface
γ_{VL}	surface energy of vapor/water interface
γ_{VS}	surface energy of vapor/ice interface
I	current
η	viscosity
φ	electric potential
φ_s	surface electric potential
k	absorption coefficient
k_B	Boltzman constant
L	thickness of the surface layer
λ_s, λ_{so}	surface charge density
λ_{sa}	surface charge absorbed on the ice interface
$\vec{m}$	dipole momentum of a water molecule
n	refractive index
n_B	concentration of Bjerrum defects
n_{H2O}	water molecule concentration in ice
n_i	charge carrier concentration, $i = 1,2,3,4$
n_i	refractive coefficient of ice
n_w	refractive coefficient of water
n_{ion}	concentration of ions
ν	frequency of ion's hops
P	pressure
$\vec{P}$	polarization vector
$\vec{P}_e$	electronic polarization vector
$\vec{P}_M$	molecular polarization vector
Q	electric charge
ρ	$r_\parallel / r_\perp$
$\rho(x)$	density of the space charge
ρ_L	water density
$r_\perp$	reflection coefficient for light polarized perpendicular to the plane of incidence
$r_\parallel$	reflection coefficient for light polarized parallel to the plane of incidence
r_o	constant
s	surface area
σ_B	Bjerrum defect conductivity
σ_B	bulk conductivity
σ_{ion}	ionic conductivity
σ_o	low-frequency bulk conductivity
σ_s	surface conductivity, Ω^{-1}

σ_{ss}	specific bulk conductivity of the ice surface layer, $\Omega^{-1}m^{-1}$
S_{st}	adhesive strength
S_c	entropy of fusion per unit mass
σ_∞	high-frequency bulk conductivity
T	temperature
t	time
τ	correlation time of molecular motion
τ_a	mean lifetime of a molecule adsorbed on the surface
τ_D	Debye relaxation time
τ_{DS}	Debye relaxation time of the surface layer of ice
τ_{MS}	Maxwell relaxation time
T_m	melting point of ice
v	velocity
x	coordinate
ω	angular frequency
ω_o	resonance frequency
W_i	electron work function of ice
W_m	electron work function of a metal
μ	chemical potential
μ_i	charge carrier mobility, $i = 1,2,3,4$ for H_3O^+, OH^- ions, D- and L-defects respectively

The Surface of Ice

VICTOR F. PETRENKO

INTRODUCTION

Since childhood, we have accustomed ourselves to matter being either solid or liquid or gas. Later, we become acquainted with the fourth kind of matter called plasma, which is very rarefied and has an extremely large electrical conductivity.

Can you imagine a simultaneous combination of certain properties of solid, liquid and plasma matter? It is present on the surface of the ice upon which we walk each winter, unsuspecting that it possesses such unique characteristics.

When we bump into a sharp corner or hurt ourselves with a needle or cut a finger with a knife, we confirm that surfaces of solids are indeed solid. This is true in so many cases that it necessarily becomes a rule.

In the case of ice, however, some simple observations make us doubt that it has a rigid and permanent surface. For example, if we bring two ice balls together, then right before our eyes, a small "neck" starts to grow between them (Fig. 1). In time, further growth will lead the two balls to become one. In this simple experiment, some substance can be considered to flow between the balls through the "neck." Since ice in bulk form is apparently solid (have you ever fallen on ice?), it is most likely the surface that flows.

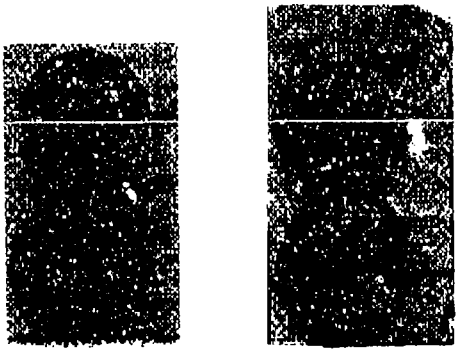

a. On contact. *b. 319 minutes later.*

Figure 1. Growth of a neck between two ice spheres 0.5 mm in diameter at –6°C (from Hobbs 1974).

In a process similar to the ice balls' unification, airy, fluffy snowflakes, after lying together for some time, sinter first into dense, heavy snow, and next into solid ice. It is this process, going on for thousands and thousands of years, that has formed the kilometer-thick ice sheets in Antarctica and Greenland (mass transport through the vapor phase and a plastic flow are also involved in this sintering process).

Evidently, the first documented guess for the existence of a special layer on the surface of ice was the work by Faraday (1859). On the grounds of his long-standing experiments on the adhesion of ice, Faraday called this layer a "liquid-like" layer. Another common expression is "quasi-liquid" layer. Now, the existence of some special layer on the ice surface has been proven by many experimental techniques. Hundreds of papers are dedicated to the investigation of the structure of this layer and its physical properties. The most essential contributions to the store of our knowledge about this liquid-like layer were made during the past two decades.

In the present report, I shall describe the results of the experimental research that provides direct information on the structure and thickness of this layer: X-ray diffraction, proton channeling, ellipsometry and NMR. Then, numerous results of studies of the physical properties of the ice surface will be considered. An analysis of these properties by means of comparing various models also allows us to obtain indirect information about the structure and thickness of the special layer on the ice surface. We shall not consider ice friction here, since several good reviews on this topic have been published recently (see, for instance, Aharon et al. [1988] and Colbeck [1992]). Nevertheless, when all the reports are united into a book, a chapter on ice friction will be included.

In conclusion, major known theoretical models, describing the structure and properties of the liquid-like layer, will be discussed.

PART I. EXPERIMENTAL RESULTS ON THE STRUCTURE AND PROPERTIES OF THE ICE SURFACE

X-RAY DIFFRACTION

When considering the structure of the quasi-liquid film on the ice surface, we must first answer the question: is the structure of the film ordered or not? That is, does the structure have a long range order? And if so, then is this structure different from that of ice? It seems that the easiest way to answer this question is to use any known X-ray diffraction technique. However, owing to the extremely small thickness of the film, it is difficult to differentiate its contribution to the diffraction from that of the ice bulk. I am aware of only one such attempt, where Kouchi et al. (1987) investigated X-ray diffraction at the surfaces of polycrystalline and monocrystalline ice in a temperature range of –0.5 to –10°C. Glancing beams were used (angle of incidence = 2°) to make the contribution of the surface as large as possible. The Kα line of the Cu X-ray spectrum was used in the experiments.

Figure 2 shows X-ray diffraction patterns of the surface of the polycrystalline ice sample obtained at –9.3, –2.1 and –1.1°C. At T = –9.3 and –2.1°C, the diffraction peaks that are characteristic for the crystal are clearly visible, although their magnitude decreases at –2.1°C. At T = –1.1 °C, those peaks virtually vanish, being replaced by a blurred, circular "halo" centered at $2\vartheta \approx 26°$. This is a clear evidence that, at this temperature, the long-range order in the arrangement of water molecules in the surface layer vanishes.

Since the intensity of the "halo" can be used to estimate the disordered layer's thickness, it is interesting to follow the temperature dependence of this intensity, which is illustrated in Figure 3. First, we can conclude from this figure that the layer's thickness is independent of the crystallographic orientation of the surface. Second, the layer ceases to be detectable by this method at $T \leq -2$°C. Unfortunately, Kouchi et al. did not attempt to estimate an absolute magnitude of the layer's thickness.

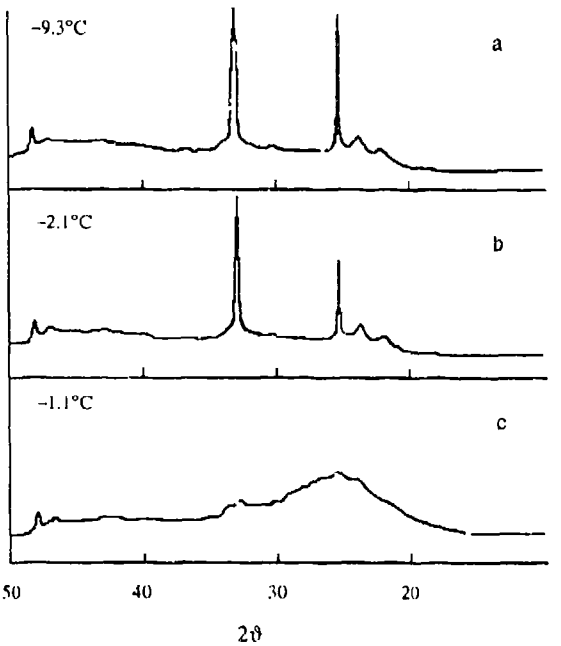

Figure 2. Intensity of the beam diffracted from the polycrystalline ice surface as a function of the angle between incident and reflected beams (after Kouchi et al. 1987).

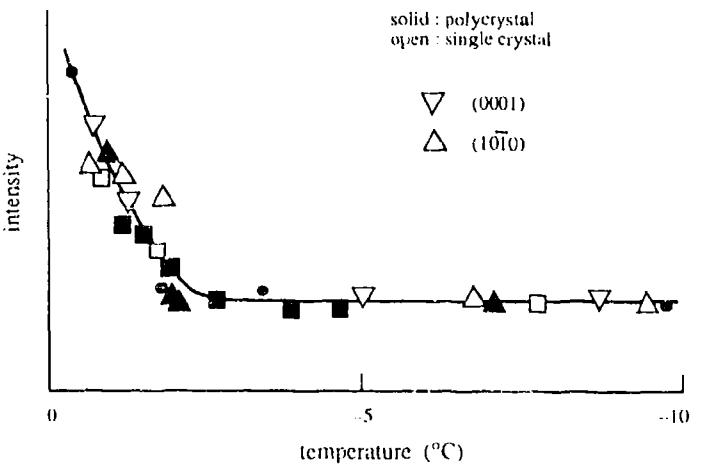

Figure 3. Changes in intensity of diffraction halo at $2\vartheta = 28°$ with temperature (after Kouchi et al. 1987).

PROTON CHANNELING

Another interesting experimental method of determining the thickness and structure of the quasi-liquid layer was used by Golecki and Jaccard (1977, 1978). This is the so-called channeling effect, discovered by Oen and Robinson (1962). The channeling effect manifests itself in the fact that, if a beam of heavy charged particles (usually protons or α particles) travels parallel to some crystallographic direction, then the particles of that beam experiencing low-angle scattering penetrate the crystal at very long distances and can stay inside the channels formed by atomic rows. The magnitude of this effect is usually expressed in terms of the ratio of the flux of backscattered particles when the direction of the flux coincides with one of the crystallographic directions to that when the direction is arbitrary.

The backscattering can take place only at nuclei of atoms that are much heavier than the particles in the beam and resembles the classic Rutherford scattering. The diffraction of such particles at the crystal lattice is insubstantial, since the characteristic de Broglie wavelength is several orders of magnitude less than the lattice constant.

Most of the backscattered particles experience only a single strong interaction with a lattice atom. Using the theory of Rutherford's scattering, we can calculate the energy of the reflected particle as a function of the scattering angle. Departures from this predicted value contain information about the depth at which the scattering took place (more exactly, about the path the particle has traveled back and forth within the matter). The loss of the kinetic energy of the particles is attributable to their interaction with the valence electrons and is almost independent of the direction of the motion. Having "calibrated" such losses for a particular material (or having calculated them theoretically), we can establish the depth at which the scattering took place with a rather high accuracy.

The channeling is extremely sensitive to the degree of perfection of a crystal structure and therefore can be efficiently used for measurements of the magnitude of thermal vibrations, the degree of disordering, the concentration of point defects and so forth. One of the comprehensive reviews on the subject is that by Gemmel (1974).

In 1977 and 1978 this effect was explored by Golecki and Jaccard for the investigation of the (0001) surface of ice crystals. The authors measured the backscattering (angle 150°) of 100-keV protons from the surface of monocrystalline ice in a wide temperature range from –2 to –130°C. They found that, at temperatures higher than –40°C, the surface layer is characterized by much higher disordering in relation to the bulk. Analysis of the behavior of the disordering process prompted Golecki and Jaccard to conclude that the disordering is caused by a significantly higher magnitude of thermal vibrations of oxygen atoms near the surface rather than the absence of symmetry in the structure. Thus, at $T = -1.8$°C the average amplitude of the thermal vibrations of oxygen atoms near the surface exceeds that of the bulk by 3.3 times. Because of that, Golecki and Jaccard suggest not using the term 'liquid-like' layer at all.

To estimate the thickness of the special surface layer of ice, Golecki and Jaccard calculated an equivalent thickness of an amorphous layer (totally disordered) that would result in the same magnitude of scattering. The results of such calculations are depicted in Figure 4. It is worth noting that the half-thickness of the layer $t/2$ obtained is extremely large. The temperature dependence of the thickness t was found to be

$$d(\text{nm}) = (94 \pm 17) - (54 \pm 14)\log(273 - T). \quad (1)$$

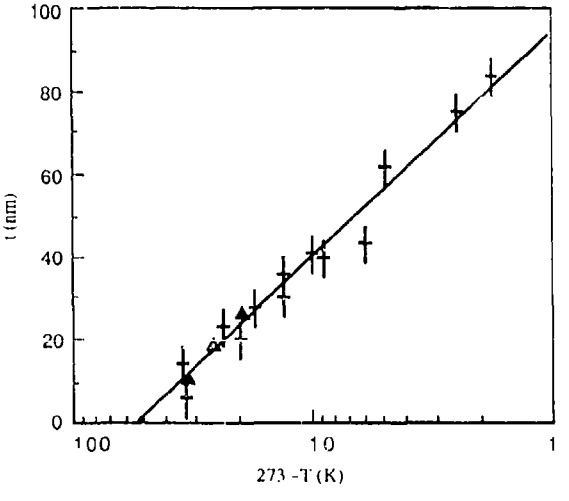

Figure 4. Equivalent "amorphous" thickness of the disordered region at the ice surface, deduced from the measurements with the aid of Meyer's (1971) theory. The solid line corresponds to least-squares fit. The density of the surface region was assumed equal to that of ice (0.917 g cm^{-3}) (after Golecki and Jaccard 1978).

OPTICAL ELLIPSOMETRY

Ellipsometry is an optical reflectance technique in which the change of the state of polarization of light upon reflection from a surface is measured. Even though the method dates back to Drude (1889), ellipsometry has recently attracted considerable attention because of a wide variety of applications in modern solid state optics, especially in the physics of surfaces, interfaces and thin films. In the study of the ice surface, optical ellipsometry was used first by Beaglehole and Nason (1980), and later by Furukawa et al. (1987a,b).

The change of the state of polarization upon reflection can be expressed in terms of the ratio of two complex reflection coefficients $r_{\parallel}$ and $r_{\perp}$ for light polarized parallel and perpendicular to the plane of incidence, r being the ratio of reflected and incident electric field strength. The complex quantity

$$\rho = \frac{r_{\parallel}}{r_{\perp}} = \tan\psi \cdot \exp(i\Delta) \qquad (2)$$

defines the two ellipsometric angles Δ and ψ. The two angles completely determine the two optical constants n (refractive index) and k (absorption coefficient) of an isotropic reflecting medium. Mathematical dependence of n and k on Δ and ψ, calculated from Fresnel's formula, was found, for example, by Bootsma and Meyer (1969).

The application of ellipsometry in surface physics is favored because in suitable cases a layer with average thickness as small as $^1/_{100}$ of a monolayer can be detected, if in the layer n and k are different from that of the bulk.

Ellipsometric data are usually analyzed with computers because the two measured variations $\delta\Delta$ and $\delta\psi$ are not sufficient to determine all parameters (optical constants, thickness) even for a single surface film.

Beaglehole and Nason (1980) employed ice monocrystals grown following the Bridgeman method using twice-distilled water. The ice surface with the orientation (0001) (basal plane) or (10$\bar{1}$0) (prismatic plane) was milled with a warm razor immediately before ellipsometrical tests. Water forming simultaneously on the ice surface was removed by the same razor, resulting in a surface of unruffled cleanness.

Measurements in the 0 to –30°C temperature range revealed a considerable distinction in the behavior of the surface layer at the basal and prismatic planes. Assuming that the refraction coefficient of the surface layer is the same as that of water, Beaglehole and Nason found that the film's thickness on the prismatic surface (d) was about 130 Å at T = –1.5°C, decreasing slowly to a monoatomic thickness at T = –10°C. They found a surface layer on the basal plane only at temperatures greater than –0.3°C.

Furakawa et al. (1987a,b) significantly advanced use of the ellipsometry technique for determining the transition layer thickness on the surface of ice. First, they used improved, more perfect ice crystals, grown from twice-distilled and degassed water. The degree of purity of ice plays an important role, since even a small salt concentration can sizably alter the thickness of the transition (quasi-liquid) layer on the ice surface. Second, they examined atomically flat (0001) and (10$\bar{1}$0) surfaces of the natural facets of a so-called negative crystal. A negative crystal is formed by pumping water vapor out of a small void inside a large monocrystal. Besides, they made their ellipsometric measurements under conditions of equilibrium between ice and its vapor.

Finally, Furakawa et al. interpreted their data, not using the assumption that the refraction coefficient of the surface film (n_i) is the same as that of water (n_w), but calculating it as a fitting parameter. They found that n_i = 1.330 for both faces (0001) and (10$\bar{1}$0), which is closer to water, n_w = 1.3327, than to ice, n_i = 1.3079. This implies that the density of the layer is quite close to that of water.

Figure 5 shows temperature dependence of the transition layer thickness as found by Furakawa et al. from their ellipsometrical measurements. As follows from this plot, the thickness of the transition layer drastically rises as temperature increas-

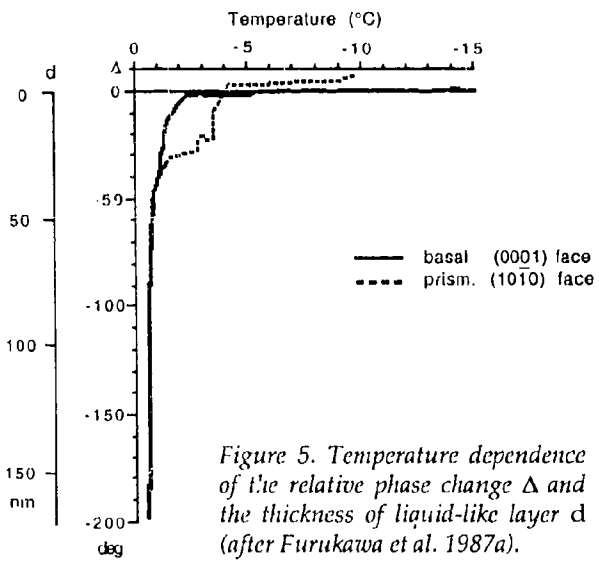

Figure 5. Temperature dependence of the relative phase change Δ and the thickness of liquid-like layer d *(after Furukawa et al. 1987a).*

es above −1 °C, exceeding 150 nm. A difference between the film's thicknesses on the (0001) face and the (10$\bar{1}$0) face is especially noticeable in the temperature range from −4 to −1 °C. Optical ellipsometry can't detect the presence of a liquid film on an ice surface at temperatures below −4 °C.

Very recently, Elbaum et al. (1993) performed optical measurements of a liquid-like layer using a simplified ellipsometry technique, which was termed Brewster reflectometry. The idea was to measure the refractive index profile near a plane interface between uniform media. If a collimated light beam with a vector E lying in the plane of incidence falls at the Brewster's angle, then the intensity of the reflected light will be zero for an interface between two homogeneous media. But, since the interface has a finite thickness, the reflectivity is slightly different from zero. Elbaum et al. assumed that the interface is composed of water vapor or its mixture with air having the refraction coefficient n = 1, a liquid film of thickness L and n =1.333 (same as water) and, finally, ice with n = 1.309. Given such conditions, the problem of the intensity of the reflected light can be solved exactly, and they used this solution to calculate the thickness of the liquid film on the ice surface from the measurements of intensity of a polarized light reflected at the Brewster's angle. Though this method has a lower sensitivity compared to conventional ellipsometry ($L \geq 12$ Å, Elbaum et al. [1993]), the described work was the first where the effect of air on the thickness and conditions of existence of the quasi-liquid layer was observed and investigated. In the absence of air, the quasi-liquid film could not be detected at the prismatic face of ice within the experimental error (12 Å). At the same time, a very thick film was observed at the basal face (0001) under the same conditions (Fig. 6). The presence of air significantly increased the liquid film thickness at the (0001) face.

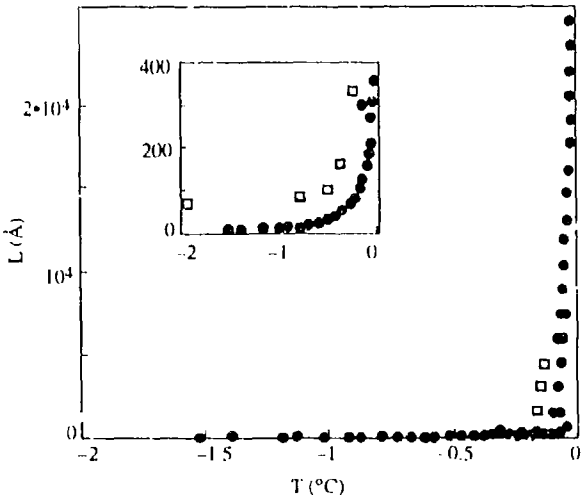

Figure 6. Collected results on the liquid-like film thickness from four reflection experiments. The inset shows the same results in smaller thickness range (after Elbaum et al. 1993).

NUCLEAR MAGNETIC RESONANCE

Clifford (1967), using Nuclear Magnetic Resonance (NMR) measurements on ice, observed a very narrow line (0.2 G) that he attributed to some form of liquid water remaining in ice down to temperature of at least −12°C. Kvlividze et al. (1970) demonstrated that this narrow resonant line is distinct from the NMR lines corresponding to protons in water and bulk ice and is caused by the liquid-like layer on the ice surface. Afterwards, NMR was used for studying the properties of the liquid-like layer on the ice surface by Bell et al. (1971), Kvlividze et al. (1974), Barer et al. (1977) and Ocampo and Klinger (1983a,b). The most comprehensive information about the physical properties of a liquid-like layer was obtained by Mizuno and Hanafuza (1987), to whom we are going to refer most often for this reason.

The phenomenon of NMR is an absorption of electromagnetic field quanta by nuclei that possess a magnetic moment and are placed in an external magnetic field B at resonance frequency ω_0

$$\omega_0 = g\,B \qquad (3)$$

where g is the giromagnetic constant.

The position of the resonant line, its shape and half-width, as well as the spin-lattice relaxation time, appear to be quite sensitive to the properties of a medium that surrounds the nuclear spins. Namely, those properties are the average distance and relative position of the spins in space, angular velocity and diffusion coefficient of molecules that contain the resonant nuclei.

Readers who are interested in this method should see the marvelous book by Abragam (1961) and also the paper by Burnett and Harmon (1972).

The NMR technique applied to ice, water or the quasi-liquid layer allows us first to distinguish three resonant lines associated with absorption by hydrogen nuclei in those three media. From the intensity of the liquid-like layer line, we can judge the approximate thickness of a particular layer. Besides, it is possible to determine the correlation

time of rotational motion of water molecules and a self-diffusion coefficient (Mizuno and Hanafuza 1987)

Since under normal conditions, the relative portion of molecules in the liquid-like layer is negligibly small, it is necessary first to increase the "surface-to-volume" ratio of the ice in question to observe NMR from this layer. The easiest way to achieve this is to pulverize water at a low temperature. As a result, microscopic ice balls are formed with a diameter about 100 μm and a net surface of about $3–5\times10^2$ cm/g. This method was used for instance by Mizuno and Hanafuza (1987). Kvlividze et al. (1974) saturated water with air prior to freezing. This leads to an appearance of a great number of microscopic air bubbles inside the ice, with a net surface of the order of $\sim10^4$ cm^2/g. Frost forming on walls of a Dewar vessel filled with liquid nitrogen has an even larger specific area of $1–2\times10^5$ cm^2/g (Kvlividze et al. 1970). Placing spherical Teflon particles ($r \approx 350$ Å) (Kvlividze et al. 1974), or Aerosil particles ($r \approx 100$ Å) (Barer et al. 1977) into water before freezing produced something comparable to the "frost" net surface of ice for NMR analysis. We have to take into account, of course, that the structure and properties of the liquid-like layer on the ice/(solid dielectric) interface might be different from ice/(water vapor + air) interface properties.

Figure 7 shows NMR spectra of the liquid-like layer of ice measured at various temperatures. To

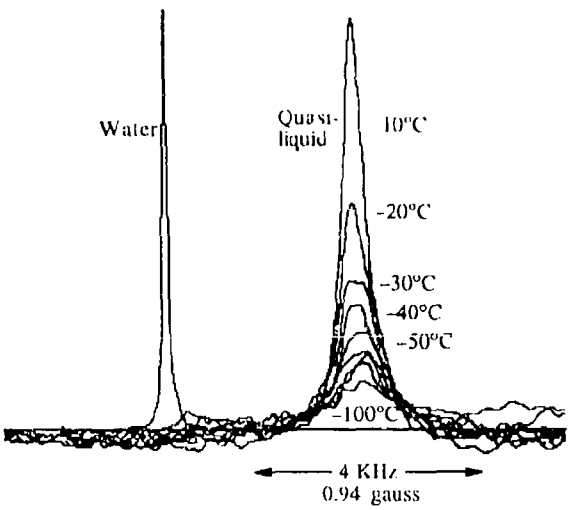

Figure 7. NMR spectra of the quasi-liquid layer of ice and water observed at 99.5 MHz. The signal of liquid water was taken at 5°C. Notice the difference in the line width between liquid water and the quasi-liquid layer (after Mizuno and Hanafusa 1987).

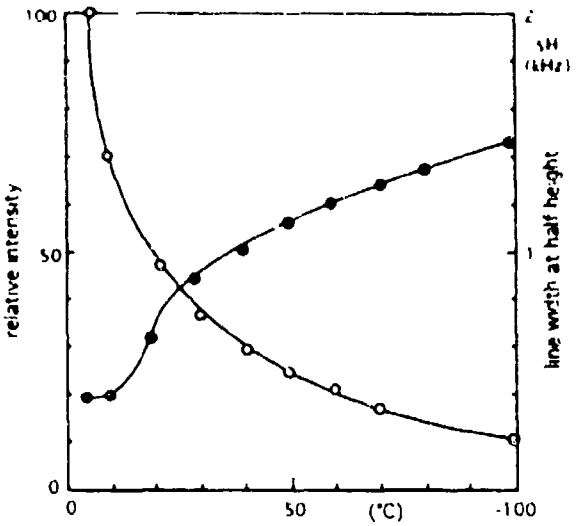

Figure 8. Intensity and line width of NMR of quasi-liquid layer against inverse temperature (after Mizuno and Hanafusa 1987).

increase the signal-to-noise ratio, the spectra were gathered 200 times at each temperature. The broad signal from crystalline ice is not seen within the range of the 20-kHz observational frequency (Mizuno and Hanafuza 1987).

The narrow signal was never detected at any temperature if bulk ice was used as a sample.

As is clear from Figure 7, the line width and the intensity vary with temperature and their temperature dependencies are shown in Figure 8. It should be noted that the line width of the liquid-like layer spectrum at –10°C is about 7 times that of ordinary water at 5°C.

Since the temperature dependencies shown in Figure 8 were measured as temperature was increased from –100 to –5°C, and since at $T \geq -10$°C a considerable sintering diminishes the total ice surface, the actual increase of the NMR signal at $T \geq -10$°C could be greater than the one shown in Figure 8.

The temperature dependence of the correlation time for rotational motion τ is shown in Figure 9. This time, which could be interpreted as the time it takes a water molecule to be reoriented in a liquid-like layer at $T = -10$°C, appears to be closer to that time for water ($\approx10^{-12}$ seconds) than for ice (2×10^{-5} seconds [Jaccard 1959]) at the same temperature. The activation energy of molecule reorientation in a liquid-like layer, which can be determined from the slope of the curve in Figure 9, is 0.291 eV and is also quite different from the corresponding value for the bulk ice (0.575 eV

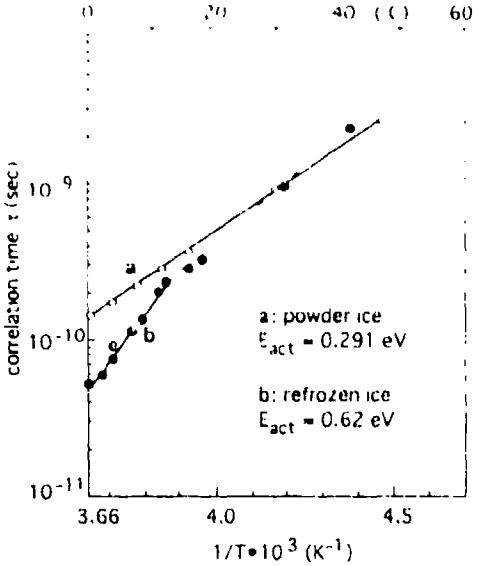

Figure 9. Correlation time for rotational motion τ of quasi-liquid layer against inverse temperature (after Mizuno and Hanafusa 1987).

[Jaccard 1959]). Therefore, comparing the rotations of a water molecule in water, the liquid-like layer and ice, we could conclude that, according to this property, the liquid-like layer is intermediate between ice and water, but it nevertheless resembles water more closely.

However, if we try to compare self-diffusion coefficients in water, the liquid-like layer and ice (see Fig. 10), we will come to an opposite conclusion, because this coefficient at 0°C in the liquid-like layer turns out to be $\approx 3\times10^{-12}$ m.^{2}/s, which is closer to ice ($\approx10^{-14}$ m^2/s) than to water (2×10^{-9} m^2/s). At the same time the activation energy of self-diffusion in the liquid-like layer (0.24 eV) is closer to that of water (≈0.24 eV) than to ice (0.65 eV).

Barer et al. (1977) studied NMR from a liquid-like layer forming at the interface between ice and Aerosil microspheres, i.e., on a frozen aqueous suspension of Aerosil. Like Mizuno and Hanafuza, they tracked the existence of the liquid-like layer much further down on the temperature scale than measurements that could be obtained from X-rays or ellipsometry (see Fig. 11). The results of their estimations of the liquid-like layer thickness at various temperatures are given in Table 1.

Table 1. Temperature dependence of the thickness of a liquid-like layer on the ice/Aerosil interface (after Barer et al. 1977).

T (°C)	-12	-10	-8	-6	-4	-2
l (Å)	11	12	14	20	27	52

In the same work (Barer et al. 1977), the viscosity of a liquid-like layer on the ice/quartz interface was measured. At T = -10°C the viscosity appeared to be $\eta = 0.17$ P, which exceeds the viscosity of supercooled water at the same temperature by an order of magnitude.

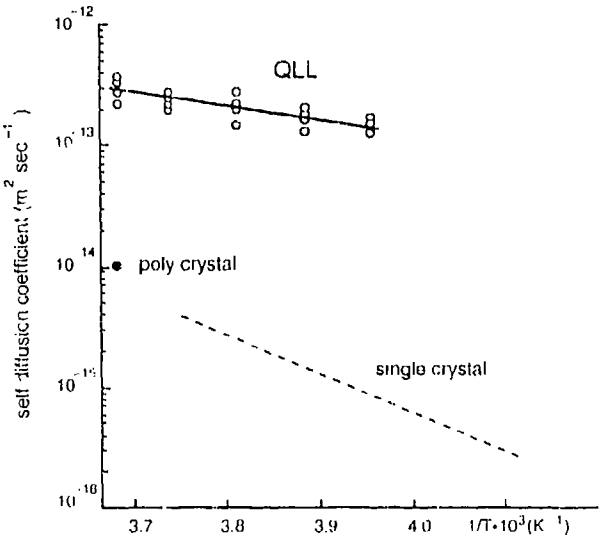

Figure 10. Diffusion coefficient of quasi-liquid layer against inverse temperature (after Mizuno and Hanafusa 1987).

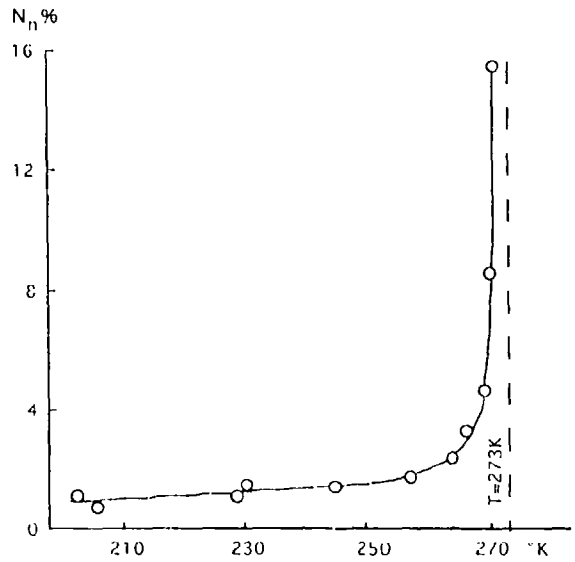

Figure 11. Temperature dependence of the relative concentration of the mobile aqueous suspension of Aerosil (after Barer et al. 1977).

ELECTRICAL CONDUCTIVITY OF THE ICE SURFACE

As we have seen in the previous sections, the surface layer of ice differs from the bulk in its structure, optical properties, molecule reorientation time and self-diffusion coefficient. It is therefore also natural to expect the ice surface to be different from the bulk in its electrical properties.

We can name several possible things that could change electrical properties of ice near the surface. The first is an increase (or decrease) of the charge carrier concentrations within the screening length, assuming that there is a potential difference φ_0 between the surface and the bulk. Such a difference may arise because of differences in the chemical potentials of charge carriers in the bulk and on the surface (electrochemical potential must be uniform everywhere) or because of adsorption of electrically charged impurities that compensate the space charge of ice at the surface. The latter arises merely from differences in solubilities of positive and negative impurity ions in ice. Second, charge carrier mobilities and the mechanisms of interaction between them might be different in the disordered surface or quasi-liquid layer.

In fact, the ice surface has an extremely high net electrical conductivity that was discovered back in the 1950s and has been studied intensely over the past 30 years. At temperatures roughly above -15°C in pure ice, the d.c. conductivity of the surface exceeds that of the bulk. A measurement of the surface conductivity is one of the simplest and most accessible ways to study the physical properties of the ice surface. In fact, a simultaneous measurement of the absolute value of the surface conductivity σ_s (with a dimension of Ω^{-1}) and of the specific volume electrical conductivity of the surface layer σ_{ss} (with a dimension of $\Omega^{-1}m^{-1}$) would allow determination of the layer's thickness L

$$L = \frac{\sigma_s}{\sigma_{ss}} . \qquad (4)$$

Measurement of charge carrier mobilities' values μ_i and their concentrations n_i is essential to understanding the nature and the structure of the quasi-liquid layer, as well as for determining the activation energies of μ_i and n_i. Researchers in this field have investigated the electrical conductivity and dielectric permittivity of the surface layer, as well as the Hall effect.

The major methodical problem in these experiments is the separation of currents flowing on the surface from the bulk currents. Usually, this is done by means of so-called guard rings (Fig. 12). A guard ring, as can be seen from this figure, is separated from the central electrode by a thin insulating ring. The guard ring and the central electrode have nearly the same potential, which provides an orientation of electrical field strength vector $\vec{E}$ (and consequently of currents) parallel to the surface of the cylinder. In this setup all subsurface currents flow through the guard ring, and their magnitude is proportional to the voltage drop across the resistor R_s. In this schematic, R_s and R_B must be much smaller than the impedance of the specimen Z_s in the whole range of the investigated frequencies.

A great majority of researchers have used the configuration shown in Figure 12, although sometimes square ice samples were used instead of cylindrical ones. Caranti and Illingworth (1983a) used the same idea (making $\vec{E}$ parallel to the surface and the use of a guard ring), although they employed a semi-spherical electrode frozen into ice.

Jaccard (1966, 1967) suggested that four-point electrodes, arranged in pairs at the opposite sides of a thin ice specimen, be used to determine the surface and bulk conductivities. However, we shall refrain from discussing this here because of serious criticism of this method expressed by Turner and Stow (1986).

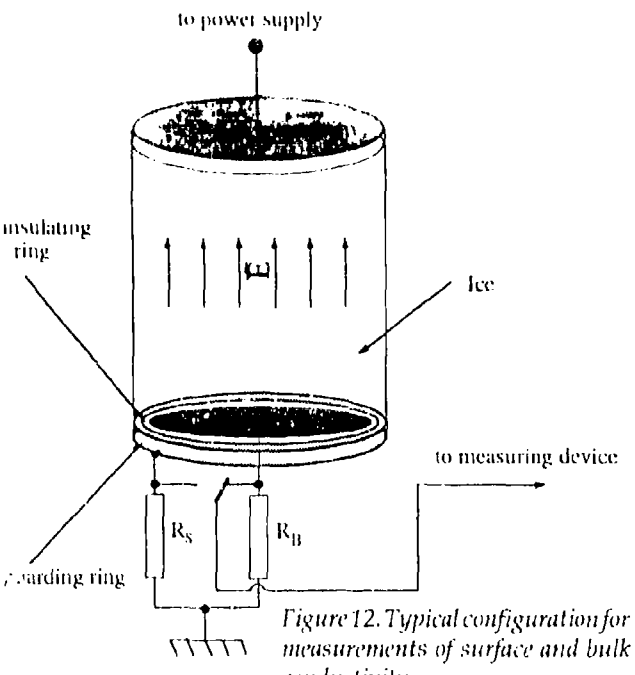

Figure 12. Typical configuration for measurements of surface and bulk conductivity.

Table 2. Surface conductivity of ice .

T (°C)	f (Hz)	σ_s (Ω^{-1})	E_s (eV)	Type of ice	Reference
-10	d.c.	3×10^{-8}	0.84 ±0.1	pure polycrystals	Camp et al. (1969)
-10	d.c.	3.9×10^{-10}	1.29	pure single crystals	Bullemer and Riehl (1966)
-10	d.c.	3.9×10^{-10}	≥ 1.3	3×10^{-4} M HF	
-10	d.c.	$(1.5–6)\times10^{-11}$	1.52	pure single crystals	Maeno (1973)
-10	d.c.	$(1–6)\times10^{-11}$	1.19	pure single crystals	Maeno and Nishimura (1978)
-10	d.c.	6×10^{-8}	0.44	1.7×10^{-4} M HH	
-10	0.1	4×10^{-9}	1.0	pure polycrystals	Caranti and Illingworth (1983a)
-10	0.1	6×10^{-8}	0.55	10^{-3} M NaCl polycrystals	
-10	107	2×10^{-8}	0.78	pure polycrystals	Caranti and Lamfri (1987)
-10	d.c.	$\approx 10^{-9}$	1.43	pure single crystals	Maidique et al. (1971)
-10	d.c.	1.5×10^{-10}	1.29	pure single crystals	Ruepp and Käss (1969)
-11	d.c.	$(1.4–6.3)\times10^{-10}$	—	pure single crystals	Jaccard (1967)
-53	d.c.	$\approx 1.5\times10^{-11}$ *		polycrystalline ice film deposited onto a dielectric substrate	Chrzanowski (1988)
-10	d.c.	$\approx 4\times10^{-9}$ †			

* Calculated from Chrzanowski's data assuming that the electrode's length was 5 mm.
† Calculated from Chrzanowski's data assuming that the activation energy is 1.2 eV.

Even a small amount of impurities in ice strongly affects the surface conductivity σ_s. This accounts for the considerable scatter in the experimental data obtained on σ_s. Data on low-frequency and d.c. surface conductivities of pure and doped ice at -10°C are summarized in Table 2. As we can see from this table, σ_s, even for pure monocrystalline ice, assumes values in a wide range, from 10^{-11} Ω^{-1} (Maeno and Nishimura 1978) up to 10^{-9} Ω^{-1} (Maidique et al. 1971). Data on activation energies E_s for the same crystals vary from a minimum value of 1.19 to 1.52 eV, with an average value of about 1.3 eV. Even a slight doping of ice leads to a considerable increase in σ_s and, as a rule, a decrease of E_s.

Typical frequency dependencies of ice bulk and surface conductivities are plotted in Figure 13. This plot shows that the frequency dependence of the bulk conductivity σ_B follows Debye's dispersion, which is well known for ice

$$\sigma_B = \sigma_0 + \frac{(\sigma_\infty - \sigma_0)\,(\tau_D\omega)^2}{1 + (\tau_D\omega)^2} \qquad (5)$$

where σ_0 is the low-frequency limit of the conductivity (or d.c. conductivity) determined by minority charge carriers. In pure ice at -10°C, those are H_3O^+ and OH^- ions. σ_∞ is the high-frequency limit of the conductivity, equal to the sum of all partial conductivities of the charge

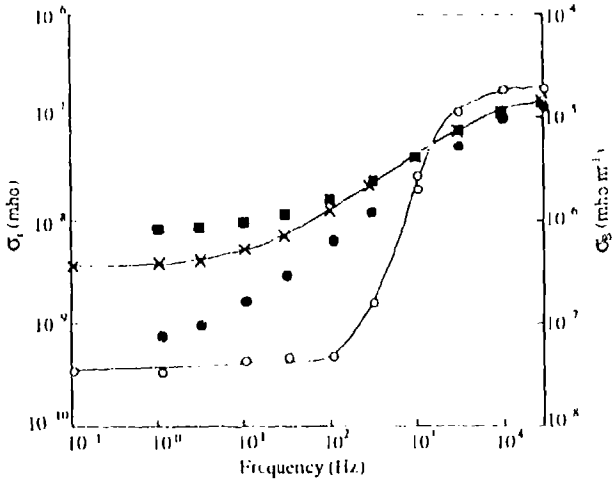

Figure 13. Variations of the real part of conductivity of pure polycrystalline ice at -10°C (after Caranti and Illingworth 1983).

carriers. Under the conditions considered, σ_∞ practically coincides with the conductivity of the majority charge carriers—Bjerrum defects, that is L- and D-defects. ω is the angular frequency and τ_D is the Debye relaxation time. I refer readers who are more interested in the electrical properties of bulk ice to the latest review on this subject (Petrenko 1993). Let us just remember that a small (compared to σ_∞) value of σ_0 results from lattice polarization arising from protonic charge carriers' motion. To prevent the polarization from increasing to infinity, ions and Bjerrum defects have to move in a consistent manner to keep their fluxes equal. An absence (or reduction) of any noticeable difference between σ_∞ and σ_0 would imply either that such a correlation in the motion of ions and Bjerrum defects is absent (or reduced) or that partial conductivity of ions is close to the conductivity of Bjerrum defects.

As can be seen from Figure 13, the frequency dependence of σ_s is much less pronounced than that of σ_B. This is especially true for the ice surface after annealing, i.e., the smoothest surface. Since some fraction of the current flowing along the surface inevitably penetrates the bulk, the remaining slight frequency dependence can be ascribed to these accompanying bulk currents. The rougher the surface is, the greater is the "bulk" contribution of the "surface" conductivity, in excellent conformity with the results shown in Figure 13. Thus, we can tell that, at least in the frequency range of 10^{-1} to 3×10^4 Hz, there is either no correlation in the motion of ions and Bjerrum defects in the subsurface layer at all (as is the case in water) or that this correlation is weak.

An alternative explanation for the weak frequency dependence of σ_s can be that the corresponding dielectric relaxation time for the subsurface layer τ_{Ds} might be several orders of magnitude more than that of the bulk τ_D. Therefore, we would search for the Debye dispersion for the liquid-like layer in a very-high-frequency range, where the standard methods for measuring σ are not applicable.

Let us try to estimate the specific conductivity of the surface layer σ_{ss} (dimensions of $\Omega^{-1}m^{-1}$), proceeding from the data in Table 2 and the results for the liquid-like layer thickness L given in the previous sections.

$$\sigma_{ss} = \frac{\sigma_s}{L} . \qquad (6)$$

Thus, taking $L = 1.2\times10^{-9}$ m ($T = -10C^\circ$ [Barer et al. 1977]) and $\sigma_s = 10^{-10}\ \Omega^{-1}$, we obtain

$$\sigma_{ss} \approx 10^{-1}\ \Omega^{-1}m^{-1}. \qquad (7)$$

If we substitute extreme values of σ_s for pure ice from $10^{-11}\ \Omega^{-1}$ up to $3\times10^{-8}\ \Omega^{-1}$, we shall get

$$\sigma_{ss} \approx (10^{-2}-3\times10^{1})\ \Omega^{-1}\,m^{-1}. \qquad (8)$$

At the same temperature, the bulk low-frequency conductance σ_0 falls in the limits (2.5×10^{-8} to 6.4×10^{-10}) $\Omega^{-1}\,m^{-1}$ (Petrenko 1993); i.e., it is from 6 to 11 orders of magnitude less than σ_{ss} from eq 8. The bulk high-frequency conductivity, $\sigma_\infty = 1.6\times10^{-5}\ \Omega^{-1}\,m^{-1}$, is also much less than σ_{ss}. If we assume that there is no correlation in the motion of ions and Bjerrum defects, then the characteristic dielectric relaxation time of the surface layer would be the Maxwell relaxation time τ_{MS}

$$\tau_{MS} = \frac{\varepsilon_0\varepsilon_\infty}{\sigma_{ss}} \approx (10^{-12} - 3\times10^{-9})\ \text{s} \qquad (9)$$

which corresponds to the frequency range

$$f = \frac{1}{2\pi\tau_{MS}} \approx (5\times10^{7} - 1.6\times10^{11})\,\text{Hz} \qquad (10)$$

where ε_0 is the vacuum dielectric permittivity and $\varepsilon_\infty = 3.2$.

Unfortunately, I am not aware of any attempts to measure σ_s as a function of frequency in the specified range, which could give more accurate values of σ_{ss} in conformity with eq 9. If in the future such measurements are carried out, then this will also allow more accurate determination of the liquid-like layer thickness L using eq 6.

The result of estimating the charge carrier concentration in the liquid-like layer using the following formula is quite interesting

$$n_i = \frac{\sigma_{ss}}{\mu_i e_i} . \qquad (11)$$

If we take $\sigma_{ss} \approx 3\times10^{1}\ \Omega^{-1}m^{-1}$ and $\mu \approx 10^{-7}\ m^2\ V^{-1}\ s^{-1}$ for ions and $\mu \approx 10^{-8}\ m^2\ V^{-1}\ s^{-1}$ for Bjerrum defects (Petrenko 1993), then an estimation using eq 11 for the n of ions and Bjerrum defects gives $3\times10^{27}\ m^{-3}$ and $5\times10^{28}\ m^{-3}$ respectively. (We used $e_1 = 0.62e$ and $e_3 = 0.38e$ [Hubmann 1979].) These are extremely large values if we recall that the concentration of water molecules in ice is about $3\times10^{28}\ m^{-3}$.

The above estimations can be much more accurate if we employ for our calculations the correlation time for rotational motion of water molecules at the ice surface, found in NMR experiments by Mizuno and Hanafuza (1987) (see Fig. 9). In bulk ice, this time coincides with the dielec-

tric relaxation time τ_D and is related to the conductivity σ_∞ by the following formula

$$\tau_D^{-1} = \Phi\left(\frac{\sigma_{ion}}{e_1^2} + \frac{\sigma_B}{e_3^2}\right) \approx \Phi\,\frac{\sigma_\infty}{e_3^2} \approx \Phi\,\frac{\sigma_{ss}}{e_3^2} \qquad (12)$$

where $\Phi = 3.85\ k_B T r_{oo}$, $r_{oo} = 2.76$ Å is oxygen-oxygen distance, "ion" and "B" subscripts correspond to ionic and Bjerrum defect conductivity and e_1 and e_3 to the electrical charges of ions and Bjerrum defects. Substituting $\tau_D = 10^{-10}$ s (from Fig. 8), $T = 263$ K and $e_3 = 0.38e$ into eq 12, we obtain for the net conductivity of the surface layer

$$\sigma_{ss} \approx 11\ \Omega^{-1}\,m^{-1} \qquad (13)$$

i.e., a value close to the upper limit found in eq 8. The corresponding concentration of Bjerrum defects in the surface layer according to eq 11 will be

$$n_B \approx 2\times10^{28}\ m^{-3}. \qquad (14)$$

If there is no correlation between fluxes of ions and Bjerrum defects in the liquid-like layer, we should use eq 9. Then

$$\sigma_{ss} \approx 0.3\ \Omega^{-1}\,m^{-1},\ n_B \approx 5\times10^{26}\ m^{-3}. \qquad (15)$$

Thus, we can conclude that the charge carrier concentration in the ice surface exceeds by many orders of magnitude that of the bulk and in some cases might correspond to a superionic state, i.e., a state in which all (or nearly all) molecules are ionized and mobile.

Caranti and Illingworth (1983a) remark in their paper that, in a.c. measurements of real and imaginary parts of the complex surface conductivity, the phase angle was always small, showing surface currents to be predominantly resistive. This is exactly what must be the case for an ordinary conductivity (without correlation between charge carrier fluxes) at frequencies much less than τ_D^{-1}.

Temperature dependencies of the surface conductivities of pure and doped ice are plotted in Figures 14 and 15. The behavior of this dependence is different at temperatures above and below –6°C. It is quite possible that a sharp rise of σ_s at $T \geq -6$°C is associated with an appearance of the liquid-like layer on the ice surface, which is detected by optical ellipsometry and X-ray diffraction methods (see previous sections). An interesting observation is the difference in σ_s corresponding to different crystallographic surfaces of ice (Fig. 15). The conductivity of the basal

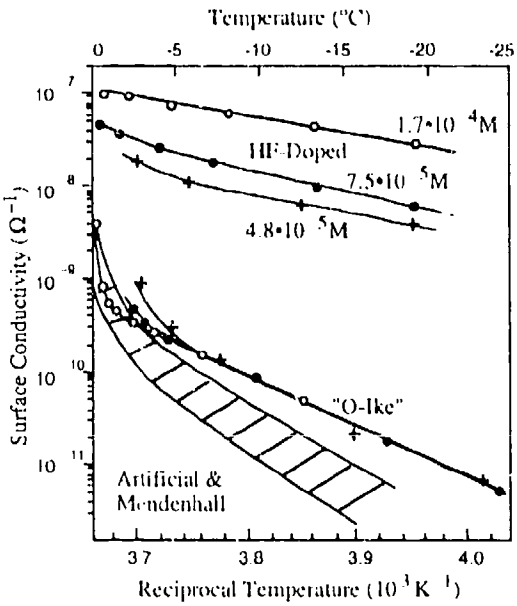

Figure 14. Temperature dependence of surface conductivity of the (0001) plane for pure and doped ice. "O-Ike" stands for ice from O-ike pond near the Syowa station in Antarctica, "Mendenhall" stands for ice from Mendenhall Glacier, Alaska (after Maeno and Nishimura 1978).

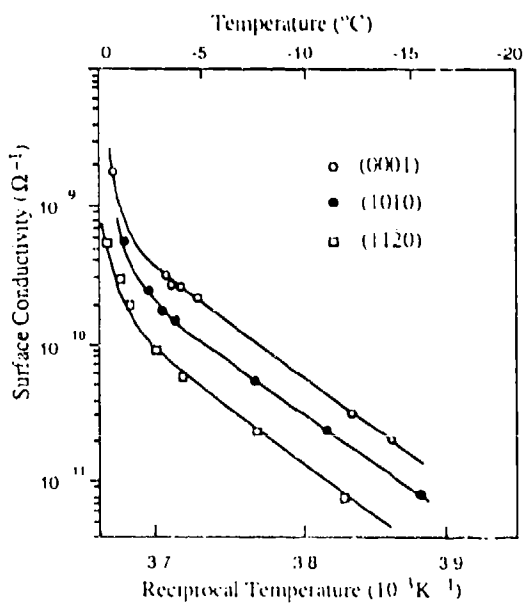

Figure 15. Surface conductivity of ice as a function of crystallographic orientation and temperature. Ice single crystals were taken from the Mendenhall Glacier, Alaska (after Maeno 1973).

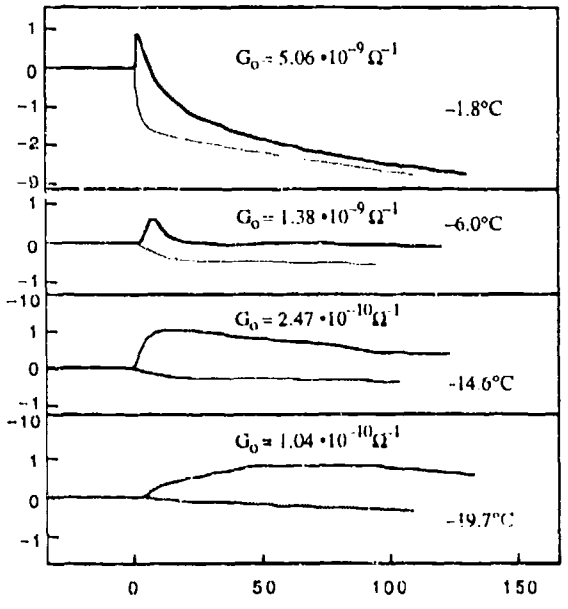

Figure 16. Variations of surface conductance after evacuation of pure water for "pure" natural ice (O-ike pond). Dotted lines indicate expected variations of the conductance calculated from measured temperature of the ice surface (after Maeno and Nishimura 1978).

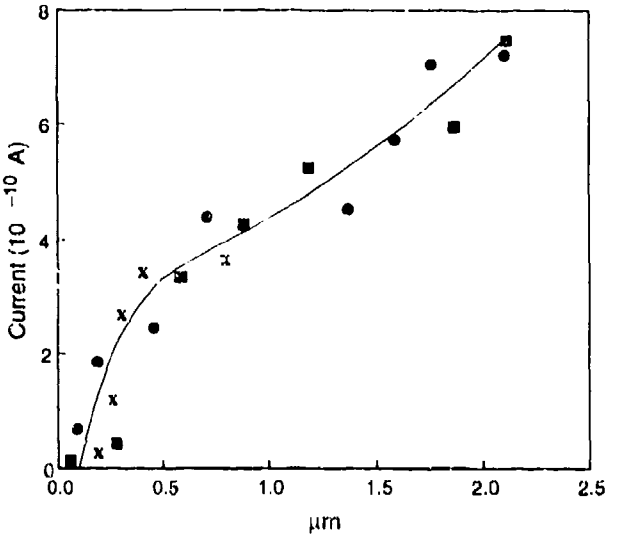

Figure 17. Typical thickness dependence of the measured current intensity obtained for ice films deposited onto a glass substrate of temperature 220 K. Three different experimental runs are shown (after Chrzanowski 1988).

(0001) surface was maximum. This result is in agreement with optical measurements by Elbaum et al. (1993) but is opposed to the results of optical ellipsometry (where liquid-like layer thickness is greater on the prismatic (10$\bar{1}$0) surface) and X-ray diffraction (where the difference between the (0001) and (10$\bar{1}$0) surfaces is negligible).

Maeno (1973) and Maeno and Nishimura (1978) found that an intense pumping out of water vapors from above the ice surface changes the surface conductivity considerably (Fig. 16). Pumping out of water vapors accelerates evaporation from the surface and its cooling. Aside from this trivial effect, a lowering of water vapor pressure above the ice increases the surface conductivity. The phenomenon discovered by Maeno shows the degree to which the conductivity of the surface layer is sensitive to physical conditions at the ice interface.

An interesting result was obtained in the work by Chrzanowski (1988), who investigated the d.c. conductivity of thin ice films deposited onto a high resistance dielectric substrate (high quality glass or quartz plate). Figure 17 demonstrates that the conductance of an ice film grows rapidly with the film's thickness until it thickens to 0.3–0.5 μm. Then, the rate of the conductance growth diminishes considerably. This result implies that the layer close to the ice/dielectric interface has a much larger specific conductivity than the bulk, and that the thickness of this layer is about 0.3–0.5 μm. This thickness (taking also into account the temperature of 220 K) exceeds considerably values found in other works. I believe that this quantity can be associated only with the screening length in ice, which was considered in detail by Petrenko and Ryzhkin (1984).

Caranti and Lamfri (1987) made a very interesting attempt to determine charge carrier mobilities in the ice surface layer. The authors used for this purpose measurements of the Hall effect and surface conductivity. Owing to the very small mobilities of charge carriers in ice, the measurements of the Hall effect are quite complicated. Caranti and Lamfri used an a.c. setup with two distinct frequencies of the magnetic field (50 Hz) and the driving current (107 Hz), measuring the Hall effect at the total frequency 157 Hz. Figure 18 shows the temperature dependence of the carrier mobilities in the ice surface determined by Caranti and Lamfri. An unusually large value of mobility (3×10^{-4} $m^2\,V^{-1}\,s^{-1}$) is striking. This is three orders of magnitude greater than the mobility of ions in water and ice and four orders greater than the mobility of Bjerrum defects in ice (Petrenko 1993). Moreover, such high mobility can not be attributed to

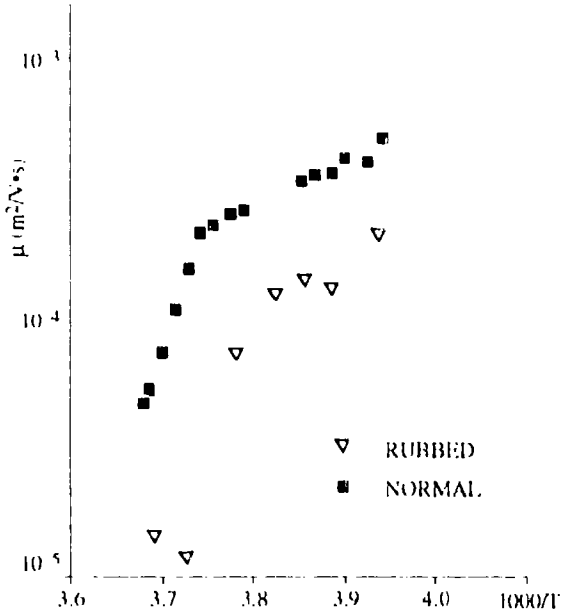

Figure 18. Hall mobility μ ($m^2 V^{-1} s^{-1}$) at 157 Hz as a function of temperature for normal and rubbed surfaces. The magnetic field B_0 was 0.38 T (after Caranti and Lamfri 1987).

Nonetheless, the result of Caranti and Zamfri is indirectly confirmed by earlier measurements of Bullemer and Riehl (1968), who tried to measure a bulk Hall effect in ice and obtained $\mu = 1.4 \times 10^{-4}\ m^2 V^{-1} s^{-1}$ at $T = -8°C$. Although Bullemer and Riehl used guard rings at the Hall electrodes to eliminate the effect of surface currents, they apparently did not succeed because they did observe the Hall effect, which is forbidden for bulk ice in principle (Sokoloff 1973, Gosar 1974). Hence, Bullemer and Riehl also determined the surface Hall mobility. It is remarkable that their result (although they used d.c. measurements) is in a good agreement with the Caranti and Lamfri result. Then, with what is this extremely high mobility associated? Perhaps with electrons in the ice surface? We do not know the answer.

Finally, Camp and Halchin (1979) studied the electrical properties of ice/ice (grain boundaries) and ice/quartz interfaces in the temperature range from 0 to –20°C and in the frequency range from d.c. to 10^7 Hz. They found that the widths of the "electrical" interfaces (ice/ice and ice/dielectric), estimated from the conductivity measurements, depend on the frequency. The higher the frequency, the thinner the surface layer in which the dielectric relaxation time is small enough for water molecules to be able to reorient. That is, the surface layer is not homogeneous: the charge carrier concentration is greater near the surface and decreases away from the surface into the bulk (see Table 3, which is a summary of results of Camp and Halchin).

Table 3. Summary of estimates of grain boundary thickness δ (after Camp and Halchin 1979). The measuring frequency is indicated in parentheses.

Sample	*Type of measurement*	*Effective grain boundary thickness*	
		–1°C	
Pure no. 2	From high frequency	δ (5×10^6) 100 Å (order of magnitude)	
Pure no. 3	From capacitance data	δ (10^6) 700 Å	
	From d.c. compared to doped ice	δ (d.c.) 2400 Å (order of magnitude)	
Pure no. 1	From capacitance data	δ (10^6) 1000 Å	
Doped	From capacitance data	–1°C	–14°C
		δ (10^6) 12 μm	3 μm
		δ (10^7) 5 μm	0.3 μm

ions at all. Even in the case of an activation-free diffusion motion of ions, their mobility cannot exceed the value

$$\mu = \frac{\nu e a^2}{k_B T} \qquad (16)$$

where ν = frequency of ion's hops between molecules
e = charge
a = length of a hop ($\approx 10^{-10}$ m).

To explain $\mu \approx 3 \times 10^{-4}\ m^2 V^{-1} s^{-1}$, we have to accept that $\nu \approx 10^{15}\ s^{-1}$, which is much greater than all possible phonon frequencies in ice (as well as in any other material).

SURFACE CHARGE AND SURFACE POTENTIAL

The study of the surface potential of ice and electric charges at the ice surface has quite a long history and continues to attract the attention of

numerous scholars. Such interest in the electrostatic properties of the surface of ice is stimulated by both fundamental problems associated with it and certain practical issues. Fundamental questions, which the study of the surface potential and the ice surface might help to resolve, include the issue of the structure of the surface of ice. For instance, if all the molecules at the ice surface are oriented "proton-outwards," as some theoretical models suggest (Fletcher 1968), this must lead to a positive charge at the surface λ_s and a positive potential of the ice surface φ_s. Both λ_s and φ_s are determined by the thickness of the surface layer d and the fraction of the oriented water molecules contained in this layer. Thus, measurement of λ_s and φ_s in conjunction with other data (d, for example) might provide valuable information on the microscopic structure and nature of the ice surface layer.

The practical issues stimulating the study of electrical properties of the ice surface, incorporate, first of all, the problem of atmospheric electricity (see details in Hobbs 1974) as well as the problem of adhesion and friction of ice and snow (Petrenko 1994).

Before we proceed to a review of experimental data, let us consider basic theoretical relationships defining the electrostatic properties of the ice surface and the most frequently employed experimental techniques used to determine of λ_s and φ_s.

Figure 19 shows schematically the distribution of the electric charge density ρ in ice near the surface ($x = 0$). The coordinate scale is chosen deliberately. First, since ice is a conductor, in equilibrium, the electric field within the bulk must be zero, i.e., $E(+\infty) = 0$. If we use the formula for the electric field strength above a charged surface

$$E = \frac{\lambda_s}{2\varepsilon_0} \tag{18}$$

we shall obtain an apparent result

$$E(+\infty) = \frac{1}{2\varepsilon_0}\int_0^{+\infty} \rho(x)dx = 0. \tag{19}$$

In other words, the sum of all charges in the surface layer of ice must be zero.

A very thin layer of the surface charge per se, with the density λ_{s0}, is composed of ions adsorbed by the surface from the air, electrons entrapped in the surface layer, etc. This layer is screened on the inner side by a much thicker layer of a space charge, composed of mobile charge carriers, i.e., predominantly Bjerrum defects and ions. Using Poisson's equation, we obtain

$$\frac{dE}{dx} = \frac{\rho(x)}{\varepsilon_0\varepsilon_\infty} \tag{20}$$

and as $d\varphi/dx = -E$, we can easily find the relationships between ρ, E and φ

$$E(x) = \int_0^x \frac{\rho(\xi)}{\varepsilon_0\varepsilon_\infty}\, d\xi; \quad \varphi(x) = -\int_0^x E(\xi)d\xi\ . \tag{21}$$

ε_∞ is high-frequency dielectric permittivity of ice.

To estimate a fraction of water molecules oriented along the electric field, i.e., with dipole moments oriented normally to the surface, we have to find the component of the polarization vector $\vec{P}$

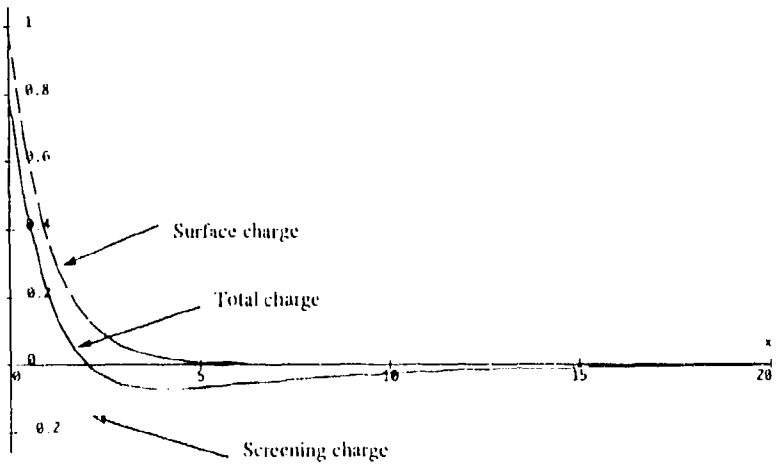

Figure 19. Space distribution of electric charges in ice near the surface. Scales are arbitrary.

that is determined by the reorientation of water molecules ($\vec{P}_M$)

$$\vec{P}_M = \vec{M}\left(\frac{n_\perp}{n_{H_2O}}\right) n_{H_2O} \tag{22}$$

where n_{H2O} and $n_\perp$ are water molecule concentration in ice and the concentration of water molecules oriented along the field respectively. Sin. e

$$\vec{P}_M = \varepsilon_0(\varepsilon_s - \varepsilon_\infty)\vec{E} = \left(\frac{\varepsilon_s - \varepsilon_\infty}{\varepsilon_\infty}\right)\int_0^x \rho(\xi)d\xi \tag{23}$$

then

$$\frac{n_\perp}{n_{H_2O}} = \frac{P_M}{M n_{H_2O}} = \left(\frac{\varepsilon_s - \varepsilon_\infty}{\varepsilon_\infty M n_{H_2O}}\right)\int_0^x \rho(\xi)d\xi. \tag{24}$$

Here, ε_s is the static dielectric permittivity of ice and M is the molecular dipole moment ($M \approx 8.66\times10^{-30}$ °C m [Hobbs 1974]).

This molecular "ordering" reaches its maximum at the surface where

$$\frac{n_\perp}{n_{H_2O}} = \frac{\varepsilon_s - \varepsilon_\infty}{\varepsilon_\infty M n_{H_2O}}\lambda_{sa} \tag{25}$$

$$\lambda_{sa} = \int_0^d \rho(\xi)d\xi. \tag{26}$$

Note that the fraction of ordered molecules in eq 25 depends only upon the density of charge λ_{sa} adsorbed by the ice surface. In other words, this result will still hold if, owing to the change of temperature or doping, the concentration of charge carriers changes, resulting in a change of the screening charge $\rho(x)$ in the bulk. Therefore, eq 25 provides a remarkable and simple way to study the ordering of water molecules in the surface layer through a measurement of the electric charge λ_{sa} adsorbed in a thin surface layer. The thickness of this layer is much less than the screening radius $æ^{-1}$.

Above we have considered the electric charge absorbed by the ice surface as a reason for the ordering orientation of water molecules. There can be an inverse phenomenon when an ordering of water molecules on the ice surface generates a surface charge. In its turn, the ordering of dipole moments of water molecules may be caused, for example, by dipole–dipole and dipole–quadrupole interactions (Fletcher 1968). Suppose this ordering is associated with polarization $P(x)$ that reaches its maximum at the surface and decays somehow to zero when $x\to\infty$ since the ice bulk is disordered. Then the surface charge λ_s associated with this polarization is

$$\lambda_s = \int_0^\infty \frac{\partial P}{\partial x}dx = \vec{P}x(0). \tag{27}$$

To find the other quantity that can be measured from an experiment, namely, the surface potential φ_s (using eq 21), we have to know how the charge $\rho(x)$ is distributed in ice; in other words, we have to know the laws of screening of an electric charge in ice. The screening of the charge λ_s will occur differently, depending on the ratio of the average thermal energy k_BT to the electrostatic energy of the charge carriers $|e_i\varphi_s|$. If the surface potential is small, so that

$$k_BT >> |e_i\varphi_s| \tag{28}$$

then in this case, as was shown by Petrenko and Ryzhkin (1984)

$$E(x) \cong \frac{\lambda_{sa}}{2\varepsilon_0\varepsilon_\infty}\exp(-æ_1 x) + \frac{\lambda_{sa}}{2\varepsilon_0\varepsilon_s}\exp(-æ_2 x) \tag{29}$$

where $æ_1^{-1}$ and $æ_2^{-1}$ are the two screening lengths determined by the major charge carriers (Bjerrum defects) and minor charge carriers (ions) respectively

$$æ_1^{-1} = \sqrt{\frac{\varepsilon_0\varepsilon_\infty k_BT}{e^2(n_3 + n_4)}} \tag{30}$$

$$æ_2^{-1} = \sqrt{\frac{e^2 k_BT}{e^2\Phi(n_1 + n_2)}} \tag{31}$$

$$\Phi \approx 3.85\, k_BT\, roo. \tag{32}$$

Since $\varepsilon_\infty << \varepsilon_s$, a large fraction of electric field (and potential) decays according to eq 29 at the distance $æ_1^{-1} << æ_2^{-1}$. This happens because of screening by major charge carriers. The rest of the potential decays at the characteristic length $æ_2^{-1}$, determined by minor charge carriers.

In the case of strong fields (large densities of the surface charge), when

$$k_BT << |e_i\varphi_s| \tag{33}$$

the screening is described by a system of nonlinear differential equations, which apparently does

not have an analytical solution. Petrenko and Maeno (1987) have found a solution by making an approximation that ignores the difference between fractional values of the electric charges of Bjerrum defects and ions. Assuming $e_3 = e_1 = q$, we obtained

$$E = \frac{\lambda_{sa}}{2\varepsilon_0 \varepsilon_\infty} \frac{1}{1 + x\text{æ}^{-1}} \tag{34}$$

where the screening length æ^{-1} now depends on λ_{sa}

$$\text{æ}^{-1} = \frac{4k_B T \varepsilon_0 \varepsilon_\infty}{q\,\lambda_{sa}}. \tag{35}$$

Equation 33 can be used in the subsurface region to a depth where the potential $|\varphi_s e_1|$ becomes comparable to $k_B T$. Further down, we should use eq 29.

Before proceeding to the discussion of experimental data, I shall point out an apparent relationship that exists between λ_{sa} and the component of the surface conductivity σ_s, which is determined by the layer λ_s of the screening charge of the protonic carriers. If in the bulk ($x = +\infty$), the charge carrier concentrations are denoted as $n_i(+\infty)$, then the corresponding values of concentrations at the surface will be

$$n_i(0) \cong n_i(+\infty) \exp\left(-\frac{e_i \varphi_i}{k_B T}\right). \tag{36}$$

In reality one of the four types of charge carriers always dominates, hence the high-frequency surface conductivity is given by

$$\sigma_s = \sum_{i=1}^{4} |e_i|\,\mu_i \int_0^{+\infty} n_i\,dx = |\lambda_s|\mu_i. \tag{37}$$

Petrenko (1994) and Petrenko and Colbeck (in press) studied an electrification arising from friction between metal and dielectric sliders on ice. Thin films rubbing against the surface of a rotating ice cylinder were used as sliders. The experiments were conducted in the –4.5 to –31.5°C temperature range and in the 0.5- to 8-m s^{-1} velocity range; the maximum pressure exerted on the ice by a slider was 1 kPa. In these experiments, we found that during sliding, the sliders pick up a significant positive charge from ice. In the case of metal sliders (stainless steel and aluminum), a large potential difference of 1600 V arises between the ice and the slider (velocity = 8 m/s, T = –31.5°C). When dielectric sliders were used (under the same conditions) strong electric fields $E = 2.1\times10^6$ V m^{-1} were produced at the ice/slider interface. From the meas-urements of the current I passing through an electrometer used as a current meter, we found that a coupled ice and slider acted as a charge generator. Thus

$$I = \frac{dQ}{dt} = \lambda_s \frac{ds}{ds} \tag{38}$$

where Q = electric charge
λ = surface charge density which the slider picks up from the ice surface
s = swept area
t = time.

Similar results were obtained in the course of field experiments on sliding of alpine skis on ice. The value of the electric charge density found is enormous: $\lambda_s = 1.6\times10^{-2}$ C m^{-2}. But even this value must be considered as the low limit for λ_s since, first, the slider is unlikely to pick up the entire charge; second, if the slider penetrated to some depth into the ice, some fraction of the unwanted screening charge can be entrapped along with λ_s.

It is interesting to make some estimates based on the value of λ_s that we found. First, such a high density of the surface charge corresponds to 0.01 electron charges per water molecule in the ice surface. Second, let us estimate the fraction of water molecules on the surface that are directed perpendicularly to the surface

$$\frac{n_\perp}{n_{H_2O}} = \frac{P(0)}{M}. \tag{39}$$

Substituting $\lambda_s = 1.6\times10^{-2}$ C m^{-2} into eq 27, we find from eq 39 that

$$\frac{n_\perp}{n_{H_2O}} = 0.2. \tag{40}$$

And remember this is the lower limit! It means that a significant fraction of water molecules at ice surface must be polarized.

Finally, using eq 37 to calculate the surface conductivity σ_s, we obtain

$$\sigma_s = 1.6\times10^{-2}\ \text{C m}^{-2}\ 1.8\times10^{-8}\ \text{m}^2\ \text{V}^{-1}\ \text{s}^{-1}$$

$$\approx 3\times10^{-10}\ \Omega^{-1} \tag{41}$$

where the value of the mobility of L-defects (which must be the major charge carriers screening a positively charged surface) at T = –10°C (Jaccard 1959) was used. The estimated value of σ_s found in eq 41 agrees in the order of magnitude to

experimental data at $T = -10°C$ (see Fig. 14 and 15). Although it seems unlikely that in such a way all properties of σ_s can be explained (the temperature dependence of μ_4 and σ_s is different, for instance), the conformity found is hardly purely incidental and implies that this process significantly contributes to the surface conductivity.

Buser and Jaccard (1978) studied a charge exchange between very small (10-μm) ice particles and various metal targets, doing the experiments at $T = -45°C$ and collision velocities of 10 m/s. They found that the amount and the sign of the charge transferred during a collision depended upon the work function of the metal target as well as the value and the sign of the external electric field, in which the particles were polarized prior to collision. To interpret their experimental results, Buser and Jaccard assumed the presence of electronic states at the ice surface in an analogy to semiconductors. These states participate in the electron exchange between ice and metal during a short (10^{-7} seconds, in the described experiments) collision. The lower limit of the density of electron surface states was found to be $\lambda_{sa}/e \geq 10^{16}$ m^2. If we assume that the amount of charge ΔQ that passes between the ice and the metal during the collision is proportional to the difference in their work functions ($W_i - W_m$), then W_i can be defined as the point of intersection with the horizontal axis on the graph of ΔQ versus W_m. In this manner, Buser and Jaccard found that $W_i = 4.3$ eV. A similar result was obtained in experiments of the same kind by Buser and Aufdermaur (1977). Caranti et al. (1985), who used the same method to determine the work function of ice, found a somewhat smaller value for W_i of 4.11±0.2 eV.

Another method used by many authors is Kelvin's method. Figure 20 illustrates the principle of measurement of the difference between a work function of the studied material (in our case W_i, the work function of ice) and that of an oscillating electrode W_m. In this method, ice (or another material) is connected electrically to the electrode that is oscillating above its surface. If $W_m \neq W_i$, electrons flow from the ice into the metal if $W_m > W_i$ or in the opposite direction if $W_m < W_i$, until the equilibrium potential difference $\Delta\varphi$ is established

$$\Delta\varphi\, e = W_m - W_i . \tag{42}$$

This potential difference produces an electric field in the space between the ice and the oscillating electrode, which forms a flat capacitor. When the electrode oscillates, the capacitance also oscillates, resulting in an alternating electric charge at the capacitor and an electric current in the circuit. At the voltage $V = -\Delta\varphi$, the magnitude of the current is minimal, which allows $W_m - W_i$ to be determined. To find the absolute value of W_i, we need to find W_m using some other method (from the extrinsic photo-effect, which has been done already for all pure metals, for instance). Kelvin's method was used to determine the work function of ice by Takahashi (1969a,b, 1970), Mazzeda et al. (1976), Caranti and Illingworth (1980, 1983a,b,c) and Caranti et al. (1985).

The approximate value of W_i found in these experiments appeared to be quite sensitive to such ambient conditions as humidity, temperature and, to a smaller degree, ice doping. A characteristic maximum value by which W_i was altered due to a change in the ambient conditions was $|\delta W_i| \leq 200$ meV. Thus, for example, Takahashi (1970) observed a buildup of a positive potential (30–80 mV) at the ice surface at the beginning of the condensation process. During further condensation, the surface potential changed its sign and reached a value of –250 mV. The effect was more pronounced at the basal (0001) plane as compared to the prismatic plane. Condensation and evaporation at the ice surface were produced through its heating or cooling, respectively; the ambient temperature was maintained constant.

The same author observed a negative potential buildup at the ice surface after its rubbing (Takahashi 1969b). This result is in qualitative agreement with the observations of Petrenko and Colbeck (in press), although we found a much larger effect.

Mazzeda et al. (1976) studied variance in W_i as a function of temperature. In these experiments, the ice surface was in equilibrium with the saturated vapor throughout the entire temperature range of 223–273 K; thus, the effect of condensation and evaporation should not have manifested. Figure 21 shows a typical temperature dependence of ΔW_{im}

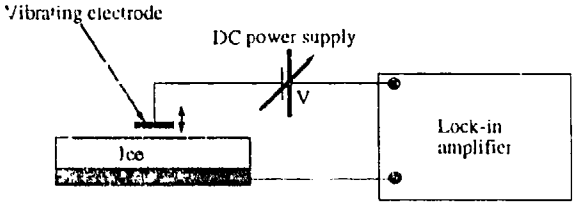

Figure 20. Kelvin's method.

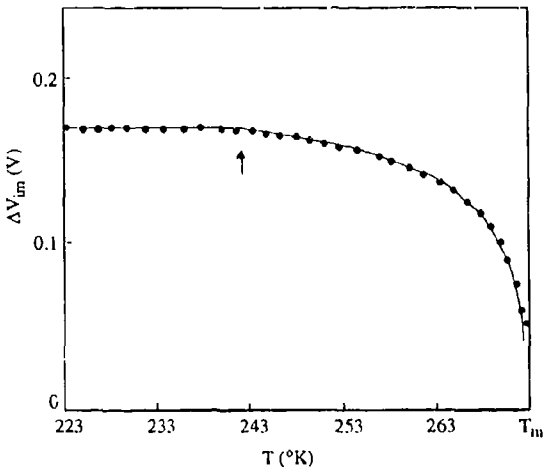

Figure 21. Temperature dependence of $\Delta W_{im} = 1/|e|\,(W_m - W_i)$ *(after Mazzeda et al. 1976).*

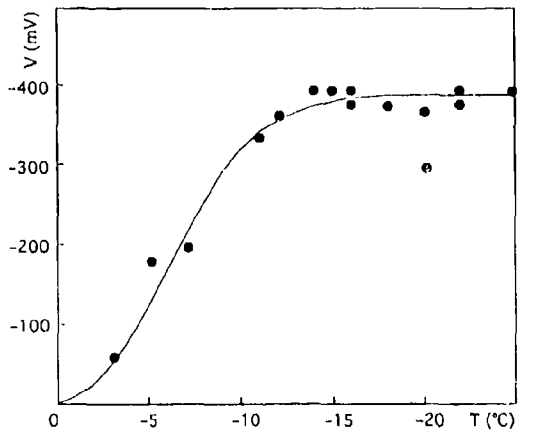

Figure 22. Change in ice surface potential when the surface was rimed with supercooled droplets (after Caranti and Illingworth 1983c).

$$\Delta W_{im} = \frac{1}{|e|}\,(W_m - W_i). \tag{43}$$

The arrow in Figure 21 indicates the temperature (≈ –30°C) at which there is a transition from a weak linear dependence to a stronger logarithmic dependence. The surface potential grew more positive relative to the bulk and reference electrode when it approached the melting point, which can be explained in terms of the formation of a double charge layer near the surface, as shown in Figure 19. Such charge distribution arises if the molecules at the surface are oriented oxygen-outwards, entrapping a positive compensating charge from the atmosphere.

Caranti and Illingworth (1980, 1983a,b,c) studied variations in the surface potential when the ice surface was rimed with supercooled droplets from an ultrasonic generator (of 50-μm radius; 1- to 2-g m^{-3} water content). A drastic change in the surface potential was observed (Fig. 22). The effect of doping by NH_3, NaCl and HF (up to concentrations of 10^{-2} M) on the amount of variation in potential was insignificant. The authors came to the conclusion that the variation in the surface potential of ice during its riming is a result of the disordered ice produced by rapid freezing of the supercooled water, since this change is proportional to the rate of freezing and relaxes with a time constant comparable to that of a mechanical relaxation.

SURFACE ELECTROCHEMICAL POTENTIAL

When the impurity concentration in ice varies from place to place, a static electric field arises from inhomogeneity in the distribution of impurities, which are the effective sources of protonic charge carriers in ice. As a result of this inhomogeneity of impurity concentration, a gradient of the charge carriers' concentrations n_i arises. The fluxes of ions and Bjerrum defects are correlated since they alter the orientation of the water molecule when they pass through it. The mathematical description of the general case, when both diffusive and drift fluxes of all four types of charge carriers must be taken into account, is quite complicated. Nevertheless, we can easily make rough estimations of the magnitude of the arising electric fields, using a simplified consideration.

Let us regard the case of one type of charge carrier of electric charge e_i and concentration n_i at a temperature T. If a diffusive flux j_D arises from inhomogeneous doping, in equilibrium it must be balanced by the opposite drift flux j_{DR}

$$j_D = j_{DR} \tag{44}$$

$$j_{DR} = \mu_i \times E;\ j_D = -D_i \times \mathrm{grad}(n_i). \tag{45}$$

Then, employing the Einstein relationship

$$D_i = \mu_i \times k_B T/e_i \tag{46}$$

we obtain for the electric field strength E

$$n_i \times E = (k_B T/e_i) \times \mathrm{grad}(n_i). \tag{47}$$

In eq 44–47, D_i, μ_i and e_i are the diffusion coefficient, the mobility and the electric charge of

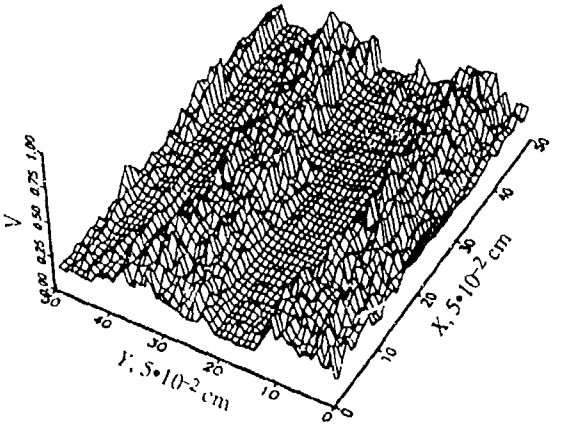

Figure 23. Static electric potential at the surface of freshwater columnar ice. An area of 2.5×2.5 cm² is shown. The columns lie along the x-axis. The potential is given in volts; T = –20°C *(from Petrenko 1992).*

the *i*th charge carrier respectively; k_B is Boltzman's constant. For the potential difference $\Delta\varphi$ between two points

$$\Delta\varphi = (\varphi_1 - \varphi_2) = (k_B T/e_i) \times \ln(n_{2i}/n_{1i}) \qquad (48)$$

where n_{1i} and n_{2i} are the concentration at points 1 and 2. Equation 48 gives $\Delta\varphi$ = 97 mV for Bjerrum defects (L- and D-defects) at T = 263 K and n_{2i}/n_{1i} = 10. A typical magnitude of the electric field associated with Bjerrum defects in ice is about 1–5 V/cm (see Fig. 23). Since $\Delta\varphi$ depends upon a ratio of impurity concentration, such an electric field exists even in very pure single crystals of ice.

I (Petrenko 1992) have studied electric potential on the surface of natural and artificial ice using a scanning microprobe connected to an electrometer (Fig. 24). The central element of the experimental setup is an X–Y pen recorder, in which a pen is replaced by a thin stainless steel electrode with a ball of 0.3 mm diameter at its end. A computer controls the position of the electrode scanning over a given area of an ice sample. Scanning was from 1×1 mm to 5×5 cm, with resolution better than or equal to ±0.5 mm. The pressure on the electrode was adjusted so finely that the electrode did not produce visible tracks on or damage to the ice surface. The velocity of the mobile electrode and the measuring time can be changed within a wide range, so that the electrode is able to measure a correct value of an electrochemical surface potential. I found that an electrode velocity of less than 10 mm s^{-1} and a measuring time longer than 10 ms were satisfactory. The potential was amplified by an electrometer preamplifier with input impedance $R_{input} \geq 10^{12}\,\Omega$ and then stored in the computer. The smooth surface of the ice samples was prepared using a microtome.

An example of the electric potential over the surface of freshwater columnar ice is shown in Figure 23. The ice columns lie along the *x*-axis. A comparison of the electric potential pattern with an optical image of the ice sample placed between two crossed polarizers reveals their similarity or even identity. In Figure 23 "rough" and "smooth" bands belong to different individual columns. The most significant gradient of potential, and hence electric field strength E = grad(φ), is located at or near grain boundaries. Generally, the distribution of the electric potential in ice follows the structural pattern of the ice: arrangement of grains, columns and boundaries between the regions of doped and normal ice.

Figure 25 depicts the electrical potential over the surface of a two-part ice sample. One part was grown from very pure deionized water and one was grown from water doped with 10^{18} molecules cm^{-3} of KOH. Those two halves, with ideal flat

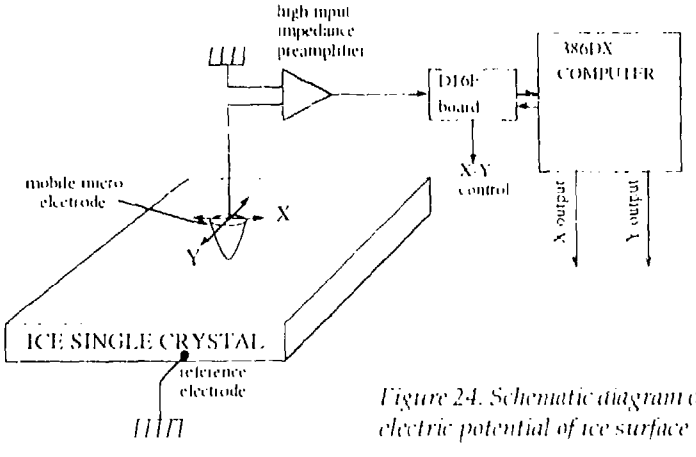

Figure 24. Schematic diagram of experimental setup for measurements of static electric potential of ice surface (from Petrenko 1992).

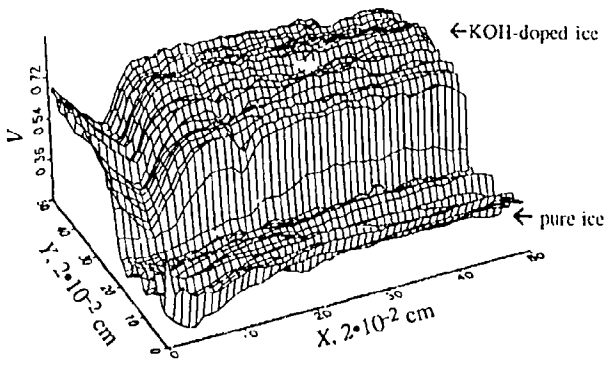

Figure 25. Electric potential on the surface of ice sample assembled of pure and KOH-doped ice. The steep step of the potential is located on the boundary between the pure and doped ice. A "ditch" seen in the potential of the doped (more positive) half corresponds to locations of grain boundaries. Dimension of the area shown is 1 × 1 cm; T = −19.5°C (from Petrenko 1992).

and smooth surfaces, were pressed together for 10 minutes at $T = -5°C$, so that they built a monolithic block. Doping ice with KOH provides negatively charged, extrinsic mobile defects: L-defects and OH^- ions (Howe and Whitworth 1989). Their diffusion into pure ice makes the pure part of the sample negatively charged and the doped part positively charged. That is precisely what we can see in Figure 25. At temperatures higher than approximately −15°C for pure ice and −22°C for saline ice, the existence of a conductive, quasi-liquid layer on the ice surface masks (or screens) the electric potential measured with this technique.

PHOTO-EMISSION OF ELECTRONS FROM THE ICE SURFACE

Nason and Fletcher (1975) studied photo-emission of electrons (extrinsic photo-effect) from the surface of ice and water. They found that the threshold of photo-emission for both ice near −10°C and water near 10°C is about 195±5 nm. This wavelength corresponds to the energy of 6.3 ±0.2 eV. The emission efficiency for liquid water was about half that for ice. Photo-emission from ice decreases steadily with decreasing temperature, apparently without any shift in the threshold value, and vanishes below approximately −160°C. This decrease of photo-emission with temperature was not related to the decrease of conductivity of ice, since the same temperature dependence of photo-emission was found for ice heavily doped with HF (5%). On the basis of similarity of photo-emissions from ice and water, the authors concluded that a quasi-liquid layer exists at the ice surface at temperatures $T >$ −160°C. Since the threshold is extremely sensitive to the value of the surface potential, its weak sensitivity to temperature variations implies, as the authors believe, that the electric structure (λ_{sa}, the screening length) of the surface layer of ice and water remains unchanged within the whole temperature range (−160 to 10°C). Nason and Fletcher believe that the most probable source of photo-electrons is the process of ionization of OH^- ions in the surface layer of ice and water. This hypothesis, obviously, contradicts the fact that a change in pH of ice from 1 to 14 does not affect photo-emission significantly.

At the present time, we can suggest an interpretation that is different. It is known that illuminating ice with light having a wavelength $\lambda \leq 190$ nm excites a bulk photo-conductivity according the following reaction

$$H_2O + h\nu \rightarrow H_2O^* \rightarrow H_2O^+ + e \qquad (49)$$

where H_2O^* denotes an excited water molecule (Khusnatdinov and Petrenko 1992). The electrons produced in this reaction can tunnel out of the ice, provided that its surface has a negative potential. Since the reaction (eq 49) begins with the excitation of a water molecule, it is not surprising that it is insensitive to the change in pH. The temperature dependence of photo-emission (as well as the difference in its values for ice and water) might result from the change in the surface electric field, since this field causes tunneling of electrons out of the subsurface layer of the ice.

SURFACE OPTICAL ABSORPTION IN INFRARED REGIONS

Interesting results about the molecular structure of the ice surface were obtained most recently from the study of infrared optical absorption spectra (Bush and Devlin 1991, Rowland and Devlin 1991, Callen et al. 1992, Devlin 1992, Nixon et al. 1992, Rowland et al. 1993). Those studies and the resulting implications were supported by computer simulations using molecular dynamics simulation methods (Bush and Devlin 1991).

The above-mentioned measurements are based on the possibility of distinguishing between lines in the IR spectra corresponding to the stretching and bending mode oscillations of non-saturated hydrogen bonds (i.e., dangling bonds) at the ice surface. The frequency of these oscilla-

tions appears to be extremely sensitive to the way in which a given water molecule is bonded to other molecules—by two or by three hydrogen bonds (2-coordinated or 3 coordinated water molecules). Molecules in the bulk are 4-coordinated. Therefore, a comparison between the intensities of 2-coordinated and 3-coordinated molecules allows us to estimate their relative concentrations. The IR absorption spectra observed in the experiments are better interpreted because of the high sensitivity of the eigen frequencies of dangling bond oscillations to the isotopic substitution of H with D. Moreover, these frequencies are quite sensitive to the process of adsorption of various gases. Thus, such measurements allow us to study ion adsorption by the ice surface at low temperatures.

Specimens of ice with large surface-to-volume ratios were produced either in the form of microscopic ice clusters suspended in gas or by vapor condensation onto a substrate, forming thin ice films. In experiments by Rowland et al. (1993), for example, crystalline ice clusters ~25 nm in diameter formed when mixtures of an inert carrier gas containing a small amount of water vapor, with a gas/H_2O ratio of ~200/1, were introduced rapidly into a cooled cluster cell to pressures of 33 kPa ($^1/_3$ bar) at temperatures below ~120 K. Increasing temperature and load pressures create larger clusters with consequently smaller surface-to-volume ratios and reduced relative surface-mode band strengths (Rowland et al. 1991).

Computer simulations using molecular dynamics methods have demonstrated that when water molecules collect to produce a small cluster, the following phenomena occur: 1) there are no molecules possessing two dangling OH bonds; 2) both 2- and 3-coordinated molecules form on the surface in approximately equal amounts, provided that the temperature is quite low (~20 K); and 3) in the annealed clusters, the 3-coordinated species are dominant. The concentration of dangling bonds is small (<< 1) even at these low temperatures. The results of spectral studies performed in the above works are in agreement with the results of computer simulations.

REGELATION (REFREEZING), SINTERING AND ADHESION

In retrospect, the studies of the quasi-liquid layer at the ice surface began with studies of thermo-mechanical effects: regelation, sintering and adhesion. The data on the physical parameters of the ice surface layer, obtained during those studies, are ambiguous and much less accurate than those obtained by modern methods. But we should keep in mind that, first, it was these phenomena that aroused such a great interest in the ice surface. Second, these phenomena are still of great practical importance. Therefore, a brief retrospective view of these studies is presented below.

Faraday (1850) observed an interesting phenomenon: if two pieces of ice are brought into slight contact at 0°C or a higher temperature, they freeze together. This discovery initiated a long and interesting argument between Faraday and Tyndall on one side and J. Thomson, his brother W. Thomson (Lord Kelvin) and Helmholtz on the other side. The Thomsons and Helmholtz held to the opinion that regelation is caused by melting under pressure in the contact zone between two pieces of ice. When the pressure is removed, water freezes again, bonding the pieces together. Faraday performed several simple but ingenious experiments that proved the erroneousness of the Thomsons' hypothesis, suggesting a regelation mechanism that is very close to the modern concept of this process. He assumed that at temperatures close to the melting point, a thin liquid film always exists at the ice surface. When two blocks of ice touch, this film first forms a "neck" connecting the two blocks. Then, since the inner part of the neck gradually turns into a bulk region of ice, it freezes, forming a solid joint between the two.

Nakaya and Matsumoto (1953) did some experimental work to verify the existence of the liquid-like layer at the ice surface. They suspended small spheres of ice (from 1.5 to 4 mm in diameter), prepared from distilled water, on cotton threads in a pendulum-like fashion. One of these pendulums was moved laterally, bringing the spheres in contact with a very small force, estimated by the authors to be less than 0.01 dyn. Then, the suspension point of one of the spheres was displaced laterally until the spheres broke free; the force can be calculated from the value of the angle ϑ (with respect to the vertical) at which they separated. Nakaya and Matsumoto also tested ice spheres containing 0.1% NaCl. In this case we would expect a thicker film on the ice surface. To explain their results, the authors had to assume that a transitional liquid-like layer exists at the ice surface at temperatures below 0°C.

Hosler et al. (1957) did similar but more accurately controlled experiments in a temperature

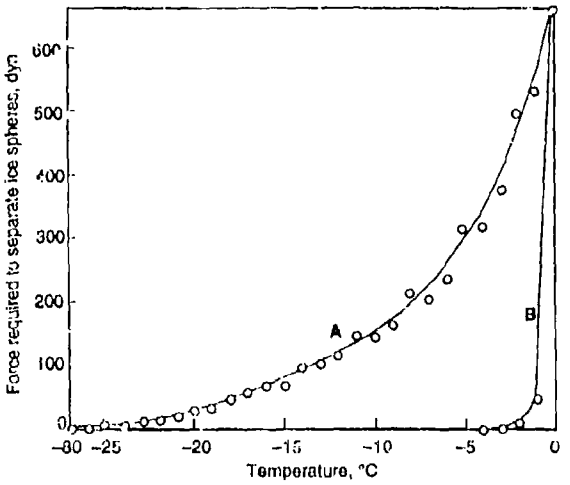

Figure 26. Separation force as a function of temperature: A—water-vapor saturated atmosphere; B—dry atmosphere (after Hosler et al. 1957).

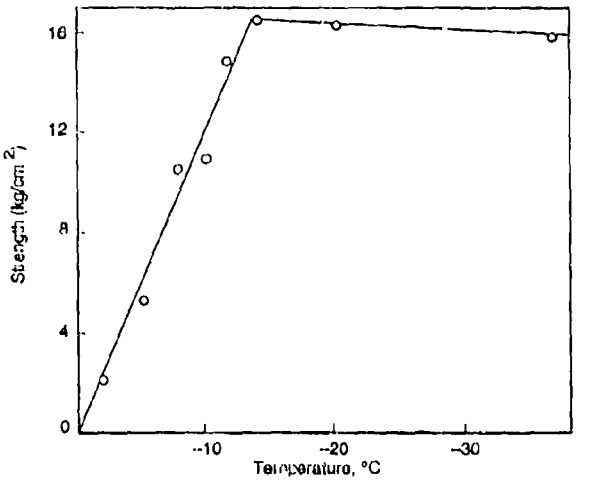

Figure 27. Strength as a function of temperature for snow–ice sandwiched between stainless steel disks, obtained by shear. Cross-sectional area 1.54 cm²; height 0.2 to 0.4 cm. Adhesive breaks at T > –13°C and cohesive breaks at T < –13°C. Each point represents an average of at least 12 tests (after Jellinek 1959).

range from –80 to 0°C in both dry and water-saturated atmospheres. Between –80 and –40°C, they observed no adhesion between spheres (Fig. 26). The lowest temperature at which adhesion was measurable in a saturated atmosphere was about –25°C, whereas in a dry atmosphere the adhesion practically ceased at –3°C. They explained this difference in terms of a rapid evaporation of the liquid-like layer from the ice surface in a dry air, which makes it very thin. Hosler et al. also found that the temperature dependence of the force at which separation occurs can be expressed in terms of a Boltzmann equation with the activation energy of 0.46 eV.

Jellinek (1957a,b; 1959; 1960; 1962), investigating the adhesive properties of ice, conducted shear and tensile experiments with ice frozen onto stainless steel and optical flat quartz plates and various polymers. In his tensile experiments, only cohesive breaks through ice were observed. Shear tests resulted in adhesive breaks along the interface, the strength of which depended on the loading rate, surface polishing, temperature and the type of the material used. A temperature dependence of the shear strength for the case of ice–snow confined between stainless steel disks is shown in Figure 27.

If we assume that the shear strength in shear-type experiments at temperatures above –13°C is determined by viscous flow of the quasi-liquid layer, then

$$\frac{d\sigma_{st}}{dv} = \frac{\eta}{L} \qquad (50)$$

where η and L are film viscosity and thickness respectively. The ratio of η/L found by Jellinek at $T = -4.5$°C was 6.99×10^4 N s/m for ice–stainless steel and 1.5×10^4 N s/m for ice–quartz. In eq 50 we have two unknowns, η and L. If the value of $L = 2.7\times10^{-9}$ m, found by Barer et al. (1977) at $T = -4$°C (see Table 1), is used, then the resulting viscosity of the quasi-liquid layer between ice and quartz will be η = 0.41 Pa s, as compared to 0.017 Pa s found by Barer et al. at even lower temperatures.

Raraty and Taber (1958) did some adhesion experiments. Their results are essentially in agreement with those of Jellinek.

A large number of experimental and theoretical works dealt with the issue of sintering of ice. Sintering plays a major role in the process of snow densification, which transforms falling snow into ice in mountain glaciers and the polar caps of Greenland and Antarctica. Several physical phenomena, such as surface and bulk diffusion, surface tension, plastic deformation and water transfer through water vapor, contribute to the sintering. The relative effect of each of the mechanisms above depends largely on conditions during sintering: temperature, humidity, impurity composition and size of ice particles. Because of this, interpreting the data on ice sintering is usually very difficult. The phenomena of small particle migra-

tion (Itagaki 1967a) on the ice surface and regelation are also similar to sintering. Studies of these things, although contributing significantly to the development of practical applications, were of little use for the determination of the fundamental parameters of the ice surface layer owing to difficulties in interpretation. As examples of excellent studies on ice sintering, I can recommend to interested readers the following papers: Kingery (1960), Hobbs and Mason (19641), Itagaki (1967c) and Maeno and Ebinuma (1983).

ADSORPTION OF GASES ON THE ICE SURFACE

When gas molecules of a mass m strike a solid surface, they can either bounce or get stuck to the surface (be entrapped) for a certain time. The latter case is called an adsorption of the molecule. If the gas molecules are in thermal equilibrium with the solid surface, the equilibrium surface concentration C_s of adsorbed molecules will depend on the flux of oncoming molecules, i.e., on the gas pressure P and temperature T and on the average time that a molecule spends on the surface.

Langmuir (1916) assumed that the maximum concentration of the adsorbed molecules C_M corresponds merely to a mono-molecular layer. Therefore, a molecule coming from a gas and colliding with an already adsorbed molecule must instantly bounce off the surface. On the basis of this assumption, simple kinetic considerations lead to the so-called Langmuir's adsorption isotherm

$$\frac{V_s}{V_M} = \frac{k_1 P}{1 + k_1 P} \tag{51}$$

where V_s is the actual volume of the adsorbed gas (which corresponds to C_s) and V_M (which corresponds to C_M) is the volume of the adsorbed gas when the entire adsorbent surface is covered with a monolayer.

$$k_1 = \frac{1}{(2\pi m k_B T)^{1/2}} \frac{\tau_a}{C_M} . \tag{52}$$

Brunauer et al. (1938) extended the result of Langmuir to the case of multilayer adsorption. This equation is known as a BET equation. They found that

$$\frac{P}{V_s(P - P_0)} = \frac{1}{V_M k_2} + \frac{(k_2 - 1)P}{V_M k_2 P_0} \tag{53}$$

where

$$k_2 = \exp\left(\frac{E_a - E_a'}{k_B T}\right). \tag{54}$$

E_a and E_a' are the heats of adsorption (i.e., the amounts of heat liberated when a molecule is adsorbed) corresponding to the first and all succeeding layers; P_0 is the saturation pressure of a gas over a plane surface at temperature T.

As we can see from eq 53, a plot of $P/V_s(P - P_0)$ versus P/P_0 must be a straight line with a slope of $(k_2 - 1)/V_M k_2$ and an intercept with a horizontal axis of $1/V_M k_2$. In this way constants V_M and k_2 can be determined; then, the surface area of the solid can be calculated. We can also find E_a, provided that the value of E_a' is known (it is usually taken to be equal to the latent heat of evaporation of the adsorbate in a liquid form). Readers interested in the theories of adsorption can find them in the book by Steele (1974), for example.

Experimental studies of gas adsorption on the ice surface are of a great practical importance for the physics of the atmosphere, meteorology, climatology and astrophysics. In addition, such studies contribute to the understanding of the ice surface structure, since adsorption is quite sensitive to both surface structure and the presence of various defects at the surface, as well as to the local fields (from the molecular dipoles, for instance) existing near the surface.

Gas adsorption by ice has been studied in a wide temperature range: from 77 to 273 K. The adsorption of gaseous nitrogen was studied by Adamson et al. (1967), Ocampo and Klinger (1983a) and Schmitt et al. (1987); the adsorption of CO_2 was studied by Ocampo and Klinger (1983); the adsorption of hydrogen was examined by Smoluchowski (1983; theoretical study); and Orem and Adamson (1969) studied the adsorption of nonpolar hydrocarbon vapors (n-alkanes). In these experiments, the surfaces of amorphous, cubical and hexagonal ice, cleaved at 77 K and annealed at higher temperatures, and natural snow were investigated.

Cubic ice, produced by the direct condensation of water vapor onto the walls of a vessel at a liquid nitrogen temperature, has the maximum net surface (11.8 m^2/g; [Adamson et al. 1967]). This surface was reduced after the ice had been annealed, and was about 1 m^2/g in the case of natural snow. The value of the adsorption heat found exceeds the heat of evaporation: 2700±20 J mol^{-1} at 77 K for the adsorption of N_2 reported by Schmitt et al. (1987); a similar value of 2512±250 J/mol was reported by Adamson et al. (1967). The adsorption heat is gen-

erally reduced after annealing (down to 1067 J mol^{-1} after 4 days [Ocampo and Klinger 1983a]).

The results of studies performed by Orem and Adamson (1969) showed that there exists a significant difference in the character of adsorbent–adsorbate interaction above and below –35°C. Between –35 and –196°C, ice acts as a low-energy adsorbent and the adsorption energy is associated with dispersion interactions, with no effect of local dipole fields. However, at temperatures above –35°C, the ice surface acquires an adsorption capability close to that of a water surface. These observations conform to the model of a quasi-liquid film at the ice surface. A similar temperature transformation in the adsorption process, but at a lower temperature (-40°C), was also noted by Ocampo and Klinger (1983a). They also found a considerable decrease in the entropy of the adsorbed gas at $T > -40$°C. Such an entropy decrease could be explained in terms of the ordering of adsorbate molecules in a strong electric field of ordered water molecules at the ice surface. As we have seen previously, this also conforms to the model of the quasi-liquid layer.

SURFACE ENERGY

A net surface free energy or simply surface energy is defined as the work required to increase the interface area by a unit area (at a constant temperature). We shall need, for a theoretical analysis, the energies of the interfaces between solid ice (S), liquid phase (L) and water vapor (V). We denote them as γ_{SL}, γ_{VS} and γ_{VL} for solid/liquid, vapor/solid and vapor/liquid interfaces respectively. All of these quantities are temperature dependent; it does not make sense to give a value to γ without indicating the temperature. The best known quantity is the most easily measured, γ_{VL}, which can be determined by a variety of experimental techniques based on the measurement of the surface tension of water. (These techniques include measurement of the height of water rise in a capillary and measurement of the wavelength of surface waves, excited by an ultrasonic generator, for example.) At the melting temperature, $\gamma_{VL} \approx 75.7$ mJ m^{-2} and increases with increasing temperature. The two other energies γ_{SL} and γ_{VS} cannot be measured quite so easily, and to determine them a certain ingenuity is required.

We shall not describe here the early and less accurate works, and shall proceed to an interesting technique suggested by Ketcham and Hobbs (1969). That technique was also used later by Hardy (1977). The technique is based on the measurement of equilibrium angles at the interfaces between two ice seeds and water vapor or water (Fig. 28). As can be seen from this figure, the triple junction in a grain-boundary groove is subjected to three forces of surface tension. Therefore, for equilibrium, the following conditions must be satisfied

$$\gamma_{gb} = 2\gamma_{VS}\cos(\vartheta_{VS}/2) \qquad (55)$$

$$\gamma_{gb} = 2\gamma_{LS}\cos(\vartheta_{LS}/2)\,. \qquad (56)$$

Since there are three unknowns γ_{gb}, γ_{LS} and γ_{VS}, we need a third equation in addition to eq 52 and 53. This equation can be the condition of equilibrium among vapor, liquid and ice in the case of incomplete wetting ($0 < \phi < \pi$). In this case

$$\gamma_{VS} = \gamma_{LS} + \gamma_{VL}\cos\phi\,. \qquad (57)$$

Using this technique for determination of the surface energies, Ketcham and Hobbs (1969) found that at 0°C

$$\gamma_{VS} = (109 \pm 3)\ \text{mJ m}^{-2}$$

$$\gamma_{LS} = (33 \pm 3)\ \text{mJ m}^{-2} \qquad (58)$$

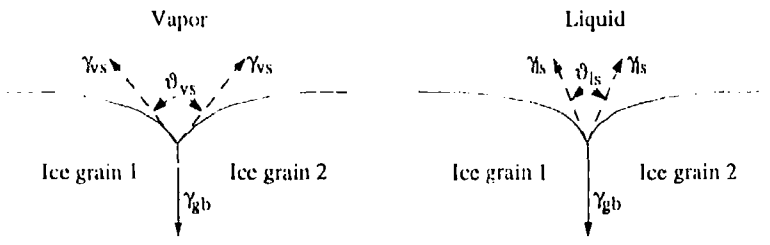

a. Vapor/solid interface. *b. Solid/liquid interface.*

Figure 28. Schematic of grain-boundary grooves (after Ketcham and Hobbs 1969).

$$\gamma_{gb} = (65 \pm 3)\ \text{mJ m}^{-2}.$$

The reader can find the data on the values of the angle ϕ in the papers by Knight (1966, 1971). Ketcham and Hobbs also calculated that the anisotropy of γ_{VS} and γ_{LS} with respect to orientation is probably small and falls within the experimental error. The value of γ_{gb} depends, of course, on the grain boundary type and must tend to zero as the angle of misorientation between the seeds tends to zero. Hardy (1977) using a similar technique, found in the case of water/ice interface a more exact value

$$\gamma_{LS} = (29.1 \pm 0.8)\ \text{mJ m}^{-2}. \qquad (59)$$

Recently, Makkonen (in press) concluded from results of measurements of ϕ (37°) that $\gamma_{LS} = 77$ mJ m^{-2} for ice at -25°C.

Finally, Kuroda and Lacmann (1982), from the number of broken bonds at the ice surface and the value of heat of sublimation of 8.5×10^{-20} J molecule^{-1}, estimated γ_{VS} on the basal (0001) and prismatic (1010) faces to be

$$\gamma_{VS}\,(0001) = 121\ \text{mJ m}^{-2}$$

$$\gamma_{VS}\,(1010) = 128\ \text{mJ m}^{-2}. \qquad (60)$$

SUMMARY OF MAIN EXPERIMENTAL RESULTS

Before we proceed to the review of theoretical models developed to explain the structure and physical properties of the ice surface, let us summarize the major experimental results so that we have a starting point for comparing them with theories. The reader undoubtedly already anticipates the difficulty of that task. The range of discrepancies in the results of different authors is too large, especially when different experimental techniques are used.

Nonetheless, let us try to establish the facts that either conform to the majority of results or to the most reliable of them. I shall also try to point out major discrepancies.

All results can be classified into several issues:

1. The presence or absence at the ice surface of a special layer, which has physical properties different from those of the bulk ice.
2. The layer thickness and its temperature domain of existence.
3. The molecular structure of this layer.
4. A comparison between measured properties of the ice surface layer (diffusion, electric conductivity, refraction coefficient, etc.) and those of water and ice.

After this is done, we shall see whether it is possible to assemble some consistent picture of the ice surface layer.

Existence of a special layer

The greatest consistency is achieved here. Experimental papers published over the past 20 years never address the question of the existence of the special layer. All authors admit to its existence. Let us join them, keeping in mind an impressive listing of experimental evidence considered above.

Thickness of the layer and the domain of its existence

Since in all cases, a strong temperature dependence of the surface properties was observed, we cannot discuss the question of the layer thickness without referring to its temperature dependence.

Figure 29 attempts to summarize all the measurements of the thickness of the surface ice layer. In those cases when a temperature dependence of some property of this layer (e.g., surface conductivity) rather than the absolute thickness was measured, this temperature dependence, normalized by the value at some temperature T_0, is plotted.

At first glance, the results presented in Figure 29 are awesome, so great are the discrepancies.

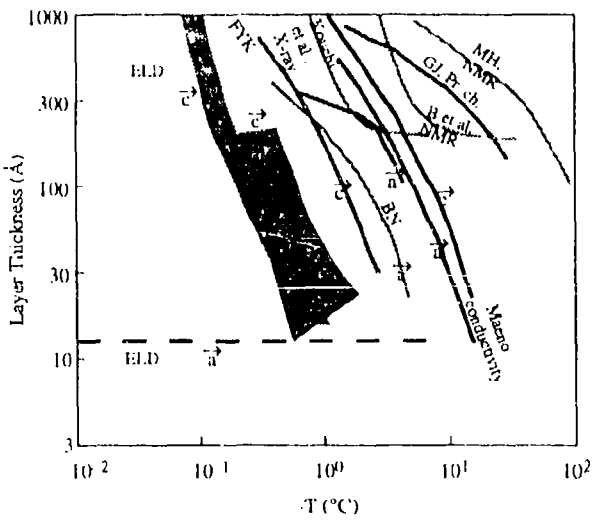

Figure 29. Temperature dependencies of quasi-liquid layer thickness taken from the papers cited in this review. Capital letters at the curves stand for first letters of the authors' names.

Thus, the layer thicknesses found by different authors differ by one to two orders of magnitude (at –10°C, $L \approx 10$ Å [Elbaum et al. 1993] and $L \approx 1000$ Å [Golecki and Jaccard 1978], for instance).

The width of the temperature domain of existence also differs by two orders of magnitude ($\Delta T \approx 1$°C [Elbaum et al. 1993] and $\Delta T \geq 100$°C [Mizuno and Hanafusa 1987]). Taking into account the thoroughness of the measurements and control of the conditions in these experiments, I feel that it is most unlikely that the described discrepancies are attributable to errors in measurement or some other error. On the contrary, I believe that all measurements were correct, but absolutely different layers on the surface of the same ice I_h were measured. In other words, the surface layer must consist of several layers, each possessing specific physical properties, different from that of the bulk.

In fact, optical investigations, based on the measurement of intensity of the light reflected from the surface, are sensitive to the molecular density of the layer. Such investigations indicate the presence of an optically dense film at the ice surface in the temperature range from 0 to approximately –4 to –5°C. The refractive index of this film $n = 1.330$, determined by Furukawa et al. (1987a,b), is very close to the refractive index of water at 0°C $n = 1.333$.

The thickness of this thinnest, "external" dense film depends not only on the temperature, but also on the type of crystallographic face, as well on the presence or an absence of air (Elbaum et al. 1993). In approximately the same temperature interval (–2.5 to 0°C), Kouchi et al. (1987) observed by means of X-ray diffraction a film with no long-range order, which is characteristic of a liquid phase.

Thus, we can conclude that in the temperature range from 0°C to "minus several degrees Celsius," a film similar in structure and density to water exists on the surface of pure ice.

A layer with increased conductivity can be detected at the ice surface at much lower temperatures (–25 to –35°C). Its maximum thickness is limited by the value of the screening length. An idea of the latter can be obtained from the work by Chrzanowski (1988): $L \cong 0.5$ μm at $T = -53$°C. Charge carrier concentration and conductivity increase within this layer as they approach the surface. Estimates made in the section on the surface charge and the surface potential indicate that the concentration of ions and Bjerrum defects near the surface can reach a value comparable to the molecular concentration (see eq 14 and 15). Such a large concentration of defects itself can be sufficient reason for a disordering of the structure.

A layer with an abnormally large amplitude of thermal vibrations is observed at even lower temperatures (≈ –50°C [Golecki and Jaccard 1978]). The thickness of this layer at $T \approx -1$°C reaches the value of 1000 Å.

Even larger is the temperature domain ($T \geq -100$°C) of a layer detected by means of NMR (Mizuno and Hanafusa 1987). This layer can be characterized as having a spin-lattice interaction different from that of the bulk, or as a layer with increased self-diffusion coefficient and rate of molecule reorientation. The thickness of this layer at the ice/Aerosil interface is 11 Å at $T = -12$°C (Barer et al. 1977).

Molecular structure of the layer

We have several sources of information about the surface layer structure. First, as was shown by Kouchi et al. (1987), in the temperature interval 0 to –2.5°C, there is no long-range order at the ice surface, which is characteristic of liquids. The disordering probably remains at lower temperatures, but the technique used does not have the necessary sensitivity to detect this. An interesting fact is that the thickness of the "liquid" layer, which is measured by X-ray diffraction, appears to be the same for (0001) and (01$\bar{1}$0) surfaces, which contradicts ellipsometrical measurements. Therefore, we cannot rule out the possibility that in these investigations different layers were observed.

Golecki and Jaccard (1977, 1978), who used a proton channeling technique, observed the presence of a disordered layer down to –50°C. This layer, with a thickness of about 1000 Å at –1°C, was interpreted as having much greater amplitude of the thermal vibrations of oxygen atoms rather than having an amorphous structure.

Additional indirect evidence of the disordering in the ice surface layer comes, as we have seen in the section on surface conductivity, from a comparison of NMR data with the data on the values of the concentrations and the mobilities of charge carriers (see eq 11–14). We found that the concentration of defective hydrogen bonds (Bjerrum defects) equals 2×10^{28} m^{-3} and is comparable to the molecular concentration of 3×10^{28} m^{-3}. Obviously, in this case it is impossible to preserve an ordered structure interconnected by hydrogen bonds corresponding to ice I_h. Moreover, since the activation energy of the L-defect mobility

(0.23 eV) is close to that of $\tau^{-1} \propto \sigma_{ss}$ (0.29 eV, Fig. 9), then according to eq 11 such high Bjerrum defect concentration and consequent inevitable disordering will persist down to very low temperatures (–60°C). We should keep in mind, however, that since the amplitude of the NMR signal decreases with decreasing temperature, the thickness of this layer must also decrease. Finally, let us remember that the results of experiments on the surface charge density and gas adsorption imply that a fraction of water molecules in the subsurface layer (at least within a single monomolecular layer) must have their dipole moments oriented normally to the surface. Such orientation is also an ordering of some kind.

Physical properties of the surface layer as compared with water and ice

As we discussed earlier, certain physical properties of the surface ice layer are intermediate between water and ice. This holds for viscosity and self-diffusion coefficient, for instance. But there are two remarkable exceptions to this rule. First, the optical density of the quasi-liquid film practically coincides with that of water at 0°C. Second, the net electric conductivity of the ice surface exceeds by many orders of magnitude the electric conductivities of both ice and water and corresponds to the upper boundary of conductivity of superionic materials.

PART II. THEORETICAL MODELS OF THE ICE SURFACE

We have seen in Part I how complicated the structure of the ice surface is and what diverse physical properties it possesses. It is clear, therefore, how difficult it is to create a theoretical model describing such physical objects as the surface layer of ice, and nobody has yet been able to devise one. Theoretical models do exist, although there are very few, that in the best case can describe satisfactorily only one of the phenomena associated with the ice surface in a limited temperature range. However, probably all the physical reasons that make the ice surface as it is were analyzed in these works. Therefore, it seems reasonable, in spite of a very limited application of existing theories, to consider and discuss them briefly.

The most simple and clear is the phenomenological model based on the idea of a possible gain in the free energy of the ice/vapor interface resulting from the formation of a liquid film on the ice surface. Obviously, this is possible only if

$$\gamma_{VS} > \gamma_{LS} + \gamma_{VL}. \tag{61}$$

Within the framework of this theory, the surface layer of ice is considered to be simple, ordinary water. If we denote the change in the Gibbs free energy per unit area resulting from melting as ΔG, obviously in thermodynamical equilibrium

$$\left(\frac{\partial \Delta G}{\partial d}\right)_T = \rho_L \Delta\mu(d) = 0 \tag{62}$$

where μ is the chemical potential, ρ_L is the water density and d is the water film thickness. The water film thickness d enters into ΔG twice

$$\Delta G = (\rho_L S_L \Delta T)\, d + \Delta\gamma(d) \tag{63}$$

where $\Delta T = T_m - T$, S_L is the entropy of fusion per unit mass and $\Delta\gamma$ is the change in the free energy of the surfaces

$$\Delta\gamma(d) = \gamma_{VL} + \gamma_{SL} - \gamma_{VS}. \tag{64}$$

$\Delta\gamma$ depends on the film's thickness implicitly because, at thickness values comparable to the interatomic distances, two interfaces begin to "sense" the presence of each other. Usually, it is assumed that

$$\Delta\gamma(d) = \Delta\gamma(\infty)\left[1 - \left(\frac{r_0}{d}\right)^2\right] \tag{65}$$

where r_0 is a constant on the order of interatomic distance (see for example Dash [1991] and Takagi [1990]). A solution of the system of eq 62–65 gives for the water film thickness

$$d = \left(\frac{2 r_0^2\, \Delta\gamma(\infty)}{\rho_L S_L (T_m - T)}\right)^{1/3}. \tag{66}$$

The reader can find examples of these calculations in the paper by Dash (1991), who also considered an ice/solid interface and took into account a small correction due to thermomolecular pressure acting on the melted layer; also in the paper by Takagi (1990), who incorporated corrections due to surface curvature. Figure 30 shows the results of such a calculation.

Fukuta (1987) and Makkonen (in press) suggested that the surface can melt because of the pressure applied to the subsurface layer by the bulk. The nature of this pressure becomes clear if we recall that a molecule on the surface is subjected to the attraction forces from the rest of the molecules and the net force is directed inside the crystal. Since the pressure lowers the melting temperature of ice, the surface melts. Fukuta, analyzing the intermolecular forces and using the dependence $T_m(P)$, valid for microscopic quantities of water and ice, estimated the thickness of the liquid film as

$$d = \frac{1.5\ \text{nm}}{\sqrt{T_m - T}}. \tag{67}$$

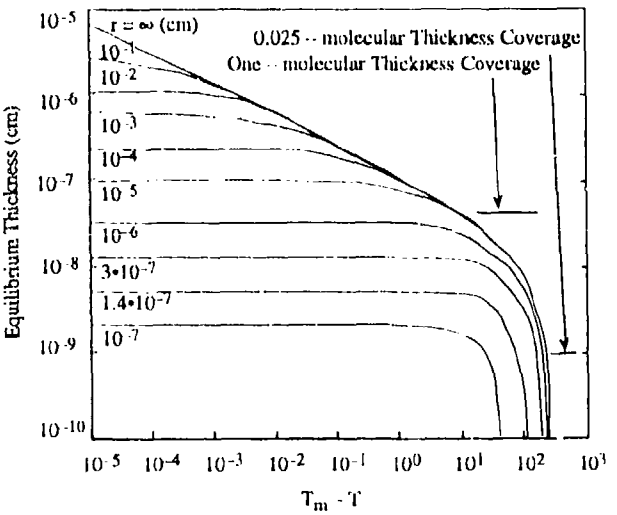

Figure 30. Calculated temperature dependence of a thickness of liquid film on an ice surface (after Takagi 1990).

Makkonen (in press), who found experimentally that eq 61 is not valid, predicted

$$d = \frac{3.5 \text{ nm } °C}{(T_m - T)} . \quad (68)$$

Within the context of Fukuta's model, the liquid film must vanish at temperatures $T < -22°C$, where the pressure just transforms ice I_h into its high pressure forms (I_{II}, I_{III} and I_{IX}) rather than into liquid.

Thus, the models just described could have been applied to the optical observations of a dense liquid film on the ice surface close to the melting point, although the estimation using eq 67 gives a much thinner thickness compared to experimental data (for example at $T = -1°C$; see Fig. 29). In addition, these phenomenological models can give nothing more in terms of properties of the liquid film than the properties of ordinary water. And these properties do not coincide at all with the properties of the liquid-like layer of ice, as we have seen previously (electrical conductivity and self-diffusion coefficient, for instance).

During a rather long period, a model proposed by Fletcher has attracted (and still continues to attract) considerable attention (see Fletcher 1962, 1963, 1968). (Note that Fletcher recently returned to the problem of the ice surface structure at much lower temperatures [see Fletcher 1992].) The key idea in Fletcher's (1968) model is the assumption that, at the ice surface, a significant fraction of molecules (denoted as α_0) is oriented with their dipole moments (i.e., protons) pointing outwards, as opposed to the bulk where molecules are oriented randomly. This would result in a large buildup of positive polarization charge at the surface. Fletcher came to his conclusion about molecule orientational ordering by analyzing the interaction between dipole and quadrupole moments of water molecules close to the surface. Fletcher estimated the energy of this interaction as 10^{-20} J per molecule, which exceeds an average thermal energy $k_B T \approx 4 \times 10^{-21}$ J.

As we have seen in the section on surface charge and surface potential, a positive electric charge of a high density, which is unambiguously related to the water molecule dipole ordering, was indeed discovered on the ice surface.

All other predictions of Fletcher's model are consequences of the molecule ordering in the surface layer. In fact, since in the bulk there is no ordering ($\alpha_0 = 1/2$), between the surface and the bulk, there should be a transitional layer with a large concentration of defective hydrogen bonds allowing molecules to reorient. This transitional disordered layer, according to Fletcher, is the liquid-like layer. Fletcher finds the equilibrium thickness of this layer thermodynamically by minimizing the Gibbs free energy of the surface and incorporating the following components of this energy: the energy associated with the surface orientation of the layer; the energy associated with the interaction of the molecular quadrupoles with the gradient of the electric field; the interaction of molecular dipoles with the total electric field; and the interfacial energy between the liquid-like layer and the ice. In addition, a "volume" reduction in G because of the melting of the layer and a lowering of the entropy because of molecule orientation are apparently also considered. An unknown fitting parameter of the theory is ε_2, the energy required to form an L-defect in the liquid-like layer. Finally, Fletcher minimizes the free energy G as a function of α_0 and the layer thickness d. I deliberately do not present the mathematical details of Fletcher's calculation because it is quite cumbersome and, more importantly, might be made more accurate in the future. Nevertheless, Fletcher's analysis of the problem and the insight that he has achieved into the physical nature of the layer are absolutely remarkable. Let us note also that within the context of this model, an unusually high electrical conductivity of the surface layer has an obvious explanation: it is ascribable to a high concentration of L-defects in the liquid-like layer. Figure 31

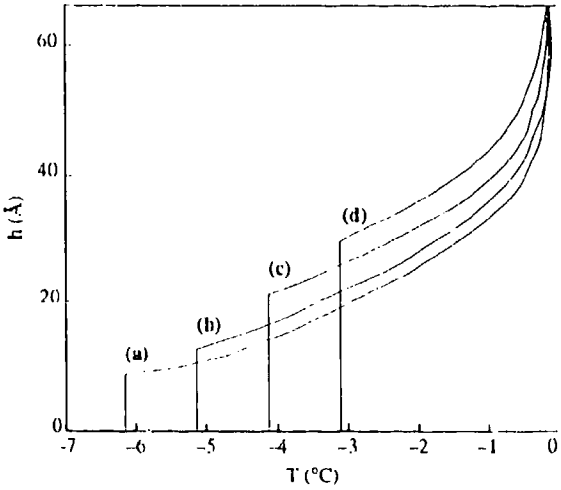

Figure 31. Calculated dependence of the equilibrium thickness, L, of the liquid-like layer on ice for various assumed values of ε_2, the energy of formation of diffuse L-defects in the liquid-like layer (after Fletcher 1968).
a—$\varepsilon_2 = 6.25 \times 10^{-3}$ eV; b—$\varepsilon_2 = 0.0188$ eV;
c—$\varepsilon_2 = 0.0625$ eV; d—$\varepsilon_2 = 0.1875$ eV.

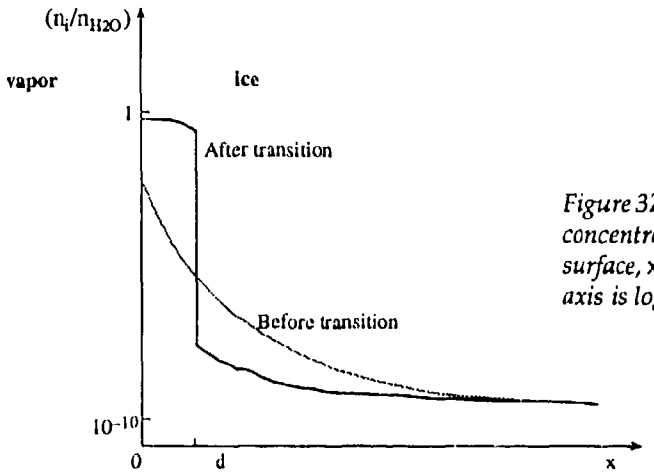

Figure 32. Schematic representation of protonic point defects concentration, n_i, as a function of a distance from the ice surface, x; d is the thickness of a superionic layer. The n_i/n_{H2O} axis is logarithmic.

shows the calculated thickness of the liquid-like layer as a function of temperature. Later, in his invited review paper, Fletcher (1973) gave an approximate expression for the thickness d of the liquid-like layer

$$d(\text{Å}) = (20 \text{ to } 50) - 25 \log_{10}(273 - T). \qquad (69)$$

Fletcher's (1992) recent calculations suggest that, at much lower temperatures, the ice surface is reconstructed by an orientation of surface dipoles into a superlattice. Such a reconstruction should occur on the (0001) basal plane below approximately 30 K and on the $(01\bar{1}0)$ prismatic plane below approximately 70 K.

On the basis of the model of the superionic state of ice invented by Ryzhkin (1985), Ossipyan and Petrenko (1988) suggested a purely electrostatic reason for surface melting that accounts for a high surface electric conductivity and the appearance of a rather thick (up to the screening length) disordered layer. The reasons for the formation of the layer are as follows. As was shown by Ryzhkin (1985), upon the increase of charge carrier concentration above a certain critical value (on the order of 10^{-8} to 10^{-4} of the molecular concentration), the activation energy of ion and Bjerrum defect formation drastically decreases, leading to a catastrophic growth of defect concentration up to 0.1–1 of the molecular concentration. This is equivalent to a phase transition into a superionic state, which can not have a regular lattice owing to a high defect concentration.

If the surface of ice is charged (which is the case in reality, as we have already seen in the section on surface charge and surface potential), this charge will be screened by ions and Bjerrum defects coming from the bulk, as shown in Figure 32. By taking into account the transition into a disordered superionic state, we can transform a smooth curve of the screening charge concentration distribution into the curve with a thin superionic layer near the surface. Within the framework of this model, the high surface conductivity of ice, the formation of the quasi-liquid disordered layer and the sharp interphase boundary (detectable by optical methods) can be quantitatively accounted for. To my knowledge, Dr. Ryzhkin is currently working on the improvement of this model.

There exists a very nontrivial and unusual model of the structure and properties of the ice layer at temperatures close to the melting point. Dzyloshinskii et al. (1961) showed that a fluid that is less polarizable than its solid phase is attracted to the solid, causing a liquid film to grow at the solid/vapor interface. Elbaum and Schick (1991) applied this idea to the ice surface. Figure 33 shows the result of their calculations. If we compare this

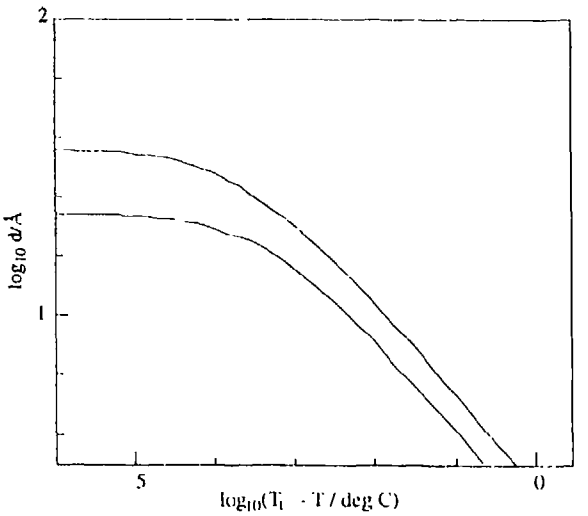

Figure 33. Calculated temperature dependence of the liquid film on ice thickness (after Elbaum and Schick 1991).

figure to the experimental results (Fig. 29), it becomes apparent that the contribution of this mechanism to the experimentally measured thickness of the quasi-liquid film is extremely small. Kroes (1992) used a molecular dynamics computer simulation to study the surface of a small cluster of water molecules. He found such ice surface characteristics as premelting and partial polarization of molecular dipoles.

LITERATURE CITED

Abragam, A. (1961) *The Principle of Nuclear Magnetic Resonance.* Oxford: Clarendon Press.

Adamson, A.W., L.M. Dormant and M. Orem (1967) Physical absorption of vapors on ice. I. Nitrogen. *Journal of Colloid Interface Science,* **25:** 206–217.

Ahagon, A., T. Kobayashi and M. Misawa (1988) Friction on ice. *Rubber Chemicals and Technology,* **61**(1): 14–35.

Barer, S.S., V.I. Kvlividze, A.B. Kurzaev, V.D. Sobolev and N.V. Churaev (1977) Thickness and viscosity of thin unfrozen layers between ice and quartz surfaces. *Doklady Akademii Nauk USSR,* **235**(3): 601–603.

Beaglehole, D. and D. Nason (1980) Transition layer on the surface of ice. *Surface Science,* **96:** 357–363.

Bell, J.D., R.W. Myatt and R.E. Richards (1971) Proton magnetic resonance evidence of a liquid phase in polycrystalline ice. *Nature,* **230:** 91–92.

Bootsma, G.A. and F. Meyer (1969) Ellipsometry in the sub-monolayer region. *Surface Science,* **14:** 52–76.

Brunauer, S., P.H. Emmet and E. Teller (1938) Adsorption of gases in multimolecular layers. *Journal of the American Chemical Society,* **60:** 309–319.

Bush, V. and J.P. Devlin (1991) Spectra of dangling OH bonds in amorphous ice: Assignment to 2- and 3-coordinated surface molecules. *Journal of Chemical Physics,* **94:** 4091–4092.

Bullemer, B. and N. Riehl (1968) Hall-Effekt an Protonen in Eis. *Physik der Kondensierten Materie,* **7:** 248–260.

Burnett, L.J. and J.F. Harmon (1972) Self-diffusion in viscous liquids: Pulse NMR measurements. *Journal of Chemical Physics,* **57:** 1293–1297.

Buser, O. and A.N. Aufdermaur (1977) Electrification by collision of ice particles on ice or metal targets. *Electrical Processes in Atmosphere* (H. Dolezalek and Reiter, Ed.). Darmstadt: Steinkopf, p. 294–301.

Buser, O. and C. Jaccard (1978) Charge separation by collision of ice particles on metals: Electronic surface states. *Journal of Glaciology,* **21**(85): 547–557.

Callen, B.W., K. Griffiths, R.V. Kasza, M.B. Jensen, P.A. Thiel and P.R. Norton (1992) Structural phenomena related to associative and dissociative adsorption of water on Ni(110). *Journal of Chemical Physics,* **97:** 3760–3774.

Camp, P.R. and D.J. Halchin (1979) Electrical properties of ice/solid interfaces. In *Proceedings of International Symposium on Snow Removal and Ice Control Research, 15–19 May, Hanover, New Hampshire.* National Research Council, Transportation Research Board, Special Report 185, p. 35–43.

Camp, P.R., W. Kiszhenick and D. Arnold (1969) Electrical conduction in ice. In *Physics of Ice* (N. Riehl, B. Bullemer and H. Engelhardt, Ed.). New York: Plenum Press. p. 450–470.

Caranti, J.M. and A.J. Illingworth (1980) Surface potential of ice and thunderstorm charge separation. *Nature,* **284:** 44–46.

Caranti, J.M. and A.J. Illingworth (1983a) Frequency dependence of the surface conductivity of ice. *Journal of Physical Chemistry,* **87:** 4078–4083.

Caranti, J.M. and A.J. Illingworth (1983b) Transient Warkman-Reynolds freezing potential. *Journal of Geophysical Research,* **88**(C13): 8483–8489.

Caranti, J.M. and A.J. Illingworth (1983c) The contact potential of rimed ice. *Journal of Physical Chemistry,* **87:** 4125–4130.

Caranti, J.M. and M.A. Lamfri (1987) Hall effect on the surface of ice. *Physical Letters A,* **126:** 47–51.

Caranti, J.M., A.J. Illingworth and S.J. Marsh (1985) The charging of ice by differences in contact potential. *Journal of Geophysical Research,* **90**(D4): 6041–6046.

Chrzanowski, J. (1988) Thickness-dependent d.c. electrical conduction in thin polycrystalline ice films deposited onto a dielectric substrate. *Journal of Materials Science Letters,* **7**:1058–1060.

Clifford, J. (1967) Proton magnetic resonance data on Ice. *Chemical Communications,* **17:** 880–881.

Colbeck, S.C. (1992) A review of the processes that control snow friction. USA Cold Regions Research and Engineering Laboratory, Monograph 92-2.

Dash, J.G. (1991) Frost heave and the surface melting of ice. In *Phase Transitions in Surface Films 2* (H. Taub et al., Ed.) New York: Plenum Press, p. 339–356.

Devlin, J.P. (1992) Molecular activity at ice surfaces: infrared bands of dangling OH bonds and induced activity of surface absorbents. In *Physics and Chemistry of Ice* (N. Maeno and T. Hondoh, Ed.). Sapporo: Hokkaido University Press, p. 183–189.

Drude, P. (1889) Über oberflächenschichten. *Annals of Physical Chemistry,* **36:** 532–560.

Dzyaloshinskii, I.E., E.M. Lifshitz and L.P. Pitae-

vskii (1961) The general theory of Van-der-Waals forces. *Advances in Physics*, **10**: 165–209.

Elbaum, M. and M. Schick (1991) Application of the theory of dispersion forces to the surface melting of ice. *Physical Review Letters*, **66**(13): 1713–1716.

Elbaum, M., S.G. Lipson and J.G. Dash (1993) Optical study of surface melting on ice. *Journal of Crystal Growth*, **129**: 491–505.

Faraday, M. (1850) Lecture given at the Royal Institution, London, June 7, 1850. Reported in *Athenaeum* 1850, p. 640.

Faraday, M. (1859) On regelation, and on the conservation of force. *Philosophical Magazine*, **17**: 162–169.

Fletcher, N.H. (1962) Surface structure of water and ice. *Philosophical Magazine*, **7**: 255–269.

Fletcher, N.H. (1963) Surface structure of water and ice—A reply and correction. *Philosophical Magazine*, **8**: 1425–1426.

Fletcher, N.H. (1968) Surface structure of water and ice II. A revised model. *Philosophical Magazine* 18: 1287–1300.

Fletcher, N.H. (1970) *The Chemical Physics of Ice*. Cambridge University Press.

Fletcher, N.H. (1973) The surface of ice. In *Physics and Chemistry of Ice* (E. Whalley, S.J. Jones and L.W. Gold, Ed.). Ottawa: Royal Society of Canada, p. 132–135.

Fletcher, N.H. (1992) Reconstruction of ice crystal surfaces at low temperatures. *Philosophical Magazine B*, **66**(1): 109–115.

Fukuta, N. (1987) An origin of the equilibrium liquid-like layer on ice. *Journal de Physique C1*, **48**: 503–509.

Furukawa, Y., M. Yamamoto and T. Kuroda (1987a) Ellipsometric study of the ice surface structure just below the melting point. *Journal de Physique C1*, **48**: 495–501.

Furukawa, Y., M. Yamamoto and T. Kuroda (1987b) Ellipsometric study of the transition layer on the surface of an ice crystal. *Journal of Crystal Growth*, **82**: 665–677.

Gemmel, D.S. (1974) Channeling and related effects in the motion of charged particles through crystals. *Review of Modern Physics*, **46**: 129–227.

Glen, J.W. (1974) Physics of ice. USA Cold Regions Research and Engineering Laboratory, Monograph MII-C2a.

Glen, J.W. (1975) Mechanics of ice. USA Cold Regions Research and Engineering Laboratory, Monograph MII-C2b.

Golecki, I. and C. Jaccard (1977) The surface of ice near 0°C studied by 100 keV proton channeling. *Physical Letters A*, **63**: 374–376.

Golecki, I. and C. Jaccard (1978) Intrinsic surface disorder in ice near the melting point. *Journal of Physics C: Solid State Physics*, **11**: 4229–4237.

Gosar, P. (1974) Note on the Hall Effect in ice. *Physics of Condensed Matter*, **17**: 183–187.

Hardy, S.C. (1977) A grain boundary groove measurement of the surface tension between ice and water. *Philosophical Magazine*, **35**: 471–484.

Hobbs, P.V. (1974) *Ice Physics*. Oxford: Clarendon Press.

Hobbs, P.V. and B.J. Mason (1964) The sintering and adhesion of ice. *Philosophical Magazine*, **9**: 181–197.

Hosler, C.L., D.C. Jensen and L. Goldshlak (1957) On the aggregation of ice crystals to form snow. *Journal of Meteorology*, **14**: 415.

Howe, R. and R.W. Whitworth (1989) The electrical conductivity of KOH-doped ice from 70 to 250 K. *Journal of the Physical Chemistry of Solids*, **50**(9): 963–965.

Itagaki, K. (1967a) Particle migration on ice surfaces. In *Physics of Snow and Ice. Proceedings of the International Conference on Low Temperature Science, Hokkaido University, Sapporo, Japan* (H. Oura, Ed.), p. 233–245.

Itagaki, K. (1967b) Self-diffusion in single crystal ice. *Journal of the Physical Society of Japan*, **22**: 427–431.

Itagaki, K. (1967c) Some surface phenomena of ice. *Journal of Colloid and Interface Science*, **25**: 218–227.

Jaccard, C. (1959) Étude théorique et expérimentale des propriétiés électriques de la glace. *Helvetica Physica Acta*, **32**: 89–128.

Jaccard, C. (1966) Four-point method for measuring the volume and surface conductivity of a thin sample. *Zeitschrift Angewandte Mathematik und Physik*, **17**: 657–663.

Jaccard, C. (1967) Electrical conductivity of the surface layers of ice. In *Physics of Snow and Ice. Proceedings of the International Conference on Low Temperature Science, Hokkaido University, Sapporo, Japan* (H. Oura, Ed.), p. 173–179.

Jellinek, H.H.G. (1957a) Tensile properties of ice adhering to stainless steel. USA Snow, Ice and Permafrost Research Establishment, Research Report 23.

Jellinek, H.H.G. (1957b) Adhesive properties of ice. USA Snow, Ice and Permafrost Research Establishment, Research Report 38.

Jellinek, H.H.G. (1959) Adhesive properties of ice. *Journal of Colloid Science*, **14**: 268–279.

Jellinek, H.H.G. (1960) Adhesive properties of ice, Part II. USA Snow, Ice and Permafrost Research Establishment, Research Report 62.

Jellinek, H.H.G. (1962) Ice adhesion. *Canadian Journal of Physics*, **40**: 1294–1309.

Ketcham, W.M. and P.V. Hobbs (1969) An experimental determination of the surface energies of ice. *Philosophical Magazine*, **19**: 1161–1173.

Khusnatdinov, N.N. and V.F. Petrenko (1992) The photoconductivity of doped ice. In *Physics and Chemistry of Ice* (N. Maeno and T. Hondoh, Ed.). Sapporo: Hokkaido University Press, p. 170–174.

Kingery, W.D. (1960) Regelation, surface diffusion and ice sintering. *Journal of Applied Physics*, **31**: 833–838.

Knight, C.A. (1966) The contact angle of water on ice. *Journal of Colloid and Interface Science*, **25**: 280–284.

Knight, C.A. (1971) Experiments on the contact angle of water on ice. *Philosophical Magazine*, **23**: 153–165.

Kouchi, A., Y. Furukawa and T. Kuroda (1987) X-ray diffraction pattern of quasi-liquid layer on ice crystal surface. *Journal de Physique C1*, **48**(3): 675–676.

Kroes, G.-J. (1992) Surface melting of the (0001) face of TIP4P ice. *Surface Science*, **275**: 365–382.

Kuroda, T. and R. Lacmann (1982) Growth kinetics of ice from the vapor phase and its growth forms. *Journal of Crystal Growth*, **56**: 189–205.

Kvlividze, V.I., V.F. Kiselev and L.A. Ushakova (1970) The existence of quasi-liquid films on the surface of ice. *Doklady Akademii Nauk USSR*, **191**(5): 1088–1090.

Kvlividze, V.I., V.F. Kiselev, A.B. Kurzaev and L.A. Ushakova (1974) The mobile water phase on ice surface. *Surface Science*, **44**: 60–68.

Langmuir, I. (1916) The evaporation, condensation and reflection of molecules and the mechanism of adsorption. *Physical Review*, **8**: 149–176.

Maeno, N. (1973) Measurements of surface and volume conductivity of single ice crystals. In *Physics and Chemistry of Ice* (E. Whalley, S.J. Jones and L.W. Gold, Ed.). Ottawa: Royal Society of Canada, p. 140–143.

Maeno, N. (1981) *The Science of Ice*. Hokkaido University Press (in Japanese).

Maeno, N. and T. Ebinuma (1983) Pressure sintering of ice and its implication to the densification of snow at polar glaciers and ice sheets. *Journal of Physical Chemistry*, **87**: 4103–4110.

Maeno, N. and H. Nishimura (1978) The electrical properties of ice surface. *Journal of Glaciology*, **21** (85): 193–205.

Maidique, M.A., A. von. Hippel and W.B. Westphal (1971) Transfer of protons through "pure" ice Ih single crystals. III. Extrinsic versus intrinsic polarization; surface versus volume conduction. *Journal of Chemical Physics*, **54**: 150–160.

Makkonen, L. (In press) Surface melting of ice. *Philosophical Magazine*.

Mazzeda, E., U. del Pennino, A. Loria and S. Mantovani (1976) Volta effect and liquid-like layer at the ice surface. *Journal of Chemical Physics*, **64**(3): 1028–1031.

Meyer, L. (1971) Plural and multiple scattering of low energy heavy particles in solids. *Physica Status Solidi (b)*, **44**: 253–268.

Mizuno, Y. and N. Hanafusa (1987) Studies of surface properties of ice using nuclear magnetic resonance. *Journal de Physique C1*, **48**: 511–517.

Nakaya, U. and A. Matsumoto (1953) Evidence of the existence of a liquid-like film on ice surfaces. USA Snow, Ice and Permafrost Research Establishment, Research Paper 4.

Nason, D. and N.H. Fletcher (1975) Photoemission from ice and water. *Journal of Chemical Physics*, **62**: 4444–4449.

Nixon, H.G., M.J. Wajcik, M.S. Devlin, J.P. Devlin and V. Bush (1992) Experimental and simulated vibrational spectra of H_2 absorbed in amorphous ice: Surface structure, energetics, and relaxation. *Journal of Chemical Physics*, **97**: 753–767.

Ocampo, J. and J. Klinger (1983a) Modification of the surface structure of ice during aging. *Journal of Physical Chemistry*, **87**: 4167–4170.

Ocampo, J. and J. Klinger (1983b) Proton mobility in the bulk and the surface of hexagonal ice. *Journal of Physical Chemistry*, **87**: 4325–4328.

Oen, O. and M.T. Robinson (1962) *Le Bombardement Ionique*. Paris: C.N.R.S.

Orem, M.W. and A.W. Adamson (1969) Physical absorption of vapor on ice. II. n-alkanes. *Journal of Colloid and Interface Science*, **31**: 278–286.

Ossipyan, Yu.A. and V.F. Petrenko (1988) The physics of ice. *Europhysics News*, **19**(5): 61–64.

Petrenko, V.F and N. Maeno (1987) Ice field transistor. *Journal de Physique C1*, **48**: 115–119.

Petrenko, V.F. (1992) Applications of electrical signals from cracks in ice micromechanics. In *Proceedings of the 11th International Symposium on Ice, Banff, University of Alberta*, p. 1140–1154.

Petrenko, V.F. (1993) Electrical properties of ice. USA Cold Regions Research and Engineering Laboratory, Special Report 93-20.

Petrenko, V.F. (1994) The effect of static electric field on friction of ice. *Journal of Applied Physics*, **76**(2).

Petrenko, V.F. and S.C. Colbeck (In press) Generation of electric fields in ice and snow friction. *Journal of Applied Physics*.

Petrenko, V.F. and I.A. Ryzhkin (1984) Dielectric properties of ice in the presence of space charge. *Physica Status Solidi (b)*, **121:** 421–427.

Raraty, L.E. and D. Tabor (1958) The adhesion and strength properties of ice. *London: Proceedings of the Royal Society*, **A245:** 184–201.

Rowland, B. and J.P. Devlin (1991) Spectra of dangling OH groups at ice cluster surfaces and within pores at amorphous ice. *Journal of Chemical Physics*, **94:** 812–813.

Rowland, B., M. Fisher and J.P. Devlin (1991) Probing ice surfaces with the dangling-OH-mode absorption: large ice clusters and microporous amorphous ice. *Journal of Chemical Physics*, **95:** 1378–1384.

Rowland, B., M. Fisher and J.P. Devlin (1993) Surface defect vibrational modes of large ice clusters. *Journal of Physical Chemistry*, **97**(11): 2485–2487.

Ruepp, R. and M. Käss (1969) Dielectric relaxation of the bulk and surface conductivity of single ice crystals. In *Physics of Ice* (Riehl et al., Ed.). New York: Plenum Press, p. 555–561.

Ryzhkin, I.A. (1985) Superionic transition in ice. *Solid State Communications*, **56**: 57–60.

Schmitt, B., J. Ocampo and J. Klinger (1987) Structure and evolution of different ice surfaces at low temperature adsorption studies. *Journal de Physique C1*, **48:** 519–525.

Smoluchowski, R. (1983) Absorption and mobility on amorphous surfaces. Application to astrophysical problems. *Journal of Physical Chemistry*, **87:** 4229–4233.

Sokoloff, J.B. (1973) Absence of a Hall effect in ice crystals. *Physics Review Letters*, **31:** 90–92.

Steele, W.A. (1974) *The Interaction of Gases with Solid Surfaces*. Oxford: Pergamon Press.

Takagi, S. (1990) Approximate thermodynamics of the liquid-like layer on an ice sphere based on an interpretation of the wetting parameter. *Journal of Colloid and Interface Science*, **137**(2): 446–455

Takahashi, T. (1969a) Electric potential of liquid water on an ice surface. *Journal of Atmospheric Science*, **26:** 1253–1258.

Takahashi, T. (1969b) Electric potential of rubbed ice surface. *Journal of Atmospheric Science*, **26:** 1259–1265.

Takahashi, T. (1970) Electric surface potential of growing ice crystals. *Journal of Atmospheric Science*, **27:** 453–462.

Turner, G.J. and C.D. Stow (1986) D.C. conductivity of the ice surface. *Solid State Communications*, **58:** 403–405.

REPORT DOCUMENTATION PAGE

Form Approved
OMB No. 0704-0188

Public reporting burden for this collection of information is estimated to average 1 hour per response, including the time for reviewing instructions, searching existing data sources, gathering and maintaining the data needed, and completing and reviewing the collection of information. Send comments regarding this burden estimate or any other aspect of this collection of information, including suggestion for reducing this burden, to Washington Headquarters Services, Directorate for Information Operations and Reports, 1215 Jefferson Davis Highway, Suite 1204, Arlington, VA 22202-4302, and to the Office of Management and Budget, Paperwork Reduction Project (0704-0188), Washington, DC 20503.

1. AGENCY USE ONLY (Leave blank)	2. REPORT DATE	3. REPORT TYPE AND DATES COVERED
	August 1994	

4. TITLE AND SUBTITLE

The Surface of Ice

5. FUNDING NUMBERS

6. AUTHORS

Victor F. Petrenko

7. PERFORMING ORGANIZATION NAME(S) AND ADDRESS(ES)

U.S. Army Cold Regions Research and Engineering Laboratory
72 Lyme Road
Hanover, New Hampshire 03755-1290

Thayer School of Engineering
Dartmouth College
Hanover, New Hampshire 03755

8. PERFORMING ORGANIZATION REPORT NUMBER

Special Report 94-22

9. SPONSORING/MONITORING AGENCY NAME(S) AND ADDRESS(ES)

Army Research Office
Research Triangle Park, North Carolina

10. SPONSORING/MONITORING AGENCY REPORT NUMBER

11. SUPPLEMENTARY NOTES

12a. DISTRIBUTION/AVAILABILITY STATEMENT

Approved for public release; distribution is unlimited.

Available from NTIS, Springfield, Virginia 22161.

12b. DISTRIBUTION CODE

13. ABSTRACT (*Maximum 200 words*)

This report examines the structure and physical properties of the surface of ice: a liquid-like layer on the ice surface, its thickness and molecular structure, surface conductivity, surface electric charge, surface potential, surface diffusion and so forth. The author reviews experimental results and theoretical models on ice adhesion, gas adsorption and ice sintering. Special attention is given to the results of studies from the last two decades. Among the experimental techniques under consideration are nuclear magnetic resonance, X-ray diffraction, optical ellipsometry, measurements of ice surface conductivity and dielectric permittivity, frictional electrification of snow and ice, proton channeling and others. In conclusion, the theoretical models of the ice surface structure and the results on molecular dynamics are considered.

14. SUBJECT TERMS

Ice
Ice surface
Liquid-like layer
Optical ellipsometry
Proton channeling
X-ray diffraction

15. NUMBER OF PAGES
45

16. PRICE CODE

17. SECURITY CLASSIFICATION OF REPORT	18. SECURITY CLASSIFICATION OF THIS PAGE	19. SECURITY CLASSIFICATION OF ABSTRACT	20. LIMITATION OF ABSTRACT
UNCLASSIFIED	UNCLASSIFIED	UNCLASSIFIED	UL

SELECTED BIBLIOGRAPHY

Ackley, S.F. and K. Itagaki (1970) Ice adhesion studies: Properties of defects in the interfacial region. In *Snow Removal and Ice Control Research: Proceedings of the International Symposium, 8–10 April, Dartmouth College, Hanover, New Hampshire.* Highway Research Board, Special Report No. MP 13, no. 115: 87–96.

Akitt, J.W. and I.H. Lilley (1967) The nature of hydrogen bonding in ice and water: ^{1}H Nuclear magnetic resonance data on ice. *Chemical Communications*, 323–324.

Bullemer, B. and N. Riehl (1966) Bulk and surface conductivity of ice. *Solid State Communications*, **4:** 447–448.

Devlin, J.P. (1990) Vibrational spectra and point defect activities of icy solids and gas phase clusters. *International Reviews in Physical Chemistry*, **9:** 29–65.

Faraday, M. (1860) Note of regelation. London. In *Proceedings of Royal Society*, **10:** 440.

Hubmann, M. (1979) Polarization processes in the ice lattice. *Zhurnal Physik B*, **32:** 127–146.

Itagaki, T. and T.M. Tobin (1973) Mass transfer along ice surfaces observed by groove relaxation technique. *Journal of Glaciology* **12**(64): 121–127.

Jellinek, H.H.G. (1967) Liquid-like (transition) layer on ice. *Journal of Colloid and Interface Science*, **25:** 192–205.

Jellinek, H.H.G. and S.H. Ibrahim (1967) Sintering of powered ice. *Journal of Colloid and Interface Science*, **25:** 245–254.

Kuhn, W. and M. Thürkauf (1958) Isotopentrennung beim Gefrieren von Wasser und Diffusionkonstanten von D und ^{18}O im eis. *Helvetica Chimica Acta*, **44:** 938–971.

Landy, M. and A. Freiberger (1967) Studies of ice adhesion. I. Adhesion of ice to plastics. *Journal of Colloid and Interface Science*, **25:** 231–244.

Murphy, E.J. (1970) The generation of electromotive forces during the freezing of water. *Journal of Colloid and Interface Science*, **32**(1): 1–11.

Tamm, I.E. (1989) *Theory of Electricity.* Moscow: Nauka.

Tobin, T.M. and T. Itagaki (1977) Mass transfer along ice surfaces observed by groove relaxation technique. Isotopes and impurities in snow and ice. In *Proceedings of the Grenoble Symposium, August/September 1975.* IAHS Publication, no. 188, p. 34–37.

Zhang, Q. and V. Bush (1990a) Condensation and structure of amorphous ice: a computational study. *Journal of Chemical Physics*, **92:** 1512–1513.

Zhang, Q. and V. Bush (1990b) Computational study of formation dynamics and structure of amorphous ice condensates. *Journal of Chemical Physics*, **92:** 5004–5016.

Time-stepping scheme:

Semi-implicit finite difference

Implicit discretization of the gradient of the surface elevation in the momentum equations and the velocity in the vertically integrated continuity equation

Explicit discretization of the convective, turbulence, and certain body force terms

Numerical solution technique: Finite difference

Type of grid: Cartesian finite difference, constant grid spacing

Coordinate transformations:

Horizontal: none

Vertical: none

Example applications: San Francisco Bay; Lagoon of Venice

Typical Δt for 3-D baroclinic circulation: 1 to 2 minutes

References:

Casulli and Cheng (1992)
Cheng, Casulli, and Gartner (1993)

Sheng-Johnson Estuarine Hydrodynamic Model

Author(s): Y. Peter Sheng and Billy H. Johnson

Organization: University of Florida, Gainesville, and WES

Contributors (modifications and enhancements):

Name of model: CH3D (Curvilinear-Grid Hydrodynamic 3-D) / CH3D-WES (WES version of CH3D)

Related models:

EHSM3D (Estuary Hydrodynamic and Sediment Model 3-D, Cartesian coordinates)

CH2D (Curvilinear-Grid Hydrodynamic 2-D Vertically Averaged)

Remarks: Dr. Sheng continues to update and make enhancements to the model. He has developed water quality/sediment transport models that interface with CH3D and EHSM3D.

WES has made significant modifications to the code that have resulted in a functionally separate version, CH3D-WES. The WES version has been modified to use either a σ-transform or a z-transform, dependent upon application. Wetting and drying is not implemented in the current WES version of the code. A water quality/aquatic ecology model has been developed to interface with CH3D-WES. A 3-D sediment transport model is currently under development for WES (anticipated completion date: October 1993).

Dimensionality: 3-D

Governing equations:

Fully nonlinear Reynolds form of Navier-Stokes with hydrostatic approximation

Continuity of Mass

Advection-Diffusion of Salinity

Advection-Diffusion of Temperature

Equation of State

Turbulence submodel:

Horizontal: Eddy viscosity

Vertical: Simplified second moment closure model

Time-stepping scheme:

Split mode solution:

Semi-implicit finite difference for the external mode (vertically averaged) solution

All terms of the internal mode solution are treated explicitly, except for the vertical turbulent diffusion terms and the bottom friction and surface slope terms in the momentum equations

Numerical solution technique: Finite difference

Type of grid: Curvilinear, staggered, boundary fitted, structured

Coordinate transformations:

Vertical: σ-coordinate system

Horizontal: curvilinear, boundary fitted

Example applications:

Lake Okeechobee; Sarasota Bay (Sheng)

Chesapeake Bay: Delaware Bay; Green Bay (WES)

Typical Δt for 3-D baroclinic circulation: 2 to 10 minutes (Equal time-steps are used for internal and external modes.)

References:

Sheng (1993)
Johnson et al. (1991)
Sheng, Parker, and Henn (1986)

Edinger-Buchak Estuarine Hydrodynamic Model

Author(s): John E. Edinger and Edward M. Buchak

Organization: J. E. Edinger Associates, Inc., Wayne, PA

Contributors (modifications and enhancements): Zenyu Zhang, University of Pennsylvania; Lixing Wu, University of Pennsylvania

Name of model: GLLVHT5 (Generalized, Longitudinal-Lateral-Vertical Hydrodynamic and Transport Model, Version 5)

Related models:

GLVHT (Generalized, Longitudinal-Vertical Hydrodynamics and Transport), the hydrodynamic basis of CE-QUAL-W2, the Corps' laterally averaged reservoir and estuary model

GLHT (Generalized Longitudinal Hydrodynamics and Transport), a 1-D river and estuary model

Remarks: Edinger Associates' models are designed for quick setup and moderate detail. According to Edinger Associates, this method permits (a) rapid issue identification; (b) low computing costs and moderate hardware requirements (an ordinary personal computer or workstation is sufficient for most studies); and (c) iterative refinement of the modeling procedure. All of Edinger's models include concurrent water quality subroutines. Mass balances within the defined computational cells are perfect to machine accuracy. Wetting and drying of the computational grid is supported.

Dimensionality: 3-D

Governing equations:

Fully nonlinear Reynolds form of the Navier-Stokes equations with hydrostatic approximation

Continuity of Mass

Constituent Transport

Equation of State relating water density to salinity and temperature

Turbulence submodel:

Horizontal: User may specify a variety of forms for computing Reynolds stresses.

Vertical: User may specify a variety of forms for computing Reynolds stresses, including Mellor-Yamada

Time-stepping scheme: A fully implicit integration divides the time-step into two halves. On the first half-time-step, the x- and y-momentum equations are substituted into the continuity equation and the resulting linear equations are solved for the water-surface elevation. The horizontal velocities are then solved algebraically from the momentum equations, followed by the vertical velocities from continuity. A second pass through this procedure assures a perfect water balance. The constituent and density equations are then solved to complete the first half-time-step.

On the second half-time-step, the horizontal velocities are solved vertically implicitly, then the vertical velocities and the water-surface elevation are solved explicitly. The constituent and density equations are solved to complete the second half-time-step. If there are significant water-surface elevation changes, a layer/cell add/subtract module is activated.

For very large grids, the code has an option to compute the main variables with a similar second-order ADI method. For this method the first half-time-step solves for u vertically implicitly and v-z by substituting the x-momentum equation into continuity. The second half-time-step reverses this procedure and solves for v vertically implicitly and u-z simultaneously. The solutions are obtained using the tridiagonal algorithm. The ADI scheme is suited to very large grids in which its inherent biasing of the buoyancy terms is negligible.

A third option is to use a first-order-in-time, second-order-in-space single-stage computation. The latter option is used for fast, preliminary simulations.

Numerical solution technique: Finite difference

Type of grid: Orthogonal finite difference

Coordinate transformations:

Vertical: variable Δz, no transformation

Horizontal: $\Delta x \neq \Delta y$, no transformation

Example applications: Sterling Harbor, Texas; Grand Lake, New Brunswick; Patuxent River Estuary, Maryland; Belledune Harbor, New Brunswick; Nechako Reservoir, British Columbia; East Waterway, Everett, Washington; Farley Storage Pond, Dothan, Alabama; Webber Cove-Barbara Weit Estuary, Prince Edward Island; Moller Bay, Alaska; Delaware Estuary, Wilmington, Delaware; Candarli Korfezi (on the Aegean Sea), Turkey; Clinton Lake, Illinois; Du Pont Cooper River Plant, Cooper River, South Carolina; Sheldon Point, Saint John Harbour, New Brunswick; Comanche Peak, Texas; Barbers Point Outfall/Barbers Point to Ewa Beach coastal area, Hawaii; Maggie Creek/Humboldt River, Nevada

Typical Δt for 3-D baroclinic circulation: 7.5 to 15 minutes

References:

Buchak, Edward M. (1993). Personal communication, 14 October.

Edinger and Buchak (1980, 1985)

Zhao-Tabios-Shen Estuarine Hydrodynamic Model

Author(s): Di Hua Zhao, Guillermo Q. Tabios, Hsieh Wen Shen

Organization: University of California, Berkeley

Contributors (modifications and enhancements):

Name of model: RBFVM-2D

Related models: none

Remarks: This model is included for review because it is the only published finite volume model currently being used for surface water flows. In its present form it is not applicable to stratified estuarine flow; however, there is great potential for 3-D model development. The finite volume method has merit for shallow surface water flow problems because wetting and drying of subdomains is handled naturally. An implicit version is being developed to alleviate the time-step restriction.

Dimensionality: 2-D vertically averaged hydrodynamics

Governing equations: 2-D shallow-water equations with constant density

Turbulence submodel:

Horizontal: neglected
Vertical: none

Time-stepping scheme: Explicit

Numerical solution technique: Finite volume method

Type of grid: Unstructured with quadrilateral and triangle elements

Coordinate transformations:

Horizontal: none

Vertical: none

Example applications: Kissimmee River Basin

Typical Δt for 2-D vertically averaged circulation: less than 1 second

Reference: Zhao, Tabios, and Shen (1992)

7 Recommended Criteria for Selecting a Hydrodynamic/ Salinity Model for the LSJRE

The State of Florida has tasked the SJRWMD to determine the ecological and water quality condition of the St. Johns River and to develop management strategies that balance multiple beneficial uses of the river. Potential beneficial uses may include water supply, navigation, industrial and residential use of shorelines, domestic and industrial waste discharges, fisheries, wildlife habitat, and recreation. From an engineering perspective, the objectives of the SJRWMD are to:

a. Understand the existing physical, chemical, and biological functions of the LSJRE.

b. Develop tools to scientifically predict the impacts of alternative management plans and engineering projects on the LSJRE.

c. Develop a methodology for evaluating the costs and benefits of alternative management plans, based on predictions.

Numerical models have the potential for integrating basinwide hydrodynamic and water quality data with scientific principles in a quantitative manner. Given the directive of the State of Florida to the SJRWMD, such sophisticated analysis tools are warranted.

The selection of a hydrodynamic model for the LSJRE is the first step in creating a comprehensive modeling and analysis system. The recommended features of a model that will meet the long-range goals of the SJRWMD, and a brief justification of each feature, are given below:

a. Minimum dimensionality: 2-D, vertically averaged estuarine hydrodynamics.

b. Potential dimensionality: 3-D, baroclinic hydrodynamics.

c. *Geometry:* boundary-fitted grid with local refinement options.

d. *Wetting and drying option:* required.

e. *Horizontal turbulent fluctuation terms:* required

f. *Vertical turbulent closure model:* documentation required.

g. *Model maintenance:* required

A brief justification of each feature is given in the following sections.

Minimum Dimensionality

The LSJRE includes approximately 110 miles (177 km) of tidally influenced river channel. Although several 1-D models have been applied to the LSJRE, the process of verifying a 1-D model frequently results in unrealistic values for roughness, channel geometry, and water quality diffusion coefficients. Two-dimensional, vertically averaged models have been found to require far less "tuning" to achieve satisfactory tidal simulations, and are more useful for making valid predictions.

The lower 100 miles (160 km) of the St. Johns River varies from 600 ft (182.9 m) to 1.5 miles (2.4 km) nominal width (Morris in preparation). The wider reaches actually fluctuate between 1.5 and 3.0 miles (4.8 km) in width, depending upon local flood conditions. A vertically averaged model will capture momentum losses due to expansions and contractions of the river channel, which affect the progression of tides and flood waves. Furthermore, lateral momentum transport occurring at junctions of the main stem with tributaries will be well represented. These characteristics are important for the ultimate computation of sediment transport and water quality, especially when the sediment load or water chemistry of the tributary is different from the main stem.

Potential Dimensionality

The LSJRE has been categorized as a highly stratified to moderately stratified estuary by Morris (in preparation), who reports a salt wedge of variable extent in the LSJRE. Vertical stratification due to salinity or temperature gradients results in vertical velocity gradients and secondary circulation, which can be described only by a 3-D model of estuarine hydrodynamics. Secondary currents can also result from flow around channel bends and from wind stress.

A 3-D model represents a substantial increase in sophistication over the 2-D, vertically averaged model. Certain modeling objectives, such as waste load allocation or flood routing, do not warrant 3-D analysis. However, if the model results are to be used for modeling salinity stratification and the

response of phytoplankton to changing salinity, then a 3-D model will be required. A prudent approach would be to select a 2-D, vertically averaged hydrodynamic model that has a 3-D counterpart either in existence or actively under development. Since most 3-D models are built upon a 2-D preliminary grid, the preparatory work of grid development, boundary condition development, and data gathering will carry over to three dimensions when the need for a 3-D study arises.

Geometry

Because the St. Johns River is bathymetrically complex, it is important to define the complexities accurately. The scales of flow phenomena vary because of the dramatic changes in width and depth along the length of the river. Either a stretched, curvilinear, boundary-fitted finite difference grid or an unstructured finite element grid (or finite volume grid) would be appropriate. A capability for rapid local refinement of the grid will be advantageous as new study areas are defined.

Wetting and Drying Option

Portions of the St. Johns River and its tributaries are adjacent to tidal and freshwater marshes. Flooding and drying of marsh areas can have a significant impact on the volume of the tidal prism, the phasing of tidal fluctuations, and the storage volume of the estuary. As part of the LSJRE ecosystem, marshes may play an important role in filtering sediments and water quality and provide habitat for fish and wildlife. A model of LSJRE hydrodynamics should be capable of handling intermittent flooding of marsh environments or representing marsh storage schematically.

Horizontal Turbulent Fluctuation Terms

Hydrodynamic circulation in the LSJRE is controlled largely by the complex geometry of the estuary. Boundary shear is important around expansions and contractions of the river, islands, and river bends. Horizontal turbulent fluctuation terms are thus required to simulate LSJRE flows adequately. Wave equation models that ignore horizontal eddy viscosity are not appropriate for this system.

Vertical Turbulent Closure Model

An advanced turbulence closure model such as the Mellor-Yamada scheme is recommended for the 3-D hydrodynamic model. A 3-D modeling study will be useful only if the model can capture the stratification behavior of the

estuary. This behavior is generally controlled by the vertical turbulence model. The vertical turbulence closure scheme of the selected model should be well documented, including guidance for selecting values of the coefficients.

Model Maintenance

The models described in this report are actively under development. The planning period for development of the SJRWMD modeling program is 3-5 years. It is desirable that the modeling tools developed under this program be useful and up to date for several years beyond the development program. Therefore, it is prudent to choose a modeling system that is designed to take advantage of new theoretical developments and new computer technology. When modeling services are contracted, provision for model maintenance and upgradability should be negotiated.

Given the above requirements, several of the models reviewed in Chapter 6 can be considered most appropriate for the LSJRE system. These models are (in no particular order):

a. RMA-10 and associated models, Ian P. King, WES.

b. CH3D, Y. P. Sheng; CH3D-WES, Y. P. Sheng and B. H. Johnson

c. ECOM, Alan F. Blumberg and George L. Mellor

Each of these models has strengths and weaknesses for the LSJRE application. For example, model *a* is the only one of the three that has a fully implemented wetting and drying scheme. Models *b* and *c* can handle marshes schematically by adding "storage nodes." Model *a* is not currently linked to a water quality model that includes phytoplankton. Models *b* and *c* are each linked to an advanced water quality model.

Models *a* and *b* are public domain models that have been applied to various estuarine flow problems by the authors at their respective institutions. WES uses both of these models, the choice of which is made according to the requirements of the specific application. Model *c* is proprietary and is available by contract with the authors.

8 Hydrodynamic Monitoring Requirements to Support Model of LSJRE

Application of a hydrodynamic/salinity model to the LSJRE will require field data to set boundary conditions and to perform model verification. The minimum data requirements are summarized in Table 1.

Table 1
Minimum Data Requirements

Data Category	Data Type	Sampling Locations	Sampling Frequency	Period of Record
Boundary conditions and initial conditions (Continued)	Tide elevation	Two or three locations at the ocean boundary	2.0-15.0 minutes	Continuous over spring-neap tidal sequence, plus long-term records from permanent tide stations (existing or to be established)
	Velocity or discharge	Tributaries, point discharges, and upstream boundary	Daily	Continuous record of length determined by seasonality of tributary flows
	Salinity	Minimally 6- to 12-point measurements throughout the estuary (vertically resolved)	Daily	Short-term records (for initial conditions)
		Tributaries, point discharges, and upstream boundary	Daily	Continuous record of length determined by seasonality of tributary flow
		Two or three locations at ocean boundary (vertically resolved)	0.5 - 1.0 hour	Continuous over one spring-neap tidal sequence for each season

(Continued)

Table 1 (Concluded)

Data Category	Data Type	Sampling Locations	Sampling Frequency	Period of Record
Boundary conditions and initial conditions	Temperature	Minimally 6- to 12-point measurements throughout the estuary (vertically resolved)	Daily	Short-term records (for initial conditions)
		Tributaries, point discharges, and upstream boundary	Daily	Continuous record of length determined by seasonality of tributary flows
		Two or three locations at ocean boundary (vertically resolved)	0.5 - 1.0 hour	Continuous over spring-neap tidal sequence
	Wind speed and direction	Point measurements throughout the estuary	Hourly	Continuous record of length determined by seasonality of local meteorology
Model verification (two or more independent data sets required)	Tidal elevation	Minimally 6- to 12-point measurements throughout the estuary and at ocean boundary	2.0 - 15.0 minutes	Continuous over spring-neap tidal sequence, plus long-term records from existing permanent tide stations
	Velocity	Minimally 6- to 12-point measurements throughout the estuary and at ocean boundary (vertically resolved)	2.0 - 15.0 minutes	Continuous over spring-neap tidal sequence
	Salinity	Minimally 6- to 12-point measurements throughout the estuary and at ocean boundary (vertically resolved)	0.5 - 1.0 hour	Continuous over spring-neap tidal sequence
	Temperature	Minimally 6- to 12-point measurements throughout the estuary and at ocean boundary (vertically resolved)	0.5 - 1.0 hour	Continuous over spring-neap tidal sequence

9 Recommended Approach for LSJRE Model Development Program

The tasks required for development of a comprehensive modeling and monitoring system for the LSJRE and an estimated timeline for accomplishing these tasks are given in Tables 2-11. The timeline estimates are hypothetical, dependent upon the satisfactory completion of preliminary tasks. Furthermore, the estimates for water quality and sediment modeling system development are subject to modification depending upon the development status of the selected model.

Table 2
Hydrodynamic Model Development Program

Task	Description
H1	Develop detailed objectives and management goals for hydrodynamic model development program.
H2	Select hydrodynamic model and contract for license, model maintenance, and consulting services.
H3	Develop limited objectives for initial, 2-D vertically averaged hydrodynamic model application (time and space scales to be simulated, hydrologic conditions for verification, questions to be answered).
H4	Develop 2-D vertically averaged hydrodynamic grid based on existing maps and surveys.
H5	Obtain preliminary boundary condition data from historic record.
H6	Perform field reconnaissance to verify map details.
H7	Perform preliminary simulations.
H8	Compare model to historical data.
H9	Analyze and document preliminary results.
H10	Determine data deficiencies and inadequacies. Recommend additions/deletions in hydrodynamic monitoring network.
H11	Perform further model simulations. Continue to test against new data.
H12	Analyze and document secondary results.
H13	Develop plans for future 2-D vertically averaged model applications. Determine if existing grid resolution, validation, and analysis system is adequate for future applications. Develop program of model maintenance and systematic application to support SJRWMD management objectives.
H14	Develop limited objectives for initial 3-D hydrodynamic model application (time and space scales to be simulated, hydrologic conditions for verification, questions to be answered).
H15	Develop 3-D hydrodynamic grid.
H16	Develop 3-D boundary condition data.
H17	Perform preliminary simulations.
H18	Compare model to historical data.
H19	Analyze and document preliminary results.
H20	Determine data deficiencies and inadequacies. Recommend additions/deletions in hydrodynamic monitoring network.
H21	Perform further model simulations. Continue to test against new data.
H22	Analyze and document secondary results.
H23	Develop plans for future 3-D model applications. Determine if existing grid resolution, verification, and analysis system is adequate for future applications. Develop program of model maintenance, enhancement, and systematic application to support SJRWMD management objectives.

Table 3
Time Line for Hydrodynamic Model Development Program

Task	Year 1	Year 2	Year 3	Year 4	Year 5
H1	-->				
H2	->				
H3	-->				
H4	---->				
H5	---->				
H6	---->				
H7	---->				
H8	---->				
H9	-----	---->			
H10	-----	---->			
H11		---------->			
H12		---------->			
H13	----------	----------	--------->		
H14	--->				
H15	--	-->			
H16		---------->			
H17		----------	-->		
H18		----------	-->		
H19		----------	-->		
H20			---------->		
H21			----------	---------->	
H22			----------	---------->	
H23		----------	----------	---------->	

Table 4
Sediment Transport Model Development Program

Task	Description
S1	Develop detailed objectives and management goals for sediment transport model development program.
S2	Review sediment modeling literature.
S3	Select sediment model and contract for license, model maintenance, model interface development (if required), and consulting services.
S4	Develop limited objectives for initial sediment model application (time and space scales to be simulated, conditions for verification, questions to be answered).
S5	Initiate/expand sediment monitoring program.
S6	Obtain sediment characterization and boundary condition data.
S7	Perform preliminary simulations.
S8	Compare model results to prototype to the extent possible with existing data.
S9	Analyze and document preliminary results.
S10	Determine data deficiencies and inadequacies. Recommend additions/deletions in sediment monitoring network.
S11	Perform further model simulations. Continue to test against new data.
S12	Analyze and document secondary results.
S13	Develop plans for future sediment dynamic model applications. Determine if existing grid resolution, verification, and analysis system is adequate for future applications. Develop program of model maintenance and systematic application to support SJRWMD management objectives.

Table 5
Time Line for Sediment Transport Model Development Program

Task	Year 1	Year 2	Year 3	Year 4	Year 5
S1	---------->				
S2	------	-->			
S3		-->			
S4		---->			
S5	------	----------	----------	----------	---------->
S6		--------->			
S7		---------	-->		
S8		---------	-->		
S9		---------	-->		
S10		---------	-->		
S11			----------	---------->	
S12			----------	---------->	
S13		---------	----------	----------	---------->

Table 6
Water Quality Model Development Program

Task	Description
Q1	Develop detailed objectives and management goals for water quality model development program.
Q2	Review water quality modeling literature.
Q3	Select water quality model and contract for license, model maintenance, model interface development (if required), and consulting services.
Q4	Develop limited objectives for initial water quality model application (time and space scales to be simulated, conditions for verification, questions to be answered).
Q5	Initiate/expand water quality monitoring program.
Q6	Obtain water quality boundary condition data.
Q7	Perform preliminary simulations.
Q8	Compare model to the extent possible with existing data.
Q9	Analyze and document preliminary results.
Q10	Determine data deficiencies and inadequacies. Recommend additions/deletions in water quality monitoring network.
Q11	Perform further model simulations. Continue to test against new data.
Q12	Analyze and document secondary results.
Q13	Develop plans for future water quality model applications. Determine if existing grid resolution, verification, and analysis system is adequate for future applications. Develop program of model maintenance and systematic application to support SJRWMD management objectives.

Table 7
Time Line for Water Quality Model Development Program

Task	Year 1	Year 2	Year 3	Year 4	Year 5
Q1	----------	---------->			
Q2	-----	---------->			
Q3		--->			
Q4		----	->		
Q5	-----	----------	----------	----------	---------->
Q6		----	------>		
Q7			---------->		
Q8			---------->		
Q9			---------->		
Q10			---------->		
Q11			---	----------	------ --->
Q12			---	----------	---------->
Q13		----	----------	----------	---------->

Table 8
Hydrodynamic Monitoring Program Development

Task	Description
HM1	Determine gauge locations, sampling intervals, maintenance schedules for hydrodynamic data stations in consultation with modelers and end users.
HM2	Develop database for hydrodynamic, sediment, and water quality field data analysis, storage, and retrieval.
HM3	Install gauges.
HM4	Collect and analyze data.
HM5	Review procedures; coordinate with modeling team; revise program as needed.

Table 9
Sediment Monitoring Program Development

Task	Description
SM1	Determine parameters, procedures, gauge locations, sampling intervals, maintenance schedules for sediment data stations.
SM2	Expand and maintain database for hydrodynamic and water quality field data analysis, storage, and retreival
SM3	Obtain samplers and equipment if required.
SM4	Collect and analyze data.
SM5	Review procedures; coordinate with modeling team; revise program as needed.

Table 10
Water Quality Monitoring Program Development

Task	Description
QM1	Determine parameters, procedures, gauge locations, sampling intervals, maintenance schedules for water quality data stations.
QM2	Expand and maintain database for hydrodynamic and water quality field data analysis, storage, and retrieval.
QM3	Obtain samplers and equipment if required.
QM4	Collect and analyze data.
QM5	Review procedures; coordinate with modeling team; revise program as needed.

Table 11
Time Line for Development of Monitoring Programs

Task	Year 1	Year 2	Year 3	Year 4	Year 5
HM1	------>				
HM2	----------	---->			
HM3	-------->				
HM4	---------	----------	----------	----------	--------->
HM5	----	----------	----------	----------	--------->
SM1	----	--->			
SM2	----	---------->			
SM3	----	----- ->			
SM4	--	----------	----------	----------	--------->
SM5	--	----------	----------	----------	--------->
QM1	----	--->			
QM2	----	---------->			
QM3	----	----->			
QM4	--	----------	----------	----------	--------->
QM5	--	----------	----------	----------	--------->

10 Other Considerations

Computer Hardware Requirements

Two-dimensional, vertically averaged models for estuarine hydrodynamics are currently being run on minicomputers and midsize workstations. The costs of cpu and memory in this class of machines have steadily decreased over the past several years, and this trend is expected to continue. Turn-around times for workstation batch jobs rival the speeds of shared-resource computers because the new chips are extremely fast and the user has local control over job processing. The advantages of a workstation environment include:

a. Graphical user interface.

b. Moderate initial cost.

c. Personal control of job schedules.

d. Multitasking.

Three-dimensional models are computationally very expensive and time-consuming. Current run times for fully nonlinear 3-D estuarine models running on minicomputers are typically about one-half of real time, depending on the size of the grid and the solution technique. Supercomputers such as the CRAY Y-MP are used for long-term 3-D simulations. However, workstation cpu power is gaining rapidly on the supercomputer market. Low-end, multi-processor machines are also being developed that can take advantage of vectorizable codes. With these advancements, a locally owned, powerful work station with periodic upgrades is likely to be the most cost-efficient solution for estuarine modeling. At the current rate of workstation development, an evaluation of computer resources and equipment upgrade is recommended every other year.

In addition to the cpu, the following equipment and software are required:

a. Digitizer.

b. Graphics monitor.

c. FORTRAN Compiler.

d. C Compiler.

e. Plotting software.

f. High-quality printer for graphics.

g. Mass data storage device.

Graphical User Interface

Estuarine models require a great deal of spatial- and time-varying data. The models generate 3-D time-series of the hydrodynamic, sediment transport, and water quality parameters. A graphical user interface is necessary to organize information, to analyze results, and to gain a physical understanding of the processes described by these data. The graphical interface should be designed to manage model input/output, visualize 3-D data, and facilitate model development and applications. Several graphical user interfaces have been developed specifically for handling data sets arising from geophysical flow models. A graphical user interface may be purchased from a third-party vendor or as part of the model license. As with other components of the modeling software, a contract for software maintenance and updates is recommended.

Costs

The cost of developing a comprehensive estuarine flow model is difficult to estimate. Costs are proportional to the degree of sophistication required to answer specific management questions. Table 12 illustrates "ballpark" figures for a small-scale model development plan using existing codes. The costs cited do not include development of new codes, interfaces, or modeling technologies that may be required to address certain complex problems. The projected costs are based on a timetable of model development similar to that described in Chapter 9. More elaborate plans will increase program costs.

Costs for implementing the hydrodynamic, water quality, and sediment monitoring programs are not included in these estimates. It is assumed that field programs will be conducted by local agencies, and therefore must be budgeted according to local labor and equipment resources. A comprehensive modeling program simply will not succeed without coordination between the monitoring program and the modeling program. The monitoring costs cited in Table 12 reflect the efforts of the modeling team to coordinate the field effort, and special reconnaissance related specifically to modeling needs.

Table 12
Costs for Small-Scale Model Development Plan

System Component	Estimated Cost				
	Year 1	Year 2	Year 3	Year 4	Year 5
Hydrodynamic Modeling System	$100,000	$100,000	$50,000	$10,000	
Sediment Transport Modeling System	$10,000	$100,000	$100,000	$50,000	$10,000
Water Quality Modeling System	$10,000	$50,000	$100,000	$100,000	$50,000
Computer Equipment Purchase and Maintenance	$50,000	$10,000	$10,000	$30,000	$10,000
Graphical User Interface	$20,000	$20,000	$10,000	$10,000	$10,000
Oversee Hydrodynamic Monitoring Program	$20,000	$20,000	$20,000	$20,000	$20,000
Oversee Sediment Monitoring Program	$20,000	$50,000	$50,000	$20,000	$20,000
Oversee Water Quality Monitoring Program	$20,000	$50,000	$50,000	$20,000	$20,000
TOTAL	$250,000	$400,000	$390,000	$260,000	$140,000

References

ASCE Task Committee on Turbulence Models in Hydraulic Computations. (1988). "Turbulence modeling of surface water flow and transport: Parts I - V," *Journal of Hydraulic Engineering*, ASCE, 114(HY9), 970-1073.

Bird, R. Byron, Stewart, Warren E., and Lightfoot, Edwin N. (1960). *Transport Phenomena*. John Wiley & Sons, New York, 160-174.

Blumberg, Alan F., and Mellor, George L. (1987). "A description of a three-dimensional coastal ocean circulation model," *Three dimensional coastal ocean models*, Norman S. Heaps, ed., American Geophysical Union, Washington, DC, 1-16.

Blumberg, Alan F., and Oey, Li-Yauw. (1985). "Modeling circulation and mixing in estuaries and coastal oceans," *Advances in Geophysics* 28A, 525-547.

Casulli, Vincenzo, and Cheng, Ralph T. (1992). "Semi-implicit finite difference methods for three-dimensional shallow water flow," *International Journal for Numerical Methods in Fluids* 15, 629-648.

Cheng, R. T., Ed. (1990). *Residual currents and long-term transport*. Springer-Verlag, New York.

Cheng, R. T., Casulli, Vincenzo, and Gartner, Jeffrey W. (1993). "Tidal, residual, intertidal mudflat (TRIM) model and its applications to San Francisco Bay, California," *Estuarine, Coastal and Shelf Science* 36, 235-280.

Cheng, R. T., Casulli, Vincenzo, and Milford, S. Nevil. (1984). "Eulerian-Lagrangian solution of the convection-dispersion equation in natural coordinates," *Water Resource Research* 20(7), 944-952.

Edinger J. E., and Buchak, E. M. (1980). "Numerical hydrodynamics of estuaries." *Estuarine and Wetland Processes with Emphasis on Modeling.* P. Hamilton and K. B. MacDonald, ed., Plenum Press, New York, 115-146.

Edinger, J. E., and Buchak, E. M. (1985). "Numerical waterbody dynamics and small computers." *Hydraulics and hydrology in the small computer age: Proceedings of the Specialty Conference,* August 13-16, Lake Buena Vista, FL. William R. Waldrop, ed., American Society of Civil Engineers, New York, 708-719.

Fletcher, C. A. J. (1988). *Computational techniques for fluid dynamics.* Volume II, 2nd ed., Springer-Verlag, Berlin.

Ford, Michael, Wang, Jia, and Cheng, Ralph T. (1990). "Predicting the vertical structure of tidal current and salinity in San Francisco Bay, California," *Water Resources Research* 26(5), 1027-1045.

Freeman, Gary Eugene. (1992). "Solving the dilemma: To wave or to oscillate? Opposing formulations of the shallow water equations in river modeling," Ph.D. diss, Texas A&M University. College Station.

Galerpin, B., and Mellor, G. L. (1990). "A time-dependent, three-dimensional model of the Delaware Bay and River system; Part 2: Three-dimensional flow fields and residual circulation," *Estuarine, coastal and shelf science* 31(3), 255-281.

Johnson, B. H., Heath, R. E., Hsieh, B. B., Kim, K. W., and Butler, H. L. (1991). "Development and verification of a three-dimensional numerical hydrodynamic, salinity, and temperature model of Chesapeake Bay," Technical Report HL-91-7, U.S. Army Engineer Waterways Experiment Station, Vicksburg, MS.

King, Ian P. (1993). "RMA-10: A finite element model for three-dimensional density stratifies flow" (working draft). Department of Civil and Environmental Engineering, University of California, Davis.

Le Méhauté, Bernard. (1976). *An introduction to hydrodynamics and water waves.* Springer-Verlag, New York.

Lee, Jonathan K., and Froehlich, David C. (1986). "Review of literature on the finite-element solution of the equations of two-dimensional surface-water flow in the horizontal plane," U.S. Geological Survey Circular 1009, U.S. Department of the Interior, Washington, DC.

Luettich, Richard A., Jr., and Westerink, Joannes J. (1991). "A solution for the vertical variation of stress, rather than velocity, in a three-dimensional circulation model," *International Journal for Numerical Methods in Fluids* 12, 911-928.

Luettich, R. A., Jr., Westerink, J. J., and Scheffner, Norman W. (1992). "ADCIRC: an advanced three-dimensional circulation model for shelves, coasts and estuaries; Report 1: Theory and methodology of ADCIRC-2DDI and ADCIRC-3DL," Technical Report DRP-92-6, U.S. Army Engineer Waterways Experiment Station, Vicksburg, MS.

Mellor, G. L., and Yamada, T. (1982). "Development of a turbulence closure model for geophysical fluid problems," *Review of Geophysics and Space Physics* 20(4), 851-875.

Morris, Frederick W. "Reconnaissance report on the Lower St. Johns River: hydrodynamics and salinity of the Lower St. Johns River" (in preparation), Volume 3, Saint Johns River Water Management District, Palatka, FL.

Rodi, W. (1987). "Examples of calculation methods for flow and mixing in stratified fluids," *Journal of Geophysical Research* 92(C5), 5305-5328.

Sheng, Y. Peter. (1993). "Hydrodynamic and transport modeling of estuarine and lake waters," *Cray Channels* 15(1), 8-11.

Sheng, Y. Peter, Parker, S. F., Henn, D. S. (1986). "A three-dimensional hydrodynamic software model (EHSM3D)," Report prepared under Contract 14-08-0001-21730 by Aeronautical Research Associates of Princeton, Inc., Princeton, NJ, for U.S. Geological Survey.

Walters, Roy A. (1987). "A model for tides and currents in the English Channel and southern North Sea," *Advances in Water Resources* 10, 138-148.

Westerink, Joannes J., and Gray, William G. (1991). "Progress in surface water modeling," *Reviews of Geophysics, Supplement*, 210-217.

Zhao, Di Hua, Tabios, Guillermo Q., III, and Shen, Hsieh Wen. (1992). "RBFVM-2D Model: river basin two-dimensional flow model using finite volume method," Program Documentation, University of California, Berkeley.

Appendix A Notation

$B(x,z)$	Width of the estuary
c	Celerity of a gravity wave
$\overline{D_x}$	One-dimensional diffusion coefficient for salinity
$\bar{D}_x, \bar{D}_y$	Turbulent diffusion coefficients for vertically averaged salinity concentration in the x- and y-directions (L^2/T)
D_x, D_y, D_z	Turbulent diffusion coefficients for salinity in the x-, y-, and z-directions (L^2/T)
$F(s,T)$	An empirically derived relationship describing the variation of water density with salinity and temperature
g	Acceleration due to gravity acting in the -z direction (L/T^2)
h	Bathymetric depth relative to datum (L)
H	Total water depth
p	Local pressure (M/LT^2)
s	Salinity concentration (M/L^3)
S	Vertically averaged salinity concentration (M/L^3)
$\bar{S}$	Cross-section averaged salinity concentration (M/L^3)
t	Time (T)
T	Temperature
$\bar{T}$	Cross-section averaged temperature

$\overline{u},\overline{v},\overline{w}$	Time-averaged mean velocities in the x-, y-, and z-directions (L/T)
u',v',w'	Turbulent fluctuation velocities in the x-, y-, and z-directions (L/T)
U	Depth-averaged horizontal velocity in the x-direction (L/T)
$\overline{U}$	Cross-section averaged velocity (L/T)
V	Depth-averaged horizontal velocity in the y-direction (L/T)
x,y,z	Right-handed Cartesian coordinate directions (L)
$\overline{\Gamma_x}$	Longitudinal tractive forces per unit volume (M/L^2T^2)
Δt	Time-step for simulation
Δx_{min}	Minimum node spacing
$\Gamma_x,\Gamma_y,\Gamma_z$	Summation of tractive and body forces (excluding gravity) per unit volume in the x-, y-, and z-directions (M/L^2T^2)
ε_{ij}	Turbulent coefficient of viscosity in the i^{th} plane in the j^{th} direction, also called eddy viscosity (M/LT)
ζ	Free surface elevation relative to fixed datum (usually mean sea level) (L)
θ_s	Source (+) or sink (-) for salinity (M/L^3T)
$\overline{\theta_s}$	Cross-section sources and sinks for salinity (M/L^3T)
μ	Viscosity of water (M/LT)
ρ	Density of water (M/L^3)
ρ_o	Reference density of water (M/L^3)
τ_{ij}	Reynolds stress component on the i^{th} plane in the j^{th} direction, for i = 1, 2, 3 and j = 1, 2 corresponding to the x-, y-, and z-directions (M/LT^2)
$\overline{\tau}_{xx}$	Cross-section averaged Reynolds stress in the longitudinal direction

REPORT DOCUMENTATION PAGE

Form Approved
OMB No. 0704-0188

Public reporting burden for this collection of information is estimated to average 1 hour per response, including the time for reviewing instructions, searching existing data sources, gathering and maintaining the data needed, and completing and reviewing the collection of information. Send comments regarding this burden estimate or any other aspect of this collection of information, including suggestions for reducing this burden, to Washington Headquarters Services, Directorate for Information Operations and Reports, 1215 Jefferson Davis Highway, Suite 1204, Arlington, VA 22202-4302, and to the Office of Management and Budget, Paperwork Reduction Project (0704-0188), Washington, DC 20503.

1. AGENCY USE ONLY (Leave blank)	2. REPORT DATE	3. REPORT TYPE AND DATES COVERED
	September 1994	Final report

4. TITLE AND SUBTITLE
Review and Evaluation of Hydrodynamic Modeling for the Lower St. Johns River Estuary

5. FUNDING NUMBERS

6. AUTHOR(S)
Lisa Roig

7. PERFORMING ORGANIZATION NAME(S) AND ADDRESS(ES)
U.S. Army Engineer Waterways Experiment Station
3909 Halls Ferry Road, Vicksburg, MS 39180-6199

8. PERFORMING ORGANIZATION REPORT NUMBER
Technical Report
HL-94-15

9. SPONSORING/MONITORING AGENCY NAME(S) AND ADDRESS(ES)
U.S. Army Engineer District, Jacksonville
P.O. Box 4970, Jacksonville, FL 32232-0019
and the St. Johns River Water Management District
St. Johns River Water Management District
Highway 100 West, Palatka, FL 32178-1429

10. SPONSORING/MONITORING AGENCY REPORT NUMBER

11. SUPPLEMENTARY NOTES
Available from National Technical Information Service, 5285 Port Royal Road, Springfield, VA 22161.

12a. DISTRIBUTION/AVAILABILITY STATEMENT
Approved for public release; distribution is unlimited.

12b. DISTRIBUTION CODE

13. ABSTRACT *(Maximum 200 words)*

The St. Johns River Water Management District and the U.S. Army Engineer District, Jacksonville, desire to quantify the hydrodynamic, sediment transport, and water quality processes of the Lower St. Johns River Estuary (LSJRE). To this end, a comprehensive numerical model development program is planned. In support of this effort, this report reviews the basic equations of estuarine hydrodynamics. Major hydrodynamic modeling technologies are compared and contrasted. The data requirements for application of a hydrodynamic model to the LSJRE are outlined. An approach for developing a system of models and monitoring programs for the LSJRE is recommended. Computer hardware and software issues that will affect the productivity of the modeling system are discussed.

14. SUBJECT TERMS	15. NUMBER OF PAGES
Estuarine modeling Hydrodynamic modeling Lower St. Johns River Estuary	76
	16. PRICE CODE

17. SECURITY CLASSIFICATION OF REPORT	18. SECURITY CLASSIFICATION OF THIS PAGE	19. SECURITY CLASSIFICATION OF ABSTRACT	20. LIMITATION OF ABSTRACT
UNCLASSIFIED	UNCLASSIFIED		